On finite element modelling of surface tension phenomena.

Saksono, Prihambodo Hendro

Department of Civil Engineering
University of Wales Swansea

ON FINITE ELEMENT MODELLING OF SURFACE TENSION PHENOMENA

Prihambodo Hendro Saksono
S.T. (ITI/Jakarta), M.Sc (Wales)

Thesis submitted to the University of Wales in candidature
for the degree of Doctor of Philosphy

C/Ph/253/02

May 2002

DECLARATION

This work has not previously been accepted in substance for any degree and is not being concurrently submitted in candidature for any degree.

Signed .....(candidate)

Date 01/05/2002

STATEMENT 1

This dissertation is being submitted in partial fulfilment of the requirements for the degree of Doctor of Philosophy.

Signed .....(candidate)

Date 01/05/2002

STATEMENT 2

This dissertation is the result of my own investigations, except where otherwise stated. Other sources are acknowledged by footnotes giving explicit references. A bibliography is appended.

Signed .....(candidate)

Date 01/05/2002

STATEMENT 3

I hereby consent for my dissertation, if accepted, to be available for photocopying and for inter-library loan, and for the title and summary to be made available to outside organisations.

Signed .....(candidate)

Date 01/05/2002

ACKNOWLEDGEMENTS

I would like to thank Prof. Djordje Perić, my supervisor, for trusting me to carry out this project and introduce me to the fascinating world of interface science, for his guidance, support and encouragement during this work.

Many thanks are also due to Dr. E.A. de Souza Neto for providing me with HYPLAS© and allow me to vandalize this code, helpful discussions on consistent linearization, and suggestions.

Also many thanks to Dr. A.J.L Crook, Dr. Z. Wei, and Dr. J.G. Yu from Rockfiled Software Ltd. for putting my surface tension formulation into ELFEN© explicit so that realistic examples can be run.

I would like to acknowledge the financial support from EPSRC of United Kingdom through Grant GR/l66724 and Government of the Republic of Indonesia through 33/IRE-BDG/1997. Also I would like to acknowledge additional financial support and encouragement received from my parents and family during my studies.

Many thanks go also to my "Computational brothers and sister" from Civil and Mechanical Engineering Departments, in alphabetical order Antonio Orlando, Arnaud G. Malan, Dhemi H. Tirmizi, Igor N. Dyson, James M. MacFadden, Kaare A. Sørensen, Mak Kok Wah, Mariella Luege, Miguel X. Rodriguez Paz, Mohamad El Hachemi, Paul D. Ledger, Rajab Said, Sava Slijepčević, Sivakumar Kulasegaram, William K. S. Pao, Wulf G. Dettmer and friends who have made my stay in Swansea enjoyable.

For the unconditional support received, I wish to express my sincere gratitude to family and friends in Indonesia.

Finally, I am especially grateful to my wife, Meily Wibisono, for bringing me back to life and her patience, understanding, and companionship during the last stage of my study, especially her encouragement for me to finish my study as soon as possible.

To My Father, Mother and Meily

To a country in chaos and a nation in confusion

SUMMARY

THE OBJECTIVE of this work is to develop a computational framework for modelling the motion of liquid phase between moving particles associated with the processing of complex multiphase materials. The liquid phase may be present at various levels of saturation and necessarily includes numerous and irregular free surfaces. In this kind of situation the surface tension is dominant and governs the interparticle motion that plays a fundamental role during material processing. This work focuses on surface tension modelling using the finite element method. Two issues related to the modelling of surface tension are addressed in this thesis, the first one is the development of a finite element procedure capable of modelling accurately the motion of the free surface boundaries between the gas and liquid phases. The second issue is finite element modelling of surface tension at such boundaries.

The finite element formulation is based on the use of the incremental flow formulation of the Lagrangian form of the initial boundary value problem governing the free surface flow. The incompressibility constraint associated with the Newtonian fluid employed in this work is imposed using the penalty method.

With regard to the surface tension model, the constitutive model commonly known as the Laplace-Young equation is employed. In the Lagrangian framework the surface tension formulation emerges naturally through the weak form of the Laplace-Young equation and the use of the surface divergence theorem reduces the continuity requirement across the element boundary from C^1 to C^0.

The performance of the finite element model of surface tension is validated by means of numerical examples for both equilibrium and dynamic cases. The finite element results are compared against both analytical solutions and experimental results.

Contents

General Notation

THROUGHOUT this disertation, an attempt has been made to maintain the notation as uniform as possible by assigning specific letter styles to the representation of each type of mathematical entity. The general scheme of notation employed is described below.

Characters. General usage

- *Italic light-face letters A, a, B, b,...*: Scalars and scalar valued functions.
- *Italic bold-face majuscules* $\boldsymbol{A}$, $\boldsymbol{B}$, ...: Second order tensors or functions whose values are second order tensors.

  Exceptions: $\boldsymbol{N}$ (material unit normal vector) and $\boldsymbol{T}$ (material unit tangent vector).
- *Italic bold-face minuscules* $\boldsymbol{a}$, $\boldsymbol{b}$, ...: Points, vectors and vector valued functions.
- *Greek light-face letters* α, β, ..., Φ, Ψ, ...: Scalars and scalar valued functions.
- *Greek bold-face minuscules* $\boldsymbol{\alpha}$, $\boldsymbol{\beta}$, ..., $\boldsymbol{\sigma}$, $\boldsymbol{\tau}$, ...: Second order tensors.
- *Script majuscules* $\mathscr{A}$, $\mathscr{B}$, ...: Spaces, sets, groups, bodies.
- *Special block-bold majuscules* $\mathbb{A}$, $\mathbb{B}$, ...: Finite element matrices and vectors.

Exceptions: $\mathbb{A}^{hydr}$ (hydrostatic part of spatial elasticity tensor), $\mathbb{A}^{visc}$ (viscous part of spatial elasticity tensor), and $\tilde{\mathbb{I}}$ (fourth-order transpose identity tensor).

- *Sans serif bold-face majuscules* A, B, ...: Second order surface tensors or functions whose values are second order surface tensors.
- *Sans serif bold-face minuscules* a, b, ...: Surface vectors or functions whose values are surface vectors.

Some commonly used characters

A	Amplitude of oscillations
$\mathbb{A}$	Spatial elasticity matrix
$\boldsymbol{B}$	Left Cauchy-Green strain tensor
$\mathscr{B}$	Three-dimensional body
$\mathbb{B}$	Standard discrete symmetric gradient matrix
$\boldsymbol{b}$	Spatial body force field
$\boldsymbol{b}_0$	Material body force field
$\boldsymbol{C}$	Right Cauchy-Green strain tensor
$\mathscr{C}$	Family of configurations
$\boldsymbol{D}$	Rate of deformation tensor
$\mathscr{D}^{visc}$	Viscous dissipation
E	Material specific internal energy
$\mathscr{E}$	Three-dimensional Euclidean space
e	Spatial specific internal energy
$\boldsymbol{F}$	Deformation gradient tensor
$\mathbb{F}^{\mathrm{EXT}}$	External global force vector
$\mathbb{F}^{\mathrm{INT}}$	Internal global force vector
F	Surface deformation gradient
G	Virtual work
G^{int}	Internal virtual work
$\mathscr{G}$	Isotropy group
$\mathbb{G}$	Standard discrete spatial gradient operator
$\boldsymbol{g}$	Spatial gradient of temperature or gravitational force vector

g	Surface gradient of surface temperature
H	Mean curvature
h_{min}	Minimum liquid bridge radius
$\boldsymbol{I}$	Second order identity tensor
$\mathscr{I}$	Time interval
$\tilde{\mathbb{I}}$	Fourth-order transpose identity tensor
I	Inclusion map
J	Jacobian of a deformation
$\mathbb{J}$	Jacobian matrix
L	Initial height of liquid bridge
$\boldsymbol{L}$	Velocity gradient tensor
L	Surface velocity gradient
l	Capillary length
K	Bulk modulus
$\mathscr{K}$	Space of kinematically admissible deformations
$\mathbb{K}$	Global stiffness matrix
$\widehat{\mathbb{K}}$	Global effective stiffness matrix
$\mathbb{M}$	Global mass matrix
$\boldsymbol{m}$	Binormal vector
$\boldsymbol{N}$	Material unit normal vector
$\boldsymbol{N}_{(i)}$	Principal directions of right stretch tensor
$\mathbb{N}$	Element shape function
n	Oscillations modes
$\boldsymbol{n}$	Spatial unit normal vector
$\boldsymbol{n}_{(i)}$	Principal directions of left stretch tensor
$\boldsymbol{o}$	Origin
$\boldsymbol{P}$	First Piola-Kirchhoff stress tensor or projection tensor
$\mathscr{P}$	Part of a body or space of pressures
p	Pressure
$\boldsymbol{p}$	Material point
$\boldsymbol{Q}$	Orthogonal tensor
$\boldsymbol{q}$	Spatial heat flux
$\boldsymbol{q}_0$	Material heat flux
q	Surface conductive heat flux

R	Unpeturbed radius
$\boldsymbol{R}$	Rotation tensor
$\mathscr{R}$	Set of real numbers
$\mathbb{R}$	Residual force vector
r	Spatial heat production density
r_0	Material heat production density
$\boldsymbol{r}$	position vector
S	Material specific entropy
$\boldsymbol{S}$	Material traction vector
s	Spatial specific entropy
$\boldsymbol{T}$	Material unit tangent vector
T	Surface stress tensor
$\boldsymbol{t}$	Traction force vector
U_m	Stretching speed
U^*	Dimensionless stretching speed
$\boldsymbol{U}$	Right stretch tensor
$\mathscr{U}$	Space of virtual displacements or unimodular transformation group
$\mathbb{U}$	Displacement vector
$\dot{\mathbb{U}}$	Velocity vector
$\ddot{\mathbb{U}}$	Acceleration vector
$\boldsymbol{u}$	Element displacement vector
V	Volume
$\boldsymbol{V}$	Left stretch tensor or material velocity vector
$\mathscr{V}$	Translation vector space associated with three dimensional Euclidean space
$\boldsymbol{v}$	Spatial velocity vector
$\boldsymbol{W}$	Spin tensor
$\boldsymbol{w}$	Weighting function
$\boldsymbol{X}$	Reference position of a material point
$\boldsymbol{x}$	Current position of a material point
α	Contact angle
β	Newmark time integration parameter
γ	Surface tension coefficient
δ	Newmark time integration parameter
$\varepsilon_{\mathscr{D}}$	A posteriori error indicator based on dissipation functional

η	Natural coordinate
Θ	Material temperature field
θ	Spatial temperature field
$\boldsymbol{\kappa}$	Injection of a body into a three dimensional Euclidean space
Λ	Static stability limit of a liquid bridge
μ	Viscosity
ξ	Natural coordinate
Π_0	Region occupied by part of a body in reference configuration
Π_t	Region occupied by part of a body in current configuration
ρ	Density
$\boldsymbol{\sigma}$	Cauchy stress tensor
$\boldsymbol{\sigma}^{hydr}$	Hydrostatic stress
$\boldsymbol{\sigma}^{visc}$	Viscous stress
τ	Period of oscillations
$\boldsymbol{\tau}$	Kirchhoff stress tensor
ϕ	Viscous potential
$\boldsymbol{\varphi}$	Motion of a three dimensional body
$\boldsymbol{\chi}$	Motion of a material surface
ψ	Helmholtz free energy function per unit mass
Ω_0	Reference configuration of a body
Ω_t	Current configuration of a body
ω_n	Frequency of oscillations
$\partial\Omega_t$	Boundary of a region occupied by a body in the current configuration
$\partial\Omega_0$	Boundary of a region occupied by a body in the reference configuration
$\partial\Omega_t^c$	Boundary with prescribed contact angle
$\partial\Omega_t^\gamma$	Boundary with prescribed surface tension
$\partial\Omega_t^\sigma$	Boundary with prescribed traction vector
$\partial\Omega_t^\varphi$	Boundary with prescribed deformation

Indices

- *Italic indices e* : Denotes a quantity associated with elements.
- *Italic indices h* : Denotes a discrete quantities.
- *Italic indices s* : Denotes a quantity associated with surfaces.
- *Italic subscripts i, j, k, l,...*: Range between 1,2,3.
- Summation on repeated subscripts is implied unless otherwise stated.

Mathematical accents

- $\widehat{(\cdot)}$: Denotes response functions.
- $\widetilde{(\cdot)}$: Denotes incremental quantities.

Symbols and operations

$\det[\cdot]$	Determinant of $[\cdot]$
$\mathrm{DIV}[\cdot]$	Material divergence of $[\cdot]$
$\mathrm{div}[\cdot]$	Spatial divergence of $[\cdot]$
$\mathrm{div}_s[\cdot]$	Surface divergence of $[\cdot]$
$\ln[\cdot]$	Tensor logarithm of $[\cdot]$
$\mathrm{tr}[\cdot]$	Trace of $[\cdot]$
$\Delta(\cdot)$	Increment of $(\cdot)$
$\nabla_s(\cdot)$	Spatial surface gradient of $(\cdot)$
$\nabla_{s_0}(\cdot)$	Material surface gradient of $(\cdot)$
$\nabla_X(\cdot)$	Material gradient of $(\cdot)$
$\nabla_x(\cdot)$	Spatial gradient of $(\cdot)$
$\dot{(\cdot)}$	Time derivative of $(\cdot)$
$\mathrm{D}(\cdot)[\boldsymbol{a}]$	Directional derivative of $(\cdot)$ in the direction of $\boldsymbol{a}$

$\dfrac{\mathrm{D}}{\mathrm{D}t}(\cdot)$	Material time derivative of $(\cdot)$
$\dfrac{\mathrm{d}}{\mathrm{d}a}(\cdot)$	Derivative of $(\cdot)$ with respect to a
$\dfrac{\partial}{\partial a}(\cdot)$	Partial derivative of $(\cdot)$ with respect to a
$\boldsymbol{A}:\boldsymbol{B}$	Double contraction of tensors
$\boldsymbol{a}\cdot\boldsymbol{b}$	Scalar product of vectors
$\boldsymbol{A}\otimes\boldsymbol{B}$, $\boldsymbol{a}\otimes\boldsymbol{b}$	Tensorial product of tensors or vectors
$\lvert(\cdot)\rvert$	Absolute value of $(\cdot)$

Notations for some sets

Bid	Set of all two dimensional subspace of the translation vector space
Invlin	Set of all invertible tensors
Lin	Set of all tensors
Lin^{+}	Set of all tensors $\boldsymbol{A}$ with $\det[\boldsymbol{A}] > 0$
Orth^{+}	Set of all proper orthogonal tensors
Sym	Set of all symmetric tensors
Unim	Set of all tensors $\boldsymbol{A}$ with $\det[\boldsymbol{A}] = 1$

Chapter 1

Introduction

Surface or interfacial phenomena, in particular the ones driven by surface tension, are frequently encountered in everyday life. Soap bubbles, the spreading of water rivulets flowing on a car wind screen during the rain, or slow moving stream of water from a tap that breaks up into drops at some distance below the tap are just a few examples of such phenomena. These phenomena also play an important role in many industrial processes involving multiphase fluids or immiscible multicomponent fluids especially when the external forces are less dominant. Improvement of the efficiency and productivity of many processes in chemical, foods, pharmaceutical industries rely heavily on the understanding of the surface tension phenomena and its role in such processes.

The fact that enormous amount of research have been carried out in the past, either theoretically or experimentally, does not mean that research activities in surface phenomena are slowing down. With the recent interest in ink jet printing and containerless material processing in zero or near zero gravity the research activities related to interfacial phenomena are increasing. The advent of digital computers in the fifties and the development of numerical methods for solving partial differential equations in the last four decades have provided a new impetus for research in surface science and have encouraged development of new theories which incorporate even more complex phenomena.

To date different numerical methods have been developed; some are well established and some still need development. Finite element method can be considered as a well established method. The finite element theory and practice have matured due to massive research activities during the last four decades and has been applied to more diverse fields and problems than any other methods. These make the finite element method the best candidate to be used to simulate industrial processes in which different fields are coupled

together. Moreover, the existence of finite element in the curriculum of engineering education and the increase in the performance of personal computer has made finite element codes routinely used by an ever increasing number of engineers.

In general, the numerical solutions of surface tension phenomena can be categorized into two main groups. The first one is associated with finding the surfaces shape under the influence of surface tension and other forms of energy, such as gravity, and subject to various constraint. This approach has variational calculus as its root. The second one is related to the solution of the partial differential equation governing the physics of the phenomena. Despite the former has been successfully applied to vast amount of problems in industry, it is limited to static equilibrium problems and because it focuses on the geometry of the surface, it is unable to explain what is happening in the interior of the fluid. The latter approach however can be used to solve static and dynamic problems, and thus, it is more suitable to model complex industrial processes such as granulation, spraying and atomization, coating, etc.

1.1 The scope of the thesis

The objective of this thesis is to develop a computational framework for modelling motion of liquid phase between moving particles. The liquid phase may be present at various levels of saturation and necessarily includes numerous and irregular free surfaces. A typical problem described by such model is encountered in granulation processes.

As a part of the wider computational developments related to combined discrete/finite element modelling of granulation processes, attention in this thesis is focused on issues related to finite element implementation of surface tension, namely

1. A finite element procedure capable of modelling accurately the deformation of the free surface boundaries between gas and liquid phases.

2. Finite element modelling of surface tension at the boundaries between gas and liquid phases.

On the application side the focus is on simulation of quasistatic and dynamic deformation of liquid drops and liquid bridges which may be in contact with stationary and/or moving solid surfaces.

1.1.1 Finite element procedure

Finite element procedures for free surface flows typically follow either Eulerian, Lagrangian, or arbitrary Eulerian-Lagrangian (ALE) descriptions. Each of these has its own advantages and disadvantages. In this work Lagrangian finite element is chosen, in particular, due to its ability to represent explicitly the free surface boundaries. The so-called incremental flow formulation is adopted so that the resulting equilibrium equations are functions of geometry changes rather than velocities. As a result this procedure provides a good platform for implementation of surface tension model.

1.1.2 Constitutive model for fluid

Only Newtonian fluid is considered in this work. Despite of its simplicity, Newtonian fluid can be used to model large number of the real fluids satisfactorily. The use of incremental flow formulation makes extension to more complicated model such as viscoelastic or viscoplastic fluids straight forward.

In this work, the incompressibility condition is enforced by using penalty method.

1.1.3 Surface tension model

The surface tension model is based on the basic form of the Laplace-Young equation with surface tension coefficient being constant. The surface tension variation along the interface, which is typically associated with the variation of temperature or chemical concentration has not been considered in this work.

Throughout this thesis the surface is assumed to be a *material surface* that is the surface always consists of the same material points. The adoption of this assumption simplifies significantly the surface tension modelling.

1.2 Layout

This thesis is divided into eight chapters, after this introductory one, the remainder of the thesis is arranged as follows:

Chapter 2 deals with the basic physical aspects of interfacial phenomena, which sets out the background for the current research. It gives a brief historical review of its development along with mechanical and thermodynamical treatments of surface tension.

Chapter 3 reviews the basic concepts of mechanics and thermodynamics of continua, including problems with interfaces.

Chapter 4 presents the finite element procedure for solution of free surface flows that appear in conjunction with surface tension problems. The finite element procedure is based on the incremental flow formulation. A short review on the adaptive remeshing procedure employed in this work is also presented.

Chapter 5 contains the weak formulation of Laplace-Young equation and its finite element implementation. The equation is considered as a boundary condition for free surfaces in which the present surface tension is described. The finite element implementation has been completed for two dimensional and axisymmetric cases and its consistent linearization associated with the Newton-Rhapson solution procedure is derived.

Chapter 6 comprises several illustrative examples of quasi-static analysis of meniscii problems using the aforementioned finite element procedure. The finite element results are compared with the solutions obtained by integrating ordinary differential equations resulting from parameterization of the Laplace-Young equation.

Chapter 7 Provides two examples in which dynamic effects are important. The first one is a droplet oscillation problem due to surface tension which has been used by many author as a benchmark test. The second example is the stretching of a liquid bridge. The deformation experienced by the liquid bridge is large requiring adaptive remeshing in order to maintain the quality of the solution.

Chapter 8 In this chapter a short summary and the conclusions of this work are presented and some suggestions for future research are given.

Bibliography

[1] C. Isenberg. *The Sience of Soap Films and Soap Bubbles.* Tieto, Clevedon, 1978.

[2] L.D. Landau and E.M. Lifshitz. *Fluid Mechanics.* Pergamon Press, New York, 2^{nd} edition, 1987.

[3] D. Perić and P.H. Saksono. On finite element modelling of surface tension: Variational formulation and applications. In W.A. Wall, K.U. Bletzinger, and K. Schweizerhof, editors, *Trends in Computational Structural Mechanics*, E. Ramm's 60^{th} Anniversary Volume, Barcelona, 2001. CIMNE.

[4] D. Perić, P.H. Saksono, and A.J.L. Crook. Some aspects of lagrangian finite element analysis of flows with free surfaces and interfaces. In *European Confrence on Computational Mechanics - ECCM 2001*, Cracow, Poland, June 2001.

[5] R.F. Probstein. *Physicochemical Hydrodynamics:An Introduction.* John Wiley & Sons, New York, 2^{nd} edition, 1994.

[6] P.H. Saksono and D. Perić. Finite element modelling of surface tension with application to equilibrium shapes of liquid drops and bridges. In *European Congress on Computational Methods in Applied Sciences and Engineering - ECCOMAS CFD 2001*, Swansea, U.K., September 2001.

Chapter 2

Surface Tension Phenomena

Uneven distribution of molecules in a region where two immiscible fluids or two different media meet gives rise to different physical and chemical processes in that region and affect the surrounding fluids. These processes manifest itself in many interesting macroscopic phenomena which are known as *surface or interfacial phenomena* (in this chapter the term surface and interfacial are used interchangeably). Since the condition in which two immiscible fluids meet occurs frequently and the fact that many natural and industrial processes are based on or influenced by these phenomena makes the surface phenomena an important subject of its own and have drawn a lot of attention from scientific community. Among different classes of surface phenomena *surface/interface tension* is the one which easily observed in every day life and, therefore, the oldest one to be studied.

In general, the approaches used for the theoretical study of surface tension phenomena can be classified into three different groups. The first group is associated with the application of mechanical principles in the behavior of particles in the neighborhood of a boundary between two immiscible fluids. The second one comprises methods in which principles of thermodynamics are applied to the infinitesimal portions of fluids composing the interfacial region, and the third group incorporates the ones which use principles of statistical mechanics to the study of the average behavior of matter at points within the interfacial region.

This chapter serves as an introductory to the surface tension phenomena. Starting with the brief history of works that had been conducted in the past on the nature and the physics of surface tension, it continues with the physics of surface tension and follows by a section on the contact angle. Sections on mechanical and thermodynamical treatments of interface region are given at the end of this chapter. The former is intended to show how the Laplace-Young equation is obtained and its generalization that takes

into account variable surface tension coefficient, while the latter shows how thermodynamics principles has been used to explain the phenomena and its dependence on thermodynamical and geometrical variables. The content of these two sections is widely available from standard fluid mechanics, physical chemistry or surface science literature [11, 12, 17, 1, 6, 13, 18].

2.1 Brief history on surface tension phenomena

It is not a surprise that the qualitative physical observations of the surface tension driven phenomena are very old field since these phenomena occur and easily observed in every day life. Pliny the Elder (23-79 A.D.) described divers who released small quantities of oil from their mouths in order to damp capillary ripples on the ocean surface and in this way provide more uniform lighting for their work [18]. Leonardo da Vinci, in the fifteenth century, studied the rise of a liquid in a capillary tube above the level of the liquid surface in the bath where the tube is inserted. The first accurate quantitative observations on capillary phenomenon were made by Francis Hawksbee in 1709.

The important concept of surface or interfacial tension was introduced by J.A. von Segner in 1751. In 1805 Thomas Young, in his essay *Cohesion of Fluids*, used the concept of surface tension to explain the rise of liquid in a capillary tube and introduced the concept of contact angle between a fluid surface and a solid surface. His works contains the solution to a number of problems that were later solved independently by Marquis de Laplace. The result, known as the Laplace-Young equation, concerns the excess pressure across a curved fluid surface or interface separating two immiscible fluids at a point.

Important theoretical contribution to the study of fluid surfaces were made by Carl Friedrich Gauss in 1830 and by Siméon Denis Poisson in 1831. Gauss rederived the Laplace-Young equation by examining the energy of the fluid surface and obtained an expression for the contact angle at the boundary. Poisson introduced the concept that the density of the fluid in the surface or interfacial regions was different from that of the bulk fluids.

Plateau's interest in the nature of the molecular forces present in the surface and the bulk of fluids had led him to the discovery of unusual surfaces formed by soap films contained by wire frames. Even though the mathematics that concerns finding the minimum area of a surface contained by a fixed boundary had been introduced by Euler, and later simplified by Lagrange,

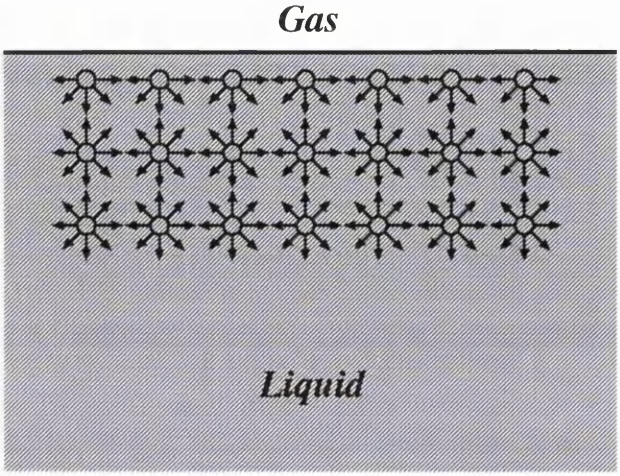

Figure 2.1: Attractive forces between molecules at the interface of two immiscible fluids

almost a century earlier, it was Plateau's experiments that provided mathematicians with a renewed motivation to investigate the problems of surface of minimum area.

2.2 Physics of surface tension

From the microscopic point of view, the boundary between two homogeneous phases or two immiscible fluids is not a simple geometrical surface but rather a region in the form of lamina or film with finite thickness known as *interfacial region* [1, 6, 17]. The thickness of this interfacial region depends on the nature of the phases and other factors and, as in bulk, the matter in the interfacial region may exist in the solid and liquid states. The material in this region is a mixture of the molecules from both contiguous homogeneous phases. Hence, the material in the interface region has different properties from those of the materials in the contiguous homogeneous phases. One of the differences is the presence of attractive intermolecular forces due to difference in molar density of chemical components that constitute the materials in interfacial region and contiguous homogeneous phases as shown in figure 2.1. Each molecule in the interior of homogeneous phases is surrounded by others on every side and therefore subject to equal attraction in all direction, while molecules in the interfacial region experience different amount of attraction from the two contiguous phases. This causes the molecule to be attracted inward the phase with stronger attractive intermolecular forces and higher energy in the interfacial region than in the interior. Since the free energy of a system tends

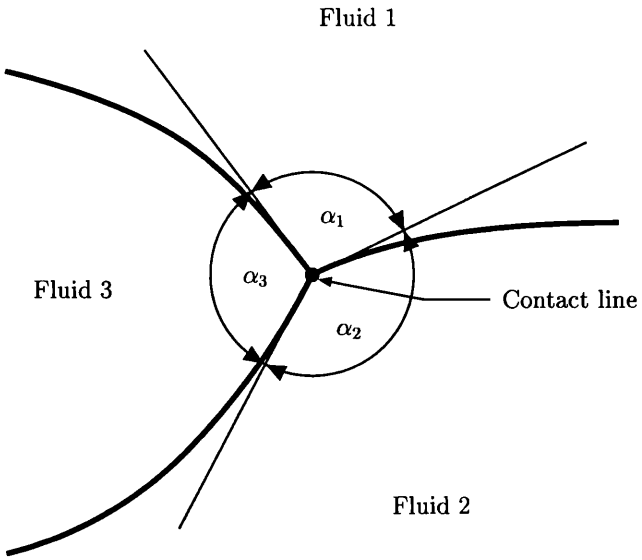

Figure 2.2: Three phases system and contact line

to a minimum, the interfacial region tends to contract spontaneously and gives an impression that the surface of a liquid were surrounded by an elastic skin in a state of tension.

It is a common practice to simplify such a system by introducing a model in which the interfacial region is replaced by an interface, which is a mathematical dividing surface of zero thickness plus two continuum phases having uniform properties right up to the interface [7]. In the solution to the problem of equilibrium, the free energy of the interfacial region results in a hypothetical tension of the same magnitude and acting in all directions parallel to the surface. This is what is generally known as the *surface tension* [1].

In general, surface tension depends on temperature and the presence of surface active materials. It decreases as the temperature is raised and vanishes when the temperature reaches a critical point. When an interface is populated by surface active materials, the surface tension decreases as the concentration of surfactant increases. At a certain saturation concentration where the interface is covered by a monolayer of surfactant the surface tension reaches a plateau [15, 17].

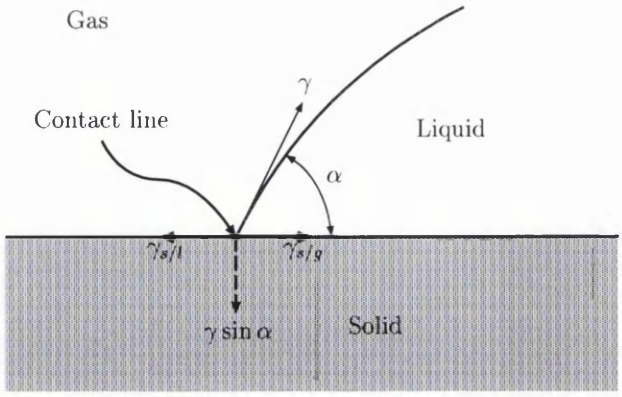

Figure 2.3: Static equilibrium of a liquid drop in a gas at line of contact with a horizontal solid surface

2.3 Contact angle

When three immiscible fluids or different phases are in equilibrium, the surfaces of separation are such that the surface tension force cancel out on the common line of intersection [12]. This condition implies that the surfaces of separation must intersect at angles determined by the values of the surface tension, as shown in figure 2.2. These angles and the common line are known as the *contact angles* and *contact line*, respectively. This phenomenon is a direct consequence of the molecular interaction among the three different materials at the vicinity of the contact line.

For cases where the phases involved are solid, liquid, and gas, and the solid phase possesses a uniform, perfectly flat surface, as in figure 2.3, the liquid may spread freely over the surface or it remains as a drop with a specific contact angle on the solid surface. This contact angle is called *static contact angle* when its value corresponds to a stationary contact line pinned on a stationary solid surface. It is a physical constant that depends upon the chemical properties of the solid and fluids [15]. The contact angle controls the radius of curvature of the drops which, in turn, regulates the pressure in the liquid drop [17].

If the liquid drop is to remain in static equilibrium without moving along the surface it is required that the horizontal component of the gas/liquid surface tension, γ, must be balanced at the contact line by other surface forces represented by solid/liquid surface tension, $\gamma_{s/l}$, and solid/gas surface tension, $\gamma_{s/g}$,

$$\gamma \cos \alpha = \gamma_{s/g} - \gamma_{s/l}. \tag{2.1}$$

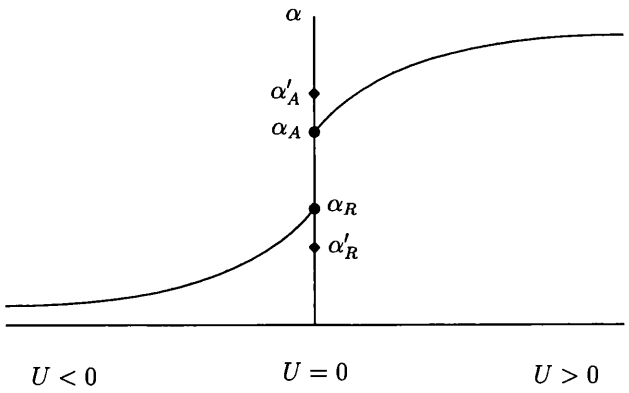

Figure 2.4: Dynamic contact angle as a function of the velocity of contact line.

By combining equation (2.1) with Dupré relation defining the *adhesion work* between liquid and solid

$$W_{s/l} = \gamma_{s/g} + \gamma - \gamma_{s/l} \tag{2.2}$$

gives

$$W_{s/l} = \gamma(1 + \cos\ \alpha) \tag{2.3}$$

Equation (2.3) shows that the contact angle, α, is determined by the relative magnitudes of the solid/liquid adhesion, $W_{s/l}$ and the liquid/gas surface tension, γ.

The above expression for the static contact angle was first derived by Young [20], based on assumption that the three material boundaries (gas/liquid, solid/liquid, and solid/gas) each possess a constant surface tension. Equation (2.1) has eluded experimental verification due to the fact that $\gamma_{s/g}$ and $\gamma_{s/l}$ cannot be easily or accurately measured. Equation (2.1) is also not completely satisfying from the mechanical point of view due to the fact that the vertical component can have arbitrary value.

Experiment shows that if the contact line is made to move over a stationary solid surface or the solid surface is made to move while the contact line is kept stationary, the observed contact angle will be different from the static contact angle. This contact angle is known as the *dynamic contact angle.* It depends upon chemistry of the solid and fluids, and the velocity of the surface and the velocity of the contact line [15]. It is found that the dynamic contact angle is related to the velocity of the contact lines U by $\partial\gamma/\partial U \geq 0$, whether or not the other fluid is a gas or an immiscible liquid [8].

Very often the value of contact angle is not obtained from the static equilibrium condition but from the extrapolated values of α in the limit as U tends to zero from positive of negative values which are known as *advancing* or *receding contact angles*, and denoted, respectively, by α_A and α_R. A typical graph of the dynamic contact angle with respect to the velocity of the contact line is shown in figure 2.4. This nonuniqueness of the value of contact angle when $U = 0$ whereby the static contact angle lies between α_A and α_R is often referred to as the *contact angle hysteresis* [8].

In general, contact angle depends on adsorption of water and impurities by the liquid and on a possible molecular re-orientation of the solid surface in the presence of water [6]. It also indirectly depends on temperature and the presence of surface active materials due to the fact that contact angle is a function of the surface tension. The roughness of the surface also has the effect of making the apparent contact angle different from the actual contact angle. Roughness increase the apparent contact angle if the actual contact angle α is greater than 90° and decrease the contact angle if the actual contact angle α is less than 90°.

2.4 Mechanics of surface tension: The Laplace-Young equation

In deriving the equation describing the surface tension phenomenon, Young considered the interface between two fluids as uniformly stretched membrane of zero thickness and defined the surface tension as a tractional force acting across any unit length of line on this fictitious membrane [14].

Let the surface of separation, of element surface area da, undergo a uniform infinitesimal displacement δh in the normal direction of every points on that surface as shown in Figure 2.5. The volume element between undisplaced and displaced surface is δh da. Let $p_{(1)}$ and $p_{(2)}$ be the pressure of fluid 1 and fluid 2, respectively, and δh has positive value if the displacement of the surface of separation is towards fluid 2. The work needed to make the above volume change is

$$\delta W_V = \int_{\partial\Omega} (-p_{(1)} + p_{(2)})\, \delta h \, \mathrm{d}a, \tag{2.4}$$

where $\partial\Omega$ is the area of the interface. The work related to the change in surface area is proportional to the change in surface area, δa

$$\delta W_S = \gamma \, \delta a, \tag{2.5}$$

where γ is the *surface tension coefficient.* Then, the total work done to displaced the surface of separation is

$$\begin{aligned} \delta W &= \delta W_V + \delta W_S, \\ &= -\int_{\partial\Omega} (p_{(1)} - p_{(2)})\, \delta h \, \mathrm{d}a + \gamma \, \delta a. \end{aligned} \tag{2.6}$$

Let R_1 and R_2 denote the principal radii of curvature of a point on the surface and take the positive value if they are drawn into fluid 1. Let $\mathrm{d}l_1$ and $\mathrm{d}l_2$ be the element length on the surface in its principal sections. As the surface undergoes infinitesimal displacements, δh, $\mathrm{d}l_1$ and $\mathrm{d}l_2$ receive increments $(\delta h/R_1)\ \mathrm{d}l_1$ and $(\delta h/R_2)\ \mathrm{d}l_2$, respectively. Hence the surface element, $\mathrm{d}a = \mathrm{d}l_1\mathrm{d}l_2$, after the displacements becomes

$$\begin{aligned} \left(1+\frac{\delta h}{R_1}\right)\left(1+\frac{\delta h}{R_2}\right)\mathrm{d}l_1\mathrm{d}l_2 &= \left(1+\frac{\delta h}{R_1}+\frac{\delta h}{R_2}+\frac{\delta h^2}{R_1R_2}\right)\mathrm{d}l_1\mathrm{d}l_2 \\ &\approx \left(1+\frac{\delta h}{R_1}+\frac{\delta h}{R_2}\right)\mathrm{d}l_1\mathrm{d}l_2. \end{aligned} \tag{2.7}$$

Thus, the surface element change by

$$\left(\frac{1}{R_1}+\frac{1}{R_2}\right)\delta h \, \mathrm{d}a.$$

The total change of area of the surface of separation is given by

$$\delta a = \int_{\partial\Omega} \left(\frac{1}{R_1}+\frac{1}{R_2}\right)\delta h \, \mathrm{d}a. \tag{2.8}$$

By substituting equation (2.8) into (2.6) and equating to zero to get the equilibrium condition, gives

$$\int_{\partial\Omega} \left\{(p_{(1)} - p_{(2)}) - \gamma\left(\frac{1}{R_1}+\frac{1}{R_2}\right)\right\}\delta h \, \mathrm{d}a = 0,$$

for every infinitesimal displacement δh. Hence

$$p_{(1)} - p_{(2)} = \gamma\left(\frac{1}{R_1}+\frac{1}{R_2}\right) = 2H\gamma, \tag{2.9}$$

where H is the mean curvature.

The Laplace-Young equation is valid only for the case in which the fluid-fluid system is in equilibrium or the viscous stress effects can be ignored.

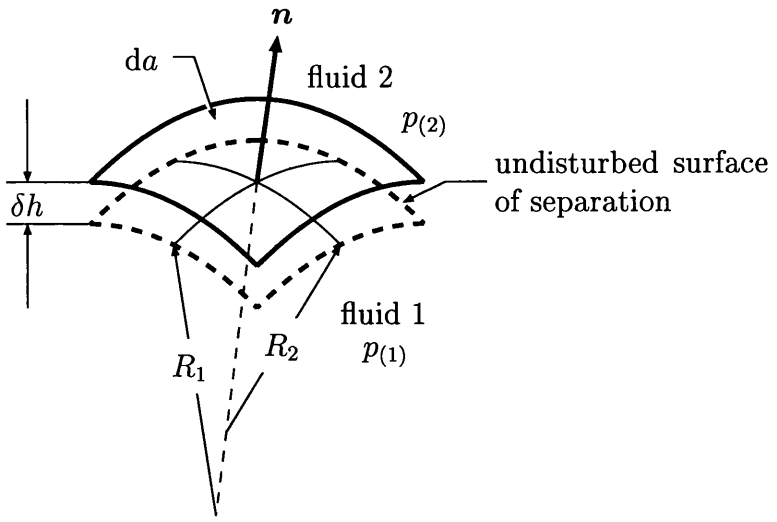

Figure 2.5: Elemental surface area in the interface between two immiscible fluids.

Therefore, tangential surface tension gradient caused by the distribution of temperature or surfactant concentration are not included into equation (2.9) [12].

If both fluids in motion are assumed to be viscous and the gradient of surface tension is taken into account, at the interface between the fluids the following boundary condition holds

$$\left(p_{(1)} - p_{(2)} - 2H\gamma\right)\boldsymbol{n} = \left(\boldsymbol{\sigma}_{(1)}^{visc} - \boldsymbol{\sigma}_{(2)}^{visc}\right)\cdot\boldsymbol{n} + \nabla\gamma \tag{2.10}$$

where $\boldsymbol{\sigma}_{(1)}^{visc}$ and $\boldsymbol{\sigma}_{(2)}^{visc}$ are the viscous stress for fluid 1 and fluid 2, respectively, and $\boldsymbol{n}$ is the unit outward normal directed toward fluid 2. The above equation is known as *Laplace-Young equation.*

Generally, the Laplace-Young equation serves as a constitutive relation that relates the mean curvature of the interface to the pressure jump in the bulk fluids. The use of single coefficient γ implies that the surface tension has no preferred direction. This is valid for most of liquid-vapor or liquid-liquid systems which either have a clean interface or hosting monolayer surfactant. However, grossly contaminated interfaces, polymerized interfaces, and biological interfaces consisting of lipids and protein exhibit more complex mechanical behavior [16]. Biological interfaces often display resistance to elastic bending or incompressible behavior that preserves the surface area.

2.5 Thermodynamics of surface tension: The Gibbs-Kelvin equation

In the phenomenological study of surface tension phenomena, the interface of two immiscible fluids can not be studied in isolation. Furthermore, the surface tension coefficient is related to the free energy of interfacial region and it is not directly measurable. In this case, thermodynamics provides a way to relate measurable variables to others that may or may not be measurable and help to identify measurable and non-measurable quantities.

The application of thermodynamic concepts to surface tension phenomena was introduced by Kelvin and explored thoroughly by Gibbs, in his treatise on heterogeneous equilibrium [9]. Later Gibbs theory on surface tension was generalized, among others, by Tolman [19], Buff [3], Buff and Saltsburg [4, 5], and Boruvka and Neumann [2] to take into account other phenomena related to surface tension, such as high curvature of the surface, contact lines, and contact angle hysteresis.

In order to obtain a simple treatment of the thermodynamic properties of a system consisting of two fluid phases which have substantially uniform distributions of matter throughout their interior but meet in a thin layer of physical inhomogeneity, Gibbs considered such a system as precisely separated into two parts by the construction of a mathematical surface of zero thickness. This surface lies within the layer of physical inhomogeneity, which passes through points in that layer which are similarly located with respect to the condition of neighboring matters. Such a surface was called by Gibbs a *dividing surface.* The main reason for introducing the dividing surface is due to the fact that there is no thermodynamic means to decide where one phase ends and where the other begins. Each phase is considered to have their bulk properties up to this surface and any excess quantities are supposed to be entirely located in this surface. Even though this is not in agreement with reality the introduction of Gibbs dividing surface will not give rise to inconsistencies [13], but there is a question on where the Gibbs dividing surface should be located. Figure 2.6 shows the possible locations of Gibbs dividing surface (GDS), assuming that the distribution of a quantity across the interface layer is as shown in figure 2.6(a). Figure 2.6(b) refers to condition where the GDS is located inside phase 2. In this case, there is an excess quantity (represented by area I) and a deficit (represented by area II) which more or less compensate each other. If the GDS is moved toward the interior of phase 2, the excess quantity become increasingly negative. On the other hand if the GDS is moved toward the interior of phase 1, the excess quantity become increasingly positive. Figure 2.6(c) shows the most realis-

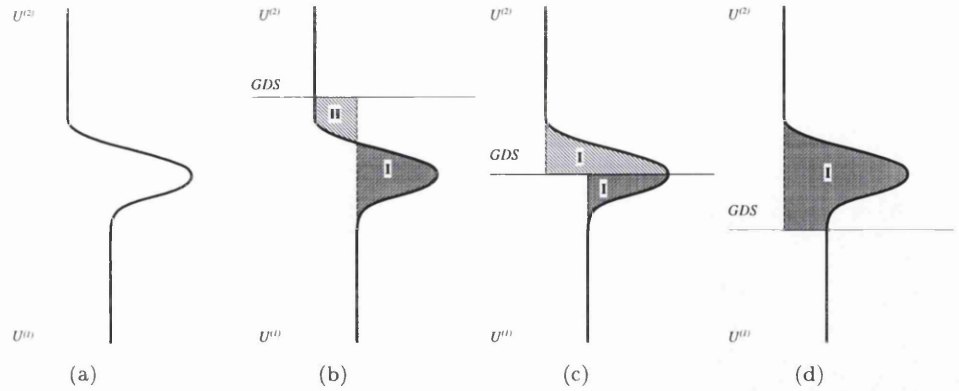

Figure 2.6: Possible distribution of a quantity in the interface between phase (1) and phase (2) and establishment of the interfacial excess quantity for the different location of the Gibbs dividing surface.

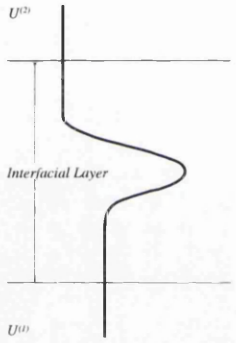

Figure 2.7: Guggenheim interfacial layer between phase (1) and phase (2).

tic condition. Both phases contribute positive excess quantity. But moving further the GDS toward the interior of phase 1 causes unrealistic magnitude of excess quantity [13].

Another approach to simplify thermodynamical treatment of two phases systems is attributed to Guggenheim [10] in which the two contiguous phases are separated by an interfacial layer of finite thickness. In this approach the surfaces separating the bulk phases and the interfacial layer are located sufficiently far outside the interfacial region and the value of excess quantities depends on the choice of the location of two surfaces and hence on the thickness of interfacial layer. However, Guggenheim's approach is less popular than the one by Gibbs.

Having made a particular choice for the dividing surface the whole volume V occupied by a two-phase system may then be regarded as a sum of two volumes, $V^{(\alpha)}$ and $V^{(\beta)}$, occupied by phases α and β, respectively, i.e.

$$V = V^{(\alpha)} + V^{(\beta)}. \tag{2.11}$$

Let E and S denote the total internal energy and total entropy of the system, respectively, and $m_1, m_2, \cdots, m_i$ denote the total amounts of i different independent components of which the system is regarded as being composed. Then these quantities can be expressed as a sum of their value for each phase and their excesses,

$$\begin{aligned}
E &= E^{(\alpha)} + E^{(\beta)} + E^{(s)} \\
S &= S^{(\alpha)} + S^{(\beta)} + S^{(s)} \\
m_1 &= m_1^{(\alpha)} + m_1^{(\beta)} + m_1^{(s)} \\
m_2 &= m_2^{(\alpha)} + m_2^{(\beta)} + m_2^{(s)} \\
&\cdots\cdots\cdots\cdots\cdots\cdots \\
m_i &= m_i^{(\alpha)} + m_i^{(\beta)} + m_i^{(s)}
\end{aligned} \tag{2.12}$$

The variation of the total energy of the system is then given by

$$\begin{aligned}
\delta E = \theta\delta S + \mu_1\delta m_1 + \mu_2\delta m_2 + \cdots + \mu_i\delta m_i - p^{(\alpha)}\delta V^{(\alpha)} - p^{(\beta)}\delta V^{(\beta)} + \\
+ \gamma\delta A + C_1\delta\kappa_1 + C_2\delta\kappa_2
\end{aligned} \tag{2.13}$$

where κ_1 and κ_2 are the curvatures. The temperature θ, chemical potentials $\mu_1, \mu_2, \cdots, \mu_i$, pressures $p^{(\alpha)}$ and $p^{(\beta)}$, surface tension coefficient γ and curvature coefficients C_1 and C_2 are coefficients having values determined by the initial equilibrium state of the system. To make it easier to analyze the effects of changes in curvature, the last two terms of equation (2.13) are substituted by

$$\frac{1}{2}(C_1 + C_2)\,\delta(\kappa_1 + \kappa_2) \quad \text{and} \quad \frac{1}{2}(C_1 - C_2)\,\delta(\kappa_1 - \kappa_2)$$

to give

$$\delta E = \theta\delta S + \mu_1\delta m_1 + \mu_2\delta m_2 + \cdots + \mu_i\delta m_i - p^{(\alpha)}\delta V^{(\alpha)} - p^{(\beta)}\delta V^{(\beta)} + \\ + \gamma\delta A + \frac{1}{2}(C_1 + C_2)\,\delta(\kappa_1 + \kappa_2) + \frac{1}{2}(C_1 - C_2)\,\delta(\kappa_1 - \kappa_2) \quad (2.14)$$

The last three terms in equation (2.14) give the variation in the internal energy of the system which would accompany a variation in the area and curvatures of dividing surface without absorption of heat, change in composition, or change in volumes containing the two phases. Further simplification of equation (2.14) can be obtained by a special choice for the location of the dividing surface. Gibbs [9] shows that it is possible to choose a particular location for the dividing surface such that the coefficient $1/2(C_1 + C_2)$ in the equation (2.14) is equal to zero. Gibbs called this particular dividing surface as the *surface of tension.*

Furthermore, for spherical and plane surface the coefficient $\delta(\kappa_1 - \kappa_2)$ is equal to zero because of the equality of κ_1 and κ_2 for these particular case. Hence, the last term in equation (2.14) can be dropped without whenever the curvature of the interphase region is small enough compared with its thickness. Since the conditions for thermodynamic equilibrium require the energy to be minimum for a given entropy, composition and total volume of the system as a whole and using equation (2.11), the equilibrium requires validity of the equation

$$\left(p^{(\alpha)} - p^{(\beta)}\right)\delta V^{(\alpha)} = \gamma\delta A \quad (2.15)$$

Relating variations in volume and surface, to the special case of a uniform displacement of the surface of tension everywhere normal to itself gives

$$p^{(\alpha)} - p^{(\beta)} = (\kappa_1 + \kappa_2)\gamma \quad (2.16)$$

For a spherical surface of radius r the previous equation leads to the familiar equation of Kelvin

$$p^{(\alpha)} - p^{(\beta)} = \frac{2\gamma}{r} \quad (2.17)$$

Gibbs treatment of interfacial region is based on assumption that all the properties of interfacial region are determined by the area and curvature of the dividing surface. The result of this treatment is general enough to have wide range of applicability. Tolman [19] considered that Gibbs treatment does not take into account the structure of the interfacial region and provides less physical insight into the underlying mechanism. Tolman improves

Gibbs treatment by giving a detailed treatment of the interfacial region. In their series of publications Buff and co-workers [3, 4, 5] three phases confluent zone and dependence on the external force were reviewed. Later the work received some criticism from Boruvka and Neumann [2]. They argued that the fundamental equation for dividing surfaces proposed by Buff and Saltzburg are insufficient without any contact angle or curvature terms being included. In their treatment, Boruvka and Neumann derived the fundamental equation not only for bulk phases and surface, but also for lines and points as the components of the fundamental equation of the whole system.

2.6 Closure

An introduction to the surface tension phenomena has been given in this chapter. The equation governing the pressure jump in the bulk fluids as a function of mean curvature of the interface is given from both mechanical and thermodynamical point of view.

The next chapter is devoted to an overview of the basics of continuum mechanics and thermodynamics for a three-dimensional body as well as for interfaces. The continuum theory of interface gives more general constitutive laws to interface to take into account complex mechanical behavior. Moreover, the three-dimensional continuum and the interface embedded in it follow the same basic principles of mechanics.

Bibliography

[1] N.K. Adam. *The Physics and Chemistry of Surfaces.* Oxford University Press, London, 3^{rd} edition, 1941.

[2] L. Boruvka and A. W. Neumann. Generalization of the classical theory of capillarity. *J. Chem. Physics.*, 66(12):5464 – 5476, 1977.

[3] F. P. Buff. Curved fluid interfaces. i. The generalized gibbs-kelvin equation. *J. Chem. Physics.*, 25(1):146 – 153, 1956.

[4] F. P. Buff and H. Saltsburg. Curved fluid interfaces. ii. The generalized neumann formula. *J. Chem. Physics.*, 26(1):23 – 31, 1957.

[5] F. P. Buff and H. Saltsburg. Curved fluid interfaces. iii. The dependence of the free energy on parameters of external force. *J. Chem. Physics.*, 26(6):1526 – 1533, 1957.

[6] J.T. Davies and E.K. Rideal. *Interfacial Phenomena.* Academic Press, New York, 1961.

[7] S.H. Davies. Contact-line problems in fluid mechanics. *J. Appl. Mech.*, 50:977 – 982, 1983.

[8] E.B. Dussan. On spreading of liquids on solid surface. static and dynamic contact lines. *Ann. Rev. Fluid. Mech.*, 11:371 – 400, 1979.

[9] J.W. Gibbs. *The Scientific Papers – Vol.1.* Dover, New York, 1961.

[10] E.A. Guggenheim. *Thermodynamics: An Advanced Treatment for Chemists and Physicists.* North-Holland, Amsterdam, 5^{th} edition, 1967.

[11] H. Lamb. *Hydrodynamics.* Cambridge University Press, Cambridge, 6^{th} edition, 1932.

[12] L.D. Landau and E.M. Lifshitz. *Fluid Mechanics.* Pergamon Press, New York, 2^{nd} edition, 1987.

[13] J. Lyklema. *Fundamentals of Interface and Colloid Science – Vol.1: Fundamentals.* Academic Press, London, 1991.

[14] S. Ono and S. Kondo. Molecular theory of surface tension in liquids. In S. Flügge, editor, *Handbuch der Physik: Vol. X*, Berlin, 1960. Springer-Verlag.

[15] C. Pozrikidis. *Introduction to Theoretical and Computational Fluid Dynamics.* Oxford University Press, New york, 1997.

[16] C. Pozrikidis. Interfacial dynamics for stokes flow. *J. Comp. Physics*, 169:250–301, 2001.

[17] R.F. Probstein. *Physicochemical Hydrodynamics: An Introduction.* John Wiley & Sons, New York, 2^{nd} edition, 1994.

[18] J.C. Slattery. *Interfacial Transport Phenomena.* Springer-Verlag, New York, 1990.

[19] R.C. Tolman. Consideration of the gibbs theory of surface tension. *J. Chem. Physics.*, 16(8):758 – 774, 1948.

[20] T. Young. An essay on the cohesion of fluids. *Philos. Trans. Royal Soc. London*, 24:65 – 87, 1805.

Chapter 3

Elements of Continuum Mechanics and Thermodynamics

This chapter is arranged into two parts. The first one reviews some basic concepts of mechanics and thermodynamics of three-dimensional continua. The material presented here is well established in continuum mechanics literature [7, 14, 15, 20]. The second part addresses more specifically the general continuum framework for interfacial phenomena paralleling the one presented in the first part.

The continuum thermodynamics theory is intended to predict the fields of mass density, motion, and temperature in a body as well as to provide a means to restrict constitutive equations which appear in the theory. In addition it also reveals symmetry due to interaction of different variables. The constitutive relations for three-dimensional continuum considered in this chapter are the ones proposed by Coleman and Noll [2] in which linear viscous fluids are a special class.

In the beginning discussion of the interface behavior was mainly done from the molecular point of view. A cogently argument on the validity and the utility of the continuum viewpoint brought by Herring [12] has triggered development of the continuum approach to interface problem. Initiated by the work of Scriven [18] on the dynamics of fluid interface it continues with the set up of thermodynamic axioms for interface embedded in three dimensional continuum by Fisher and Leitman [4, 5]. In their works, Fisher and Leitman consider only non-deformable interface with the constitutive relations limited to rigid surface conductor. Later, Moeckel [16] extends the considerations into a deformable interface with inviscid fluid interface constitutive relations and take into consideration two different classes of inter-

face; material interface and propagating interface. Another important work on continuum interface is of Gurtin and Murdoch [10] where the authors provide a mathematical framework on the study of mechanical behaviour of material interface with attention focused on elastic interface. The continuum thermodynamic treatment of this class of interface is carried out by Murdoch [17]. In their study on stability analysis of fluid motion when an interface is present between two fluids, Lindsay and Straughan [13] rely on the thermodynamic arguments of linear viscous interface fluid introduced by Scriven [18]. Recently, a series of works by Gurtin and co-workers [8, 1, 11, 3, 9] deal with the mathematical framework of propagating interface in order to model interfacial problems where material diffusion at phase changes play an important role.

The introduction of the continuum theory to the interfacial problem generalizes the constitutive relations for an interface embedded in a three dimensional continuum. This provides a foundation for modelling more complex interface behavior that occurs in nature and consider Laplace-Young equation as a special case.

In general the phase interface has no natural material structure; but by assuming that the thickness of the interfacial region is small and if the diffusion into the interfacial zone is not significant, it is possible to model the interface as a material surface in thermomechanical interaction with its environment [17]. Considering the nature of problems addressed in this thesis all the interfaces will be modelled as material surfaces.

To maintain consistency in the notation used throughout this chapter, *direct notation* for surfaces introduced by Gurtin and Murdoch [10] is employed.

3.1 Mechanics and Thermodynamics of Continua

3.1.1 Kinematics of deformation

Let $\mathscr{E}$ denotes a three-dimensional euclidean space with the corresponding translation vector space $\mathscr{V}$. A body, $\mathscr{B}$ is a set of points with a structure defined by a family $\mathscr{C}$ of configurations such that

$$\text{each } \kappa \in \mathscr{C} \text{ is an injection of } \mathscr{B} \text{ into } \mathscr{E}.$$

If a region $\kappa_0(\mathscr{B}) = \Omega_0 \subset \mathscr{E}$, with a regular boundary $\partial\Omega_0$ is considered as a *reference configuration*, a *deformation* of $\mathscr{B}$ is defined by a smooth

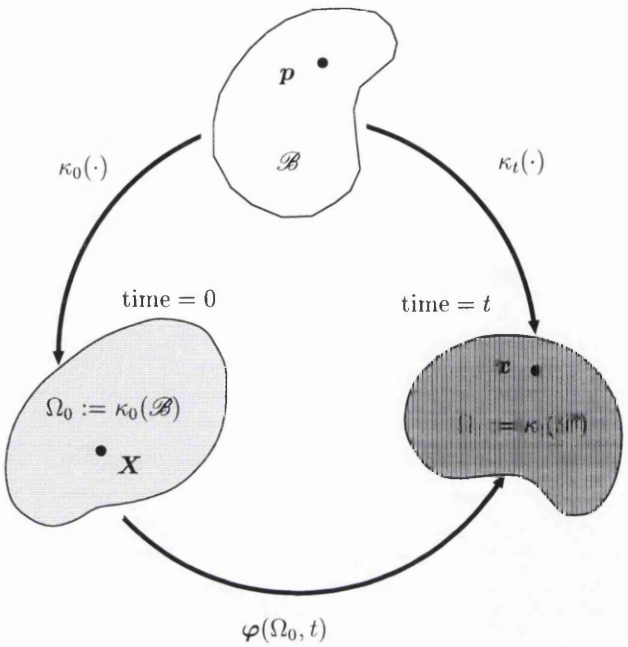

Figure 3.1: Configuration and deformation of a material body at time 0 and t.

invertible function $\boldsymbol{\varphi} : \Omega_0 \to \mathscr{E}$ that map every material point $\boldsymbol{p} \in \mathscr{B}$ from its reference position $\boldsymbol{X} \in \Omega_0$ to a current position

$$\boldsymbol{x} = \boldsymbol{\varphi}(\boldsymbol{X}). \tag{3.1}$$

The *displacement* of $\boldsymbol{p}$, denoted by $\boldsymbol{u}(\boldsymbol{X})$, is defined by

$$\boldsymbol{u}(\boldsymbol{X}) := \boldsymbol{\varphi}(\boldsymbol{X}) - \boldsymbol{X}, \tag{3.2}$$

where $\boldsymbol{u}(\boldsymbol{X}) \in \mathscr{V}$. Equation (3.2) can be rearranged as

$$\boldsymbol{x} = \boldsymbol{X} + \boldsymbol{u}(\boldsymbol{X}). \tag{3.3}$$

A *motion* of $\mathscr{B}$ is a smooth one-parameter family of deformations, $\boldsymbol{\varphi}(\cdot, t)$, with the time, $t \in \mathscr{I}$, as the parameter. Mathematically, it is defined as

$$\boldsymbol{\varphi} : \Omega_0 \times \mathscr{I} \to \mathscr{E}, \tag{3.4}$$

where $\mathscr{I} \subset \mathscr{R}$ is the time interval. The place occupied by the material point $\boldsymbol{p}$ at time t is given by

$$\boldsymbol{x} = \boldsymbol{\varphi}(\boldsymbol{X}, t) = \boldsymbol{\varphi}(\kappa_0(\boldsymbol{p}), t) \tag{3.5}$$

and the region of $\mathscr{E}$ occupied by the body $\mathscr{B}$ at time t is given by

$$\Omega_t = \varphi(\Omega_0, t) = \varphi(\kappa_0(\mathscr{B}), t) \tag{3.6}$$

Trajectory of body $\mathscr{B}$ is defined as

$$\mathcal{T} = \{(\boldsymbol{x}, t) : \boldsymbol{x} \in \Omega_t, t \in \mathscr{I}\} \tag{3.7}$$

Let Φ be a general time dependent field (either scalar, vector or tensor) defined over the body $\mathscr{B}$. Φ is said to be *material field* if its domain is $\Omega_0 \times \mathscr{I}$. On the other hand, if its domain is $\mathcal{T}$ then Φ is said to be a *spatial field.* The *spatial description* Φ_s of a material field $\Phi(\boldsymbol{X}, t)$ is defined by

$$\Phi_s(\boldsymbol{x}, t) = \Phi(\varphi^{-1}(\boldsymbol{x}, t), t) \tag{3.8}$$

and the *material description* Φ_m of a spatial field $\Phi(\boldsymbol{x}, t)$ is defined by

$$\Phi_m(\boldsymbol{X}, t) = \Phi(\varphi(\boldsymbol{X}, t), t) \tag{3.9}$$

From now on, the subscripts s and m denoted the material and spatial descriptions of general fields will be dropped to avoid notational complexity. In general, the description employed will be evident either from the context or from the argument used ($\boldsymbol{X}$ or $\boldsymbol{x}$).

Material time derivative of a field Φ, denoted by $\dot{\Phi}$, is obtained by taking the derivative of Φ with respect to time t holding $\boldsymbol{X}$ fixed,

$$\dot{\Phi} = \frac{\partial}{\partial t}\Phi(\boldsymbol{X}, t). \tag{3.10}$$

Material gradient of a field Φ, denoted by $\nabla_{\boldsymbol{X}}\Phi$ is defined by

$$\nabla_{\boldsymbol{X}}\Phi = \frac{\partial}{\partial \boldsymbol{X}}\Phi(\boldsymbol{X}, t). \tag{3.11}$$

Similarly, *spatial time derivative* Φ' and *spatial gradient* $\nabla_{\boldsymbol{x}}$ of a field Φ are defined, respectively, by

$$\Phi' = \frac{\partial}{\partial t}\Phi(\boldsymbol{x}, t) \tag{3.12}$$

$$\nabla_{\boldsymbol{x}}\Phi = \frac{\partial}{\partial \boldsymbol{x}}\Phi(\boldsymbol{x}, t) \tag{3.13}$$

The *material velocity vector* $\boldsymbol{V}$ and the *material acceleration vector* $\boldsymbol{A}$ are defined as

$$\boldsymbol{V}(\boldsymbol{X},t) = \frac{\partial \boldsymbol{\varphi}(\boldsymbol{X},t)}{\partial t} \tag{3.14}$$

$$\boldsymbol{A}(\boldsymbol{X},t) = \frac{\partial \boldsymbol{V}(\boldsymbol{X},t)}{\partial t} = \frac{\partial^2 \boldsymbol{\varphi}(\boldsymbol{X},t)}{\partial t^2}. \tag{3.15}$$

By using equation (3.8) the *spatial velocity vector* and the *spatial acceleration vector* can be obtained as follows

$$\boldsymbol{V}(\boldsymbol{X},t) = \boldsymbol{V}(\boldsymbol{\varphi}^{-1}(\boldsymbol{x},t),t) = \boldsymbol{v}(\boldsymbol{x},t) \tag{3.16}$$

$$\boldsymbol{A}(\boldsymbol{X},t) = \boldsymbol{A}(\boldsymbol{\varphi}^{-1}(\boldsymbol{x},t),t) = \boldsymbol{a}(\boldsymbol{x},t). \tag{3.17}$$

3.1.2 The deformation gradient. Polar decomposition

The *deformation gradient* of the motion $\boldsymbol{\varphi}$ is a second order tensor defined by

$$\boldsymbol{F}(\boldsymbol{X},t) = \nabla_{\boldsymbol{X}} \boldsymbol{\varphi}(\boldsymbol{X},t). \tag{3.18}$$

Since $J \equiv \det[\boldsymbol{F}] > 0$ then $\boldsymbol{F} \in \mathrm{Lin}^+$. $\boldsymbol{F}$ is a *two point* tensor which relate the reference configuration with the current configuration.

Polar decomposition theorem [20, 7] allows the deformation gradient $\boldsymbol{F}$ to be decomposed uniquely into

$$\boldsymbol{F} = \boldsymbol{R}\boldsymbol{U} = \boldsymbol{V}\boldsymbol{R}, \tag{3.19}$$

where $\boldsymbol{R} \in \mathrm{Orth}^+$ is a proper orthogonal tensor, known as the rotation tensor, which measures the local rigid rotation of points near $\boldsymbol{p}$. $\boldsymbol{U}$ and $\boldsymbol{V}$ are, respectively, the right and left stretch tensor which measure local stretching from $\boldsymbol{p}$. In terms of $\boldsymbol{F}$, $\boldsymbol{U}$ and $\boldsymbol{V}$ can be expressed as

$$\boldsymbol{U}^2 = \boldsymbol{C} = \boldsymbol{F}^T\boldsymbol{F}, \qquad \boldsymbol{V}^2 = \boldsymbol{B} = \boldsymbol{F}\boldsymbol{F}^T. \tag{3.20}$$

Since $\boldsymbol{U}$ and $\boldsymbol{V}$ are symmetric and positive definite, they may be represented by their eigen values $\lambda_{(i)}$, $i = 1,2,3$, known as the *principal stretches*, and their corresponding eigen vectors which form mutually orthogonal basis known as the *principal directions*.

$$\boldsymbol{U} = \sum_{i=1}^{3} \lambda_{(i)} \boldsymbol{N}_{(i)} \otimes \boldsymbol{N}_{(i)}, \qquad \boldsymbol{V} = \sum_{i=1}^{3} \lambda_{(i)} \boldsymbol{n}_{(i)} \otimes \boldsymbol{n}_{(i)} \tag{3.21}$$

Here, $\boldsymbol{N}_{(i)}$ and $\boldsymbol{n}_{(i)}$, $i = 1,2,3$ are the principal directions for $\boldsymbol{U}$ and $\boldsymbol{V}$, repectively. Note also that the values of $\lambda_{(i)}$ are the same for $\boldsymbol{U}$ and $\boldsymbol{V}$.

3.1.3 Velocity gradient. Rate of deformation tensor

The spatial field known as the *velocity gradient* is defined by

$$\boldsymbol{L} := \nabla_{\boldsymbol{x}} \boldsymbol{v} = \dot{\boldsymbol{F}}\, \boldsymbol{F}^{-1}. \tag{3.22}$$

This spatial tensor field can be decomposed into a symmetric $\boldsymbol{D}$ and a skew $\boldsymbol{W}$ parts such that

$$\boldsymbol{L} = \boldsymbol{D} + \boldsymbol{W}, \tag{3.23}$$

where $\boldsymbol{D} = \frac{1}{2}[\boldsymbol{L} + \boldsymbol{L}^T]$ and $\boldsymbol{W} = \frac{1}{2}[\boldsymbol{L} - \boldsymbol{L}^T]$ measure the rate of stretching and the rate of rotation, respectively.

3.1.4 Isochoric motion

Given a part $\mathscr{P} \subset \mathscr{B}$, the region of space occupied by $\mathscr{P}$ at the time t is written as

$$\Pi_t = \boldsymbol{\varphi}(\Pi_0, t) = \boldsymbol{\varphi}(\boldsymbol{\kappa}_0(\mathscr{P}), t)$$

and its volume is given by

$$\mathrm{vol}(\Pi_t) = \int_{\Pi_t} \mathrm{d}v = \int_{\Pi_0} \det[\boldsymbol{F}]\, \mathrm{d}V$$

Thus, the rate of change of the volume of Π_t can be expressed as

$$\begin{aligned} \frac{\mathrm{d}}{\mathrm{d}t}\mathrm{vol}(\Pi_t) &= \int_{\Pi_0} \frac{\partial}{\partial t}\det[\boldsymbol{F}]\, \mathrm{d}V \\ &= \int_{\Pi_t} \mathrm{div}[\boldsymbol{v}]\, \mathrm{d}v \end{aligned} \tag{3.24}$$

A motion $\boldsymbol{\varphi}$ is called *isochoric* if for every part $\mathscr{P}$ of $\mathscr{B}$ and time t

$$\frac{\mathrm{d}}{\mathrm{d}t}\mathrm{vol}(\Pi_t) = 0 \tag{3.25}$$

which implies that

$$\frac{\partial}{\partial t}\det[\boldsymbol{F}] = 0 \quad \text{or} \quad \mathrm{div}[\boldsymbol{v}] = 0$$

For a motion to be isochoric the volume of each part must be constant throughout the motion.

3.1.5 Stress measures

Let $\varphi(\mathcal{S}_0, t)$ be an oriented surface in $\varphi(\Omega_0, t)$ with positive normal $\boldsymbol{n}(\boldsymbol{x}, t)$ at $\boldsymbol{x} \in \varphi(\Omega_0, t)$. Then the force per unit area exerted across $\varphi(\mathcal{S}_0, t)$ at $\boldsymbol{x}$ depends on $\varphi(\mathcal{S}_0, t)$ only through its normal $\boldsymbol{n}(\boldsymbol{x}, t)$ at $\boldsymbol{x}$. Moreover, this depedency on $\boldsymbol{n}(\boldsymbol{x}, t)$ is linear. This implies the existence of a second order tensor field $\boldsymbol{\sigma}(\boldsymbol{x}, t) \in$ Sym called the *Cauchy stress* such that the vector $\boldsymbol{t}(\boldsymbol{x}, \boldsymbol{n}, t)$ representing the force per unit area acting across any surface $\varphi(\mathcal{S}_0, t)$ with normal $\boldsymbol{n}(\boldsymbol{x}, t)$ at $\boldsymbol{x}$ is given by

$$\boldsymbol{t}(\boldsymbol{x}, \boldsymbol{n}, t) = \boldsymbol{\sigma}(\boldsymbol{x}, t)\boldsymbol{n}(\boldsymbol{x}, t). \tag{3.26}$$

In many situations the deformed configuration $\varphi(\Omega_0, t)$ is not known in advance. It is then necessary to introduce stress tensor which gives the force measured per unit area in the reference configuration. This stress tensor is called the *first Piola-Kirchhoff stress tensor* and defined by

$$\boldsymbol{P} := J\,\boldsymbol{\sigma}\boldsymbol{F}^{T}. \tag{3.27}$$

Here $\boldsymbol{P}$ is a function of $(\boldsymbol{X}, t)$ and $\boldsymbol{\sigma}$ is evaluated at $(\boldsymbol{X}, t)$ using the relation $\boldsymbol{X} = \varphi^{-1}(\boldsymbol{x}, t)$.

3.1.6 Conservation of mass

If the mass of the body is conserved throughout the motion, then the following equality must hold

$$\int_{\Omega_t} (\dot{\rho} + \rho \operatorname{div}[\boldsymbol{v}])\, \mathrm{d}v = 0. \tag{3.28}$$

The local form of mass conservation obtained from the localization theorem is then

$$\dot{\rho} + \rho \operatorname{div}[\dot{\boldsymbol{u}}] = 0. \tag{3.29}$$

3.1.7 Momentum balance laws

Let $\boldsymbol{t}(\boldsymbol{x}, t, \boldsymbol{n})$ be the surface force acting on an oriented surface $\mathcal{S}_t$ in Ω_t with positive unit normal $\boldsymbol{n}(\boldsymbol{x}, t)$ at $\boldsymbol{x}$ and let $\boldsymbol{b}$ be the body force acting on Ω_t. The momentum balance laws assert that for every configuration Ω_t and time t

$$\int_{\partial\Omega_t} \boldsymbol{t}(\boldsymbol{n})\,\mathrm{d}a + \int_{\Omega_t} \boldsymbol{b}\,\mathrm{d}v = \int_{\Omega_t} \rho\dot{\boldsymbol{v}}\,\mathrm{d}v \tag{3.30}$$

$$\int_{\partial\Omega_t} \boldsymbol{r}\times\boldsymbol{t}(\boldsymbol{n})\,\mathrm{d}a + \int_{\Omega_t} \boldsymbol{r}\times\boldsymbol{b}\,\mathrm{d}v = \int_{\Omega_t} \rho\boldsymbol{r}\times\dot{\boldsymbol{v}}\,\mathrm{d}v \tag{3.31}$$

where $\boldsymbol{r}$ is the position vector

$$\boldsymbol{r}(\boldsymbol{x}) = \boldsymbol{x} - \boldsymbol{o}$$

and $\boldsymbol{o}$ is the origin.

The necessary and sufficient condition for the momentum balance to be satisfied is that there exist a spatial tensor field, $\boldsymbol{\sigma}$, called the Cauchy stress tensor such that

1. For each unit vector $\boldsymbol{n}$
$$\boldsymbol{t}(\boldsymbol{n}) = \boldsymbol{\sigma}\boldsymbol{n},$$
2. $\boldsymbol{\sigma}$ is symmetric,
3. $\boldsymbol{\sigma}$ satisfies the equation of motion
$$\mathrm{div}[\boldsymbol{\sigma}] + \boldsymbol{b} = \rho\dot{\boldsymbol{v}}.$$

3.1.8 Continuum thermodynamics

It is necessary to introduce some additional scalar and vector fields defined over Ω_t in order to state the fundamental laws of thermodynamics. The scalar fields $\theta(\boldsymbol{x},t)$, $e(\boldsymbol{x},t)$, $s(\boldsymbol{x},t)$, and $r(\boldsymbol{x},t)$ represent, respectively, the temperature, specific internal energy, specific entropy, and the density of heat production, while vector fields $\boldsymbol{b}(\boldsymbol{x},t)$ and $\boldsymbol{q}(\boldsymbol{x},t)$ stand for, respectively, body force and heat flux.

The first principle

The first principle of thermodynamics constitutes the third conservation law, i.e. the conservation of energy. This principle states that *the time rate of change of kinetic energy and internal energy in a body is equal to the rate of work done on the body plus the changes in all other forms of energy such as heat, magnetic, electrical, and chemical energy per unit time* [21]. Considering only heat energy involved, in its global form the first principle of thermodynamics can be expressed mathematically as

$$\frac{\mathrm{D}}{\mathrm{D}t}\int_{\Omega_t}\frac{1}{2}\rho\boldsymbol{v}\cdot\boldsymbol{v}\,\mathrm{d}v+\frac{\mathrm{D}}{\mathrm{D}t}\int_{\Omega_t}\rho e\,\mathrm{d}v=\int_{\partial\Omega_t}\boldsymbol{t}\cdot\boldsymbol{v}\,\mathrm{d}a+\int_{\Omega_t}\rho\boldsymbol{b}\cdot\boldsymbol{v}\,\mathrm{d}v - \int_{\partial\Omega_t}\boldsymbol{q}\cdot\boldsymbol{n}\,\mathrm{d}a+\int_{\Omega_t}\rho r\,\mathrm{d}v, \quad (3.32)$$

with its corresponding local form

$$\rho\dot{e}=\boldsymbol{\sigma}:\nabla\boldsymbol{v}-\mathrm{div}[\boldsymbol{q}]+\rho r. \quad (3.33)$$

Using the fact that inner product of a symmetric tensor and an unsymmetric tensor is zero the energy conservation equation can be written as

$$\rho\dot{e}=\boldsymbol{\sigma}:\boldsymbol{D}-\mathrm{div}[\boldsymbol{q}]+\rho r. \quad (3.34)$$

The second principle. Clausius-Duhem inequality

The second principle of thermodynamics postulates that *for every process admissible in a body consisting of a given material and for every part* $\mathscr{P}\in\mathscr{B}$ *of this body the entropy production is non-negative* [2]. Let $\boldsymbol{q}/\theta$ is regarded to be a vectorial *flux of entropy* and r/θ to be a scalar *supply of entropy.* Then the entropy production in its spatial form is given by

$$\frac{\mathrm{D}}{\mathrm{D}t}\int_{\Omega_t}\rho s\,\mathrm{d}v-\int_{\Omega_t}\rho\frac{r}{\theta}\,\mathrm{d}v+\int_{\partial\Omega_t}\frac{\boldsymbol{q}}{\theta}\cdot\boldsymbol{n}\,\mathrm{d}a\geq 0 \quad (3.35)$$

Under suitable smoothness assumptions the second principle can be written in its local form as follows

$$\rho\dot{s}-\rho\frac{r}{\theta}+\mathrm{div}\left[\frac{\boldsymbol{q}}{\theta}\right]\geq 0 \quad (3.36)$$

By combining the first and the second principles of thermodynamics, the fundamental inequality can be obtained

$$\rho\dot{s}-\frac{1}{\theta}(\rho\dot{e}-\boldsymbol{\sigma}:\boldsymbol{D}+\mathrm{div}[\boldsymbol{q}])+\mathrm{div}\left[\frac{\boldsymbol{q}}{\theta}\right]\geq 0. \quad (3.37)$$

Using the identity

$$\mathrm{div}\left[\frac{\boldsymbol{q}}{\theta}\right]=\frac{1}{\theta}\mathrm{div}[\boldsymbol{q}]-\frac{1}{\theta^2}\,\boldsymbol{q}\cdot\nabla\theta.$$

and introducing the *Helmholtz free energy function per unit mass* defined as

$$\psi=e-\theta s \quad (3.38)$$

the fundamental inequality (3.37) results in the *Clausius-Duhem inequality*

$$\boldsymbol{\sigma} : \boldsymbol{D} - \rho(\dot{\psi} + s\dot{\theta}) - \frac{1}{\theta}\, \boldsymbol{q} \cdot \boldsymbol{g} \geq 0 \tag{3.39}$$

where $\boldsymbol{g} := \nabla\theta$.

3.1.9 Constitutive axioms

The kinematics, stresses and conservation laws apply to any continuum body for all times. In order to be able to distinguish one material from another additional equations must be introduced in the form of constitutive laws. Let $\Theta(\boldsymbol{X}, t)$, $E(\boldsymbol{X}, t)$, $S(\boldsymbol{X}, t)$, $r_0(\boldsymbol{X}, t)$, $\boldsymbol{b}_0(\boldsymbol{X}, t)$ and $\boldsymbol{q}_0(\boldsymbol{X}, t)$ denote material fields defined over $\Omega_0 \times \mathscr{I}$ which are the material counterparts of $\theta(\boldsymbol{x}, t)$, $e(\boldsymbol{x}, t)$, $s(\boldsymbol{x}, t)$, $r(\boldsymbol{x}, t)$, $\boldsymbol{b}(\boldsymbol{x}, t)$ and $\boldsymbol{q}(\boldsymbol{x}, t)$, repectively. A *thermokinetic* process of $\mathscr{B}$ is a pair of fields

$$\boldsymbol{\varphi}(\boldsymbol{X}, t), \qquad \Theta(\boldsymbol{X}, t). \tag{3.40}$$

A *calorodynamic* process is defined by the set

$$\{\boldsymbol{P}(\boldsymbol{X}, t),\, E(\boldsymbol{X}, t),\, S(\boldsymbol{X}, t),\, r_0(\boldsymbol{X}, t),\, \boldsymbol{b}_0(\boldsymbol{X}, t),\, \boldsymbol{q}_0(\boldsymbol{X}, t)\} \tag{3.41}$$

Thermodynamic determinism

The principle of thermodynamically compatible determinism [21] postulates that *the thermokinetic process to which a neighborhood of a point $\boldsymbol{p} \in \mathscr{B}$ has been subjected determines a calorodynamic process for $\mathscr{B}$ at $\boldsymbol{p}$.* A body $\mathscr{B}$ is said to be a *viscous body with heat conduction* if its calorodynamic process is related to thermokinetical process by the constitutive relations of the forms

$$\begin{aligned} \boldsymbol{P} &= \widehat{\boldsymbol{P}}(\boldsymbol{F}, \Theta, \boldsymbol{G}, \dot{\boldsymbol{F}}), \\ E &= \widehat{E}(\boldsymbol{F}, \Theta, \boldsymbol{G}, \dot{\boldsymbol{F}}), \\ S &= \widehat{S}(\boldsymbol{F}, \Theta, \boldsymbol{G}, \dot{\boldsymbol{F}}), \\ \boldsymbol{q}_0 &= \widehat{\boldsymbol{q}}_0(\boldsymbol{F}, \Theta, \boldsymbol{G}, \dot{\boldsymbol{F}}). \end{aligned} \tag{3.42}$$

Using the relations $\theta(\boldsymbol{x}, t) = \Theta(\boldsymbol{X}, t)$, $e(\boldsymbol{x}, t) = E(\boldsymbol{X}, t)$, $s(\boldsymbol{x}, t) = S(\boldsymbol{X}, t)$, $r(\boldsymbol{x}, t) = r_0(\boldsymbol{X}, t)$, $\boldsymbol{b}(\boldsymbol{x}, t) = \boldsymbol{b}_0(\boldsymbol{X}, t)$, $\boldsymbol{q}(\boldsymbol{x}, t) = 1/J\, \boldsymbol{F}\, \boldsymbol{q}_0(\boldsymbol{X}, t)$, $\boldsymbol{\sigma}(\boldsymbol{x}, t) = 1/J\, \boldsymbol{P}(\boldsymbol{X}, t)\boldsymbol{F}^T$ and equation (3.38) the constitutive relations (3.42) can be written as

$$\begin{aligned} \boldsymbol{\sigma} &= \widehat{\boldsymbol{\sigma}}(\boldsymbol{F},\theta,\boldsymbol{g},\dot{\boldsymbol{F}}), \\ \psi &= \widehat{\psi}(\boldsymbol{F},\theta,\boldsymbol{g},\dot{\boldsymbol{F}}), \\ s &= \widehat{s}(\boldsymbol{F},\theta,\boldsymbol{g},\dot{\boldsymbol{F}}), \\ \boldsymbol{q} &= \widehat{\boldsymbol{q}}(\boldsymbol{F},\theta,\boldsymbol{g},\dot{\boldsymbol{F}}). \end{aligned} \tag{3.43}$$

The equilibrium and the dynamic responses

The response functions in (3.43) can be split into the so-called *equilibrium* and *dynamic* responses. The equilibrium response is defined for processes in which $\boldsymbol{F}$ and θ constant. In particular the equilibrium stress response functions $\widehat{\boldsymbol{\sigma}}^{eq}$ are defined by [24]

$$\widehat{\boldsymbol{\sigma}}^{eq}(\boldsymbol{F},\theta) = \widehat{\boldsymbol{\sigma}}(\boldsymbol{F},\theta,\boldsymbol{0},\boldsymbol{0}), \tag{3.44}$$

and the dynamic stress response function $\widehat{\boldsymbol{\sigma}}^{dyn}$ is defined by

$$\widehat{\boldsymbol{\sigma}}^{dyn}(\boldsymbol{F},\theta,\boldsymbol{g},\boldsymbol{L}) = \widehat{\boldsymbol{\sigma}}(\boldsymbol{F},\theta,\boldsymbol{g},\boldsymbol{L}) - \widehat{\boldsymbol{\sigma}}^{eq}(\boldsymbol{F},\theta). \tag{3.45}$$

To within errors of order $O(|\boldsymbol{L}| + |\boldsymbol{g}|)$ the dynamic response function at $(\boldsymbol{F},\theta)$ have the forms [24]

$$\begin{aligned} \widehat{\boldsymbol{\sigma}}^{dyn}(\boldsymbol{F},\theta,\boldsymbol{g},\boldsymbol{L}) &= \widehat{\boldsymbol{V}}(\boldsymbol{F},\theta)[\boldsymbol{L}] + \widehat{\boldsymbol{D}}(\boldsymbol{F},\theta)[\boldsymbol{g}], \\ \widehat{\boldsymbol{q}}(\boldsymbol{F},\theta,\boldsymbol{g},\boldsymbol{L}) &= -\widehat{\boldsymbol{K}}(\boldsymbol{F},\theta)[\boldsymbol{g}] - \widehat{\boldsymbol{E}}(\boldsymbol{F},\theta)[\boldsymbol{L}], \end{aligned} \tag{3.46}$$

where the values of $\widehat{\boldsymbol{V}}, \widehat{\boldsymbol{D}}, \widehat{\boldsymbol{K}}$, and $\widehat{\boldsymbol{E}}$ at $(\boldsymbol{F},\theta)$ are

$$\widehat{\boldsymbol{V}} = \partial_{\boldsymbol{L}}\widehat{\boldsymbol{\sigma}}^{dyn}, \quad \widehat{\boldsymbol{D}} = \partial_{\boldsymbol{g}}\widehat{\boldsymbol{\sigma}}^{dyn}, \quad \widehat{\boldsymbol{E}} = -\partial_{\boldsymbol{L}}\widehat{\boldsymbol{q}}, \quad \widehat{\boldsymbol{K}} = -\partial_{\boldsymbol{g}}\widehat{\boldsymbol{q}}. \tag{3.47}$$

A viscous material with heat conduction is said to be linear if $\boldsymbol{\sigma}^{dyn}$ and $\boldsymbol{q}$ depend linearly on $\boldsymbol{L}$ and $\boldsymbol{g}$.

Consequences of the Clausius-Duhem inequality

The dissipation principle requires that constitutive function must be such that the Clausius-Duhem inequality holds in every smooth admissible process. The necessary and sufficient conditions that a viscous body with heat conduction satisfies the dissipation principle are that

i.) the constitutive functions $\widehat{\psi}$, and $\widehat{s}$ are independent of the nonequilibrium variables $\boldsymbol{g}$ and $\boldsymbol{L}$, i.e.

$$\widehat{\psi}(\boldsymbol{F},\theta,\boldsymbol{g},\boldsymbol{L}) \;=\; \widehat{\psi}(\boldsymbol{F},\theta). \tag{3.48}$$

ii.) the equilibrium thermostatic relations

$$\widehat{\boldsymbol{\sigma}}^{eq}(\boldsymbol{F},\theta) = \rho\partial_{\boldsymbol{F}}\widehat{\psi}(\boldsymbol{F},\theta), \quad \widehat{s}(\boldsymbol{F},\theta) = -\partial_{\theta}\widehat{\psi}(\boldsymbol{F},\theta), \tag{3.49}$$

hold for each $(\boldsymbol{F},\theta) \in \text{Invlin} \times \mathscr{R}^{+}$.

iii.) the internal dissipation inequality

$$\widehat{\boldsymbol{\sigma}}^{dyn}(\boldsymbol{F},\theta,\boldsymbol{g},\boldsymbol{L}) : \boldsymbol{L} - \widehat{\boldsymbol{q}}(\boldsymbol{F},\theta,\boldsymbol{g},\boldsymbol{L}) \cdot \frac{\boldsymbol{g}}{\theta} \geq 0, \tag{3.50}$$

holds for each $(\boldsymbol{F},\theta,\boldsymbol{g},\boldsymbol{L}) \in \text{Invlin} \times \mathscr{R}^{+} \times \text{Vect} \times \text{Lin}$.

Following the work of Coleman and Noll [2], only a class of material which the authors called *elastic material with heat conduction and viscosity* will be considered. For this material the authors assumed that $\widehat{\boldsymbol{\sigma}}^{dyn}$ is independent of $\boldsymbol{g}$ and $\widehat{\boldsymbol{q}}$ independent of $\boldsymbol{L}$. The constitutive equations for this material have the forms

$$\begin{aligned} \boldsymbol{\sigma} &= \widehat{\boldsymbol{\sigma}}^{eq}(\boldsymbol{F},\theta) + \widehat{\boldsymbol{V}}(\boldsymbol{F},\theta)[\boldsymbol{L}], \\ \psi &= \widehat{\psi}(\boldsymbol{F},\theta), \\ s &= \widehat{s}(\boldsymbol{F},\theta), \\ \boldsymbol{q} &= \widehat{\boldsymbol{q}}(\boldsymbol{F},\theta,\boldsymbol{g}). \end{aligned} \tag{3.51}$$

Material objectivity

The constitutive equations (3.51) must obey the *principle of material frame-indifference* or *material objectivity* [2, 22]. This principle states that an admisible process must remain admissible under a change of frame or observer.

Let $\boldsymbol{\varphi}$ and $\boldsymbol{\varphi}^{*}$ be motions of $\mathscr{B}$. Then $\boldsymbol{\varphi}$ and $\boldsymbol{\varphi}^{*}$ are related by a change in observer if

$$\boldsymbol{\varphi}^{*}(\boldsymbol{p},t) = \boldsymbol{y}(t) + \boldsymbol{Q}(t)\boldsymbol{\varphi}(\boldsymbol{p},t), \tag{3.52}$$

where $\boldsymbol{y}(t)$ is a point and $\boldsymbol{Q}(t)$ is an orthogonal tensor. Under such a change scalar fields (such as θ, ψ, and s) remain unaffected, but $\boldsymbol{F}$, $\boldsymbol{\sigma}$, $\boldsymbol{L}$, and $\boldsymbol{g}$ transform as follows:

$$\begin{aligned} \boldsymbol{F} &\rightarrow \boldsymbol{F}^* = \boldsymbol{Q}\boldsymbol{F}, \\ \boldsymbol{\sigma} &\rightarrow \boldsymbol{\sigma}^* = \boldsymbol{Q}\boldsymbol{\sigma}\boldsymbol{Q}^T, \\ \boldsymbol{L} &\rightarrow \boldsymbol{L}^* = \boldsymbol{Q}\boldsymbol{D}\boldsymbol{Q}^T + \dot{\boldsymbol{Q}}\boldsymbol{Q}^T, \\ \boldsymbol{g} &\rightarrow \boldsymbol{g}^* = \boldsymbol{Q}\boldsymbol{g}. \end{aligned} \tag{3.53}$$

This principle shows that the dynamic stress response depends on $\boldsymbol{L}$ only through its symmetric part $\boldsymbol{D}$. The expression for constitutive relations of elastic material with heat conduction and viscosity now take form

$$\begin{aligned} \boldsymbol{\sigma} &= \widehat{\boldsymbol{\sigma}}^{eq}(\boldsymbol{F},\theta) + \widehat{\boldsymbol{V}}(\boldsymbol{F},\theta)[\boldsymbol{D}], \\ \psi &= \widehat{\psi}(\boldsymbol{F},\theta), \\ s &= \widehat{s}(\boldsymbol{F},\theta), \\ \boldsymbol{q} &= \widehat{\boldsymbol{q}}(\boldsymbol{F},\theta,\boldsymbol{g}). \end{aligned} \tag{3.54}$$

The principle of material frame-indifference also imposes restrictions on the constitutive functionals (3.54). It requires that the following identities hold.

$$\begin{aligned} \boldsymbol{\sigma}^* &= \widehat{\boldsymbol{\sigma}}^{eq}(\boldsymbol{Q}\boldsymbol{F},\theta) + \widehat{\boldsymbol{V}}(\boldsymbol{Q}\boldsymbol{F},\theta)[\boldsymbol{Q}\boldsymbol{D}\boldsymbol{Q}^T], \\ \psi &= \widehat{\psi}(\boldsymbol{Q}\boldsymbol{F},\theta), \\ s &= \widehat{s}(\boldsymbol{Q}\boldsymbol{F},\theta), \\ \boldsymbol{q}^* &= \widehat{\boldsymbol{q}}(\boldsymbol{Q}\boldsymbol{F},\theta,\boldsymbol{Q}\boldsymbol{g}), \end{aligned} \tag{3.55}$$

for any transformation of the form (3.53).

Material symmetry

The symmetry group of a material is the set of density preserving changes of reference configuration which leave the response of the material unaltered [2]. The symmetry group $\mathcal{G}$ of a viscous material with heat conduction is the set of all unimodular tensor $\boldsymbol{H}$ for which the following identities hold:

$$\begin{aligned} \widehat{\boldsymbol{\sigma}}^{eq}(\boldsymbol{F},\theta) &= \widehat{\boldsymbol{\sigma}}^{eq}(\boldsymbol{F}\boldsymbol{H},\theta), \\ \widehat{\boldsymbol{V}}(\boldsymbol{F},\theta)[\boldsymbol{D}] &= \widehat{\boldsymbol{V}}(\boldsymbol{F}\boldsymbol{H},\theta)[\boldsymbol{D}], \\ \widehat{\psi}(\boldsymbol{F},\theta) &= \widehat{\psi}(\boldsymbol{F}\boldsymbol{H},\theta), \\ \widehat{s}(\boldsymbol{F},\theta) &= \widehat{s}(\boldsymbol{F}\boldsymbol{H},\theta), \\ \widehat{\boldsymbol{q}}(\boldsymbol{F},\theta,\boldsymbol{g}) &= \widehat{\boldsymbol{q}}(\boldsymbol{F}\boldsymbol{H},\theta,\boldsymbol{g}). \end{aligned} \tag{3.56}$$

for all scalars θ, all vectors $\boldsymbol{g}$ and all tensors $\boldsymbol{F}$ and $\boldsymbol{D}$.

A viscous material with heat conduction is a *linear viscous fluid with heat conduction* if the symmetry group $\mathscr{G}$ is the full unimodular transformation group $\mathscr{U}$, i.e. $\mathscr{G} = \mathscr{U}$, for one and hence all reference configurations.

Linear viscous fluids

The fact that $\mathscr{G} = \mathscr{U}$ implies that the constitutive equations for linear viscous fluid with heat conduction can depend on the deformation gradient $\boldsymbol{F}$ only through its determinant $J = \det[\boldsymbol{F}]$ or, equivalently, through the specific volume $v = 1/\rho$. The equilibrium stress response is now reduced to

$$\widehat{\boldsymbol{\sigma}}^{eq}(v,\theta) = \partial_v \widehat{\psi}(v,\theta)\boldsymbol{I}. \tag{3.57}$$

The principle of material objectivity requires that

$$\boldsymbol{Q}\widehat{\boldsymbol{V}}(v,\theta)[\boldsymbol{D}]\boldsymbol{Q}^T = \widehat{\boldsymbol{V}}(v,\theta)[\boldsymbol{Q}\boldsymbol{D}\boldsymbol{Q}^T], \tag{3.58}$$

holds for every $\boldsymbol{D} \in \text{Sym}$ and $\boldsymbol{Q} \in \text{Orth}^+$. For the equality (3.58) to hold the dynamic stress response function has to be of the form

$$\widehat{\boldsymbol{V}}(v,\theta)[\boldsymbol{D}] = 2\mu\boldsymbol{D} + \lambda \,\text{tr}[\boldsymbol{D}]\boldsymbol{I}. \tag{3.59}$$

where μ and λ are scalar functions of v and θ. Substituting equations (3.57) and (3.59) into (3.54_1) the expression for the stress tensor can be written as

$$\boldsymbol{\sigma} = -p(v,\theta)\boldsymbol{I} + 2\mu(v,\theta)\boldsymbol{D} + \lambda(v,\theta)\,\text{tr}[\boldsymbol{D}]\boldsymbol{I}, \tag{3.60}$$

where $p(v,\theta) = -\partial_v \widehat{\psi}(v,\theta)$.

For the case of temperature independent and incompressible fluid, in which the responses functions are temperature independent and the density of the fluid is constant, the equation (3.60) becomes

$$\boldsymbol{\sigma} = -p\boldsymbol{I} + 2\mu\boldsymbol{D}^{dev}. \tag{3.61}$$

3.2 Mechanics and Thermodynamics of Material Interface

3.2.1 Surface kinematics

A *material surface* is a set of points $\mathscr{S}$ each of whose configurations is a bijection of $\mathscr{S}$ onto a surface in $\mathscr{E}$. The deformations are defined by smooth

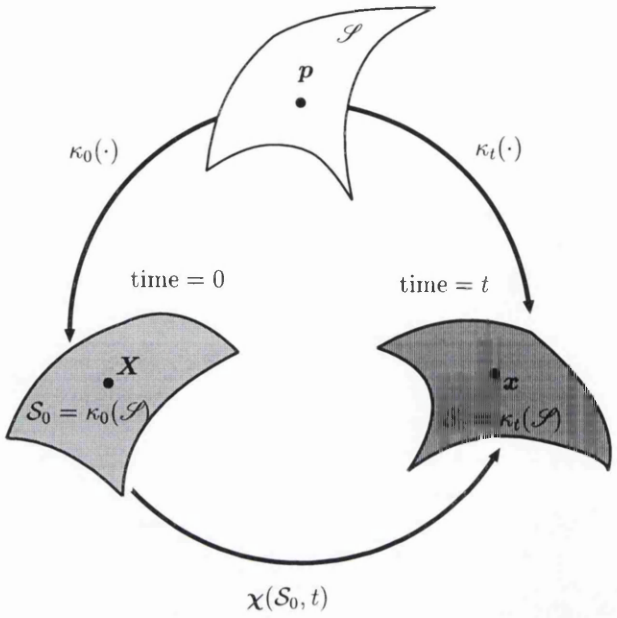

Figure 3.2: Configuration and motion of a material surface $\mathscr{S}$ at time 0 and t.

invertible functions $\boldsymbol{\chi} : \mathcal{S}_0 \to \mathcal{S}_t$ in $\mathscr{E}$, where $\mathcal{S}_0$ is the reference configuration of the material surface $\mathscr{S}$ with boundary $\partial\mathcal{S}_0$.

A motion $\boldsymbol{\chi}$ of a material surface $\mathscr{S}$ is a smooth one parameter family of deformations of $\mathscr{S}$

$$\boldsymbol{\chi} : \mathcal{S}_0 \times \mathscr{I} \to \mathscr{E}, \tag{3.62}$$

where $\mathscr{I}$ is an open interval in $\mathscr{R}$, satisfying

i.) $\kappa_t(\cdot) : \mathscr{S} \to \mathscr{E}$ is a configuration for every $t \in \mathscr{I}$, and

ii.) $\boldsymbol{\chi} : \kappa_0(\mathscr{S}) \times \mathscr{I} \to \mathscr{E}$, defined by

$$\boldsymbol{\chi}(\kappa_0(\boldsymbol{p}), t) = \kappa_t(\boldsymbol{p})$$

,

is of class C^2 for every configuration κ of $\mathscr{S}$.

Associating each material point $\boldsymbol{p} \in \mathscr{S}$ with its position in the reference configuration $\boldsymbol{X} \in \mathcal{S}_0$, the velocity and acceleration of the material point $\boldsymbol{p}$ in the motion $\boldsymbol{\chi}$ at time t are denoted by $\dot{\boldsymbol{\chi}}(\boldsymbol{X}, t)$ and $\ddot{\boldsymbol{\chi}}(\boldsymbol{X}, t)$, respectively. Let $\bar{\mathsf{F}} \in \mathrm{Lin}(\mathscr{T}_X, \mathscr{V})$ such that

$$\bar{\mathsf{F}}(\boldsymbol{X},t) = \nabla_{s_0}\boldsymbol{\chi}(\boldsymbol{X},t), \tag{3.63}$$

where ∇_{s_0} is the surface gradient with respect to $\mathcal{S}_0$.

The perpendicular projection of $\bar{\mathsf{F}}$ onto the tangent plane in current configuration is defined as

$$\mathsf{F} = \boldsymbol{P}\bar{\mathsf{F}}. \tag{3.64}$$

Note that $\mathsf{F} \in \mathrm{Invlin}(\mathscr{T}_X, \mathscr{T}_x)$ and

$$\mathsf{IF} = \bar{\mathsf{F}}, \tag{3.65}$$

where $\mathsf{I} \in \mathrm{Lin}(\mathscr{T}_X, \mathscr{V})$ is the inclusion map. F is termed *surface deformation gradient* of $\boldsymbol{\chi}$. The gradient of velocity field with respect to the current configuration $\mathcal{S}_t$ is

$$\begin{aligned} \mathsf{L}(\boldsymbol{x},t) &= \nabla_s \boldsymbol{v}(\boldsymbol{x},t) \\ &= \dot{\bar{\mathsf{F}}}(\boldsymbol{X},t)\,\mathsf{F}^{-1}(\boldsymbol{X},t) \end{aligned} \tag{3.66}$$

3.2.2 Fundamental laws of thermodynamics for a material surface

To discuss thermodynamics of material surfaces five additional variables need to be introduced. These additional variables are *surface temperature* $\theta_s(\boldsymbol{x},t)$, *surface internal energy per unit area* $e_s(\boldsymbol{x},t)$, *surface entropy per unit area* $s_s(\boldsymbol{x},t)$ and *radiative heat supply from the environment* $r(\boldsymbol{x},t)$ which exists for every configuration of $\mathscr{S}$ and for all $t \in \mathscr{I}$ and a tangential vector field called *surface conductive heat flux* q satisfying $\mathsf{q}(\boldsymbol{x},t) \in \mathscr{T}_{\boldsymbol{x}}$ for all $t \in \mathscr{I}$.

Conservation of mass

The local equivalent of conservation of mass on a surface can be expressed as

$$\dot{\rho}_s + \rho_s \,\mathrm{div}_s[\boldsymbol{v}] = 0 \tag{3.67}$$

where ρ_s is surface density. By decomposing spatial velocity $\boldsymbol{v}$ into a component parallel to $\mathcal{S}_t$ and a component normal to it

$$\boldsymbol{v} = \boldsymbol{v}_s + v_n\,\boldsymbol{n},$$

Equation (3.67) can be written as

$$\dot{\rho}_s + \rho_s \operatorname{div}_s[\boldsymbol{v}_s] - 2H\rho_s v_n = 0, \tag{3.68}$$

where H is the mean curvature.

Balance of momentum

Let the mechanical interaction between adjancent parts of $\mathcal{S}_t$ be represented by the tensor $\overline{\mathsf{T}}(\boldsymbol{x}, t) \in \mathrm{Lin}(\mathscr{T}_{\boldsymbol{x}}, \mathscr{V})$ for every $\boldsymbol{x} \in \mathcal{S}_t$ and $\mathsf{b} = \mathsf{t}^{(1)} + \mathsf{t}^{(2)} + \mathsf{b}_s$, where vector fields $\mathsf{t}^{(1)}$ and $\mathsf{t}^{(2)}$ denote the tractions upon subsurface s of $\mathcal{S}_t$ by the environment from each of the two sides of $\mathcal{S}_t$ and b_s is the surface body force. The local form of the balance of linear momentum implies that the range of $\overline{\mathsf{T}}(\boldsymbol{x}, t)$ lies in $\mathscr{T}_{\boldsymbol{x}}$. Let *surface stress tensor* T denotes $\overline{\mathsf{T}}$ when its codomain is restricted to $\mathscr{T}_{\boldsymbol{x}}$. The local momentum balance is then expressed as

$$\begin{aligned} \rho_s \dot{\boldsymbol{v}} &= \operatorname{div}_s \mathsf{T} + \mathsf{b}, \\ \mathsf{T} &\in \mathrm{Sym}(\mathscr{T}_x). \end{aligned} \tag{3.69}$$

First principle of thermodynamics

Assume that the interfaces do not support temperature discontinuity. Under a sufficient smoothness assumption the local form of energy balance is given as

$$\dot{e}_s + e_s \operatorname{div}_s[\boldsymbol{v}] = \mathsf{T}{:}D\boldsymbol{v} + r + \operatorname{div}_s[\mathsf{q}]. \tag{3.70}$$

Second principle of thermodynamics

The second principle of thermodynamics for a material surface in the form of the Clausius-Planck inequality is given by

$$\dot{s}_s + s_s \operatorname{div}_s[\boldsymbol{v}] + \operatorname{div}_s\left[\frac{\mathsf{q}}{\theta_s}\right] - \frac{r}{\theta_s} \geq 0. \tag{3.71}$$

By introducing the *surface free energy*

$$\psi_s = e_s - \theta_s s_s,$$

into inequality (3.71) and after some algebra the second principle of thermodynamics for a material surface can be written in the form of Clausius-Duhem inequality as

$$\dot{\psi}_s + \dot{\theta}_s s_s + (\psi_s \mathbf{1} - \mathsf{T}) : D\boldsymbol{v} + \frac{1}{\theta_s}\mathsf{q}\cdot\mathsf{g} \leq 0, \tag{3.72}$$

where $\mathbf{1}$ is the identity on current tangent space and $\mathsf{g} := \nabla_s \theta_s$.

3.2.3 Constitutive equations for material surface

Let $(\boldsymbol{\chi}, \theta_s)$ be a thermokinetic process for $\mathscr{S}$, and F the deformation gradient associated with the motion $\boldsymbol{\chi}$. A calorodynamic process for a material surface is a set of fields

$$\mathsf{T}(\boldsymbol{x},t), \qquad \mathsf{q}(\boldsymbol{x},t), \qquad e_s(\boldsymbol{x},t), \qquad s_s(\boldsymbol{x},t), \qquad \mathsf{b}(\boldsymbol{x},t), \qquad r(\boldsymbol{x},t),$$

over a the region $\mathcal{S}_t$ such that (3.69), (3.70), and (3.72) are satisfied. Consider a class of material surface as the one for which constitutive equations of the forms

$$\begin{aligned} \mathsf{T}(\boldsymbol{x},t) &= \widehat{\mathsf{T}}(\mathsf{F},\theta_s,\mathsf{g}), \\ \psi_s(\boldsymbol{x},t) &= \widehat{\psi}_s(\mathsf{F},\theta_s,\mathsf{g}), \\ s_s(\boldsymbol{x},t) &= \widehat{s}_s(\mathsf{F},\theta_s,\mathsf{g}), \\ \mathsf{q}(\boldsymbol{x},t) &= \widehat{\mathsf{q}}(\mathsf{F},\theta_s,\mathsf{g}), \end{aligned} \tag{3.73}$$

hold for every $\boldsymbol{x} \in \mathcal{S}_t = \boldsymbol{\chi}(\kappa(\mathscr{S},0),t)$ and for every $t \in \mathscr{I}$, where $\boldsymbol{x} = \boldsymbol{\chi}(\boldsymbol{X},t)$.

The principle of material frame indifference implies that if $\mathsf{F} = \mathsf{RU}$ is the polar decomposition of F then

$$\begin{aligned} \mathsf{T}(\boldsymbol{x},t) &= \mathsf{R}\widehat{\mathsf{T}}(\mathsf{U},\Theta_s,\mathsf{G})\mathsf{R}, \\ \psi_s(\boldsymbol{x},t) &= \widehat{\psi}_s(\mathsf{U},\Theta_s,\mathsf{G}), \\ s_s(\boldsymbol{x},t) &= \widehat{s}_s(\mathsf{U},\Theta_s,\mathsf{G}), \\ \mathsf{q}(\boldsymbol{x},t) &= \mathsf{R}\widehat{\mathsf{q}}(\mathsf{U},\Theta_s,\mathsf{G}), \end{aligned} \tag{3.74}$$

are the reduced constitutive equations, where $\mathsf{U} \in \mathrm{Psym}(\mathscr{T}_{\boldsymbol{X}})$, $\Theta_s : \mathcal{S}_0 \times \mathscr{I} \to \mathscr{R}^+$, and $\mathsf{G} \in \mathscr{T}_{\boldsymbol{X}} = \nabla_{s_0}\Theta_s$.

Necessary and sufficient conditions that every admissible thermodynamic process of a homogeneous material surface of this class be compatible with the Clausius-Duhem inequality are that [17]

i.) $\widehat{\mathsf{T}}$, $\widehat{\psi}$, and $\widehat{s}$ be a function of U, and Θ_s.

ii.) $\mathsf{T} = \psi_s \mathsf{1} + \mathsf{R}\left(\frac{\partial \widehat{\psi}_s}{\partial \mathsf{U}}\right)\mathsf{F}^T$.

iii.) $\widehat{s} = -\frac{\partial \widehat{\psi}}{\partial \Theta_s}$.

iv.) $\mathsf{q}\cdot\mathsf{g} \leq 0$.

3.2.4 Material surface symmetry

The symmetry group $\mathscr{G}(\boldsymbol{X})$ for $\boldsymbol{X}$ is the group of all $\mathsf{H} \in \mathrm{Unim}(\mathscr{T}_X)$ such that

$$\begin{aligned} \widehat{\mathsf{T}}(\mathsf{F},\theta_s) &= \widehat{\mathsf{T}}(\mathsf{FH},\theta_s), \\ \widehat{\psi}_s(\mathsf{F},\theta_s) &= \widehat{\psi}_s(\mathsf{FH},\theta_s), \\ \widehat{s}_s(\mathsf{F},\theta_s) &= \widehat{s}_s(\mathsf{FH},\theta_s), \\ \widehat{\mathsf{q}}(\mathsf{F},\theta_s,\mathsf{g}) &= \widehat{\mathsf{q}}(\mathsf{FH},\theta_s,\mathsf{g}), \end{aligned} \tag{3.75}$$

for every $\mathsf{F} \in \mathrm{Invlin}(\mathscr{T}_X, \mathscr{T}_x)$ with $\mathscr{T}_x \in \mathrm{Bid}(\mathscr{V})$. A homogeneous material surface point $\boldsymbol{p}$ may be described as fluid if for every configuration κ, $\mathscr{G}_\kappa(\boldsymbol{X}) = \mathrm{Unim}(\mathscr{T}_X)$.

3.2.5 Inviscid fluid surface

For a fluid material surface, the response functions $\widehat{\mathsf{T}}$, $\widehat{\psi}_s$, $\widehat{s}_s$, and $\widehat{\mathsf{q}}$ can depend upon U only through $J = \det[\mathsf{U}]$. Then the surface stress is given by

$$\begin{aligned} \mathsf{T}(\boldsymbol{x},t) &= \left(\psi_s + J\frac{\partial \widehat{\psi}_s}{\partial J}\right)\mathsf{1}, \\ &= \gamma\,\mathsf{1}. \end{aligned} \tag{3.76}$$

When equation (3.76) holds the surface stress is called surface tension [10, 17]. Note that here the surface tension and surface energy are not generally the same.

Considering $\mathsf{T} = \gamma\mathsf{1}$ and using the relations $\mathrm{div}_s[\mathsf{1}] = 2H\boldsymbol{n}$, equation (3.69) can be written as

$$2\gamma H\boldsymbol{n} + \nabla\gamma + \mathsf{b} = \rho_s \dot{\boldsymbol{v}}. \tag{3.77}$$

Furthermore, by assuming that the surface inertial force can be neglected and the fluid is viscous, $\mathsf{b} = (\boldsymbol{\sigma}^{(1)} - \boldsymbol{\sigma}^{(2)})\boldsymbol{n}$ equation (3.77) becomes

$$(\boldsymbol{\sigma}^{(2)} - \boldsymbol{\sigma}^{(1)})\boldsymbol{n} = 2\gamma H\boldsymbol{n} + \nabla\gamma. \tag{3.78}$$

If both fluids are considered to be inviscid, the surface body force is given by $\mathsf{b} = (p^{(1)} - p^{(2)})\boldsymbol{n}$, Upon assuming that γ is constant

$$(p^{(2)} - p^{(1)}) = 2\gamma H, \tag{3.79}$$

which is the well known Laplace-Young equation that gives the pressure jump across the interface as a function of mean curvature.

3.3 Closure

In this chapter the continuum mechanics and thermodynamics of three dimensional body and material interface have been reviewed. In particular, the constitutive relations for linear viscous fluids and inviscid fluid surface are given, which will be used throughout this thesis.

By using the same thermodynamic axioms and principles as the ones established for three dimensional continua, the Laplace-Young equation can be obtained. This modern continuum thermodynamic treatment of material interface generalizes the Laplace-Young equation, thus allowing more complex behavior to be modelled. Unlike the earlier mechanical or thermodynamical treatments of interface which consider surface energy per unit area and surface tension equivalent, the adopted treatment, in general, makes differentiation between the two.

In the next chapter aspects of finite element analysis of free surface flow problem in the Lagrangian framework will be presented. Emphasis is placed on the use of the so-called incremental flow formulation to approximate the rate type of constitutive equations describing the linear viscous fluid. The consistent linearization of the weak form of initial boundary value problem associated with the Newton-Raphson iterative procedure will be discused in detail.

Bibliography

[1] S. Angenent and M.E. Gurtin. Multiphase thermomechanics with interfacial structure 2. evolution of an isothermal interface. *Arch. Rat. Mech. Anal.*, 108:323 – 391, 1989.

[2] B.D. Coleman and W. Noll. The thermodynamics of elastic materials with heat conduction and viscosity. *Arch. Rat. Mech. Anal.*, 13:168 – 178, 1963.

[3] F. Davi and M.E. Gurtin. On the motion of a phase interface by surface diffusion. *J. Appl. Math. Phys.*, 41:782 – 811, 1990.

[4] G.M.C. Fisher and M.J. Leitman. On continuum thermodynamics with surface. *Arch. Rat. Mech. Anal.*, 30:225 – 262, 1968.

[5] G.M.C. Fisher and M.J. Leitman. Continuum thermodynamics with surfaces: Restrictions on constitutive equations. *Quart. Appl. Math.*, 28:303 – 311, 1970.

[6] M.E. Gurtin. Modern continuum thermodynamics. In S. Nemat-Naser, editor, *Mechanics Today: Vol. 1*, New York, 1972. Pergamon Press.

[7] M.E. Gurtin. *An Introduction to Continuum Mechanics.* Academic Press, New York, 1981.

[8] M.E. Gurtin. Multiphase thermomechanics with interfacial structure 1. heat conduction and capillary balance law. *Arch. Rat. Mech. Anal.*, 104:195 – 221, 1988.

[9] M.E. Gurtin. On thermomechanical laws for the motion of a phase interface. *J. Appl. Math. Phys.*, 42:370 – 388, 1991.

[10] M.E. Gurtin and A.I. Murdoch. A continuum theory of elastic material surfaces. *Arch. Rat. Mech. Anal.*, 57:291 – 323, 1975.

[11] M.E. Gurtin and A. Struthers. Multiphase thermomechanics with interfacial structure 3. evolving phase boundaries in the presence of bulk modulus. *Arch. Rat. Mech. Anal.*, 112:97 – 160, 1990.

[12] C. Herring. The use of classical macroscopic concepts in surface energy problems. In R. Gomer and C.S. Smith, editors, *Structure and Properties of Solid Surfaces*, Chicago, 1953. University of Chicago Press.

[13] K.A. Lindsay and B. Straughan. A thermodynamic viscous interface theory and associated stability problems. *Arch. Rat. Mech. Anal.*, 71:307 – 326, 1978.

[14] L.E. Malvern. *Introduction to the Mechanics of a Continuous Medium.* Prentice-Hall, Englewood Cliffs, New Jersey, 1969.

[15] J.E. Marsden and T.J.R. Hughes. *Mathematical Foundations of Elasticity.* Prentice-Hall, Englewood Cliffs, New Jersey, 1983.

[16] G.P. Moeckel. Thermodynamics of an interface. *Arch. Rat. Mech. Anal.*, 57:254 – 280, 1975.

[17] A.I. Murdoch. A thermodynamical theory of elastic material interfaces. *J. Mech. Appl. Math.*, 29:245 – 275, 1976.

[18] L.E. Scriven. Dynamics of a fluid interface: Equation of motion for newtonian surface fluids. *Chem. Engng. Sci.*, 12:98 – 108, 1960.

[19] E.A. de Souza Neto. *Aspects of Continuum Modelling and Numerical Simulation of Internal and Surface Damage in Finitely Deformed Solids.* PhD thesis, Dept. of Civil Engineering, Univ. Coll. of Swansea, 1994.

[20] A.J.M. Spencer. *Continuum Mechanics.* Longman, Essex, 1980.

[21] C. Truesdell. *Rational Thermodynamics.* McGraw-Hill, New York, 1982.

[22] C.A. Truesdell and W. Noll. The non-linear field theories of mechanics. In S. Flügge, editor, *Handbuch der Physik: Vol. III/3*, Berlin, 1965. Springer-Verlag.

[23] C.A. Truesdell and R. Toupin. The classical field theories. In S. Flügge, editor, *Handbuch der Physik: Vol. III/1*, Berlin, 1960. Springer-Verlag.

[24] M. Šilhavý. *The Mechanics and Thermodynamics of Continuous Media.* Springer-Verlag, Berlin, 1997.

Chapter 4

Finite Element Procedure for Incremental Formulation of Lagrangian Free Surface Fluid Dynamics

Numerical simulation of surface tension phenomena involves free surfaces in which the positions vary with time in a manner not known *a priori.* Like velocity and pressure fields, the shape and position are determined as part of the problem solution. Therefore, a numerical method capable of handling free surface problem is required to simulate these phenomena.

Most existing finite difference (FD) and finite element (FE) methods for solving multiphase/free-surface flows fall into two categories, namely, *front capturing* which uses a fixed mesh throughout the calculation and *front tracking* which allows the mesh to deform in time so that it remains surface intrinsic. It is clear that in order to be able to capture the interface a special technique is required when fixed mesh is used. Marker and Cell (MAC) appears to be the first technique developed for such purpose by Harlow and Welch [12]. The MAC technique uses massless marker particles which travel with the fluid to trace the fluid and the interface. Difficulty arise when the surface tension effect has to be incorporated in the calculation due to required detailed knowledge of the fluid interface orientation in order to make accurate estimates of surface curvature. A paper by Daly [7] provides a technique for including surface tension effects into the FD with MAC method. Later Hirt and Nichols [15] introduced another technique to capture the interface, known as the *Volume of fluid* (VOF) technique. The VOF technique modifies the MAC technique by replacing the discrete marker particles with a continuous field variable, the so-called *color function.* This function assigns

a unique constant (color) to each fluid and has a sharp gradient at the fluid interface. In order to incorporate the surface tension effect into VOF code, Brackbill *et. al.* [6] proposed a continuum surface force (CSF) model in which the interface condition, represented by Laplace-Young equation, is implied in the momentum equation rather than explicitly imposed, thus the location of the interface is no longer explicitly required in the calculation. The combination of the VOF technique and the CSF model became very popular, due to its ability for handling large deformation and topological changes such as separation and merging problems, and has been used by a number of authors [17, 35]. However, front capturing methods are less accurate compared to front tracking methods.

In the front tracking technique, which usually involves FD or FE method in Lagrangian description, imposing interface condition is a lot simpler and more accurate compared to front capturing technique, because interface always coincides with sides of computational mesh. Although for flows undergoing large distortion it requires frequent updating of the computational mesh, which can be a complex and time consuming procedure, its ease in handling free-surface and interfaces makes it applicable to a wide variety of problems and has been preferred by a number of authors [14, 1, 30].

In addition to the aforementioned Eulerian and Lagrangian descriptions used in the numerical simulation of free surface flow some authors use the so-called arbitrary Lagrangian-Eulerian (ALE) description [13, 29, 34] to overcome the difficulties in both Eulerian and Lagrangian descriptions.

4.1 Lagrangian free-surface flow: continuum formulation

4.1.1 Strong form of initial boundary value problem

Let $\mathscr{B}$ be a generic continuum body, which initially occupies a reference configuration Ω_0, a subset of three dimensional Euclidean space $\mathscr{E}$, with boundary $\partial\Omega_0$ (subject to a motion $\boldsymbol{\varphi}$ such that for every time $t \in \mathscr{I}$, $\mathscr{I} = [0, T]$). The deformation $\boldsymbol{\varphi} : \Omega_0 \times \mathscr{I} \longrightarrow \mathscr{E}$ maps each material particle $\boldsymbol{p} \in \mathscr{B}$ from its initial position $\boldsymbol{X} \in \Omega_0$ into its current position $\boldsymbol{x} \in \Omega_t$.

Denote by $\boldsymbol{P}(\boldsymbol{X}, t)$ the first Piola-Kirchhoff stress tensor such that the traction vector $\boldsymbol{S}(\boldsymbol{X}, t, \boldsymbol{N})$ is related to the first Piola-Kirchhoff stress tensor through $\boldsymbol{S} = \boldsymbol{PN}$, where $\boldsymbol{N}(\boldsymbol{X})$ is a unit normal vector in the initial configuration. The local form of the (linear) momentum balance can be expressed as

$$\mathrm{DIV}[\boldsymbol{P}] + \rho_0 \boldsymbol{b}_0 = \rho_0 \ddot{\boldsymbol{\varphi}} \quad \text{in} \quad \Omega_0 \times \mathscr{I}, \tag{4.1}$$

where $\boldsymbol{b}_0$ is the body force density in initial configuration, and $\ddot{\boldsymbol{\varphi}}$ is the material acceleration field.

For some common fluids such as air, water and liquids of low molecular weight linear viscous type of constitutive law can be used to describe their behaviour. In isothermal case, assuming that the fluid is isotropic, this constitutive law relates the Cauchy stress tensor of viscous fluid $\boldsymbol{\sigma}$ and the rate of deformation $\boldsymbol{d}$ in a linear fashion,

$$\boldsymbol{\sigma} = -p\boldsymbol{I} + \lambda(\rho)\ \mathrm{tr}[\boldsymbol{D}]\boldsymbol{I} + 2\ \mu(\rho)\ \boldsymbol{D},$$

where p is the hydrostatic pressure, $\boldsymbol{I}$ is the identity tensor, λ and μ are the viscosity coefficients which are in general function of density ρ. If the fluid is incompressible, then ρ is constant and $\mathrm{tr}[\boldsymbol{D}] = 0$. The consequence of this particular constraint is an arbitrary hydrostatic pressure which can be superimposed on the stress field without causing any deformation. Such a hydrostatic pressure is not determined by constitutive equation but can only be found through the equations of motion or of equilibrium, and the boundary conditions. Thus for an incompressible viscous fluid,

$$\boldsymbol{\sigma} = -p\boldsymbol{I} + 2\ \mu\ \boldsymbol{D}^{dev}, \tag{4.2}$$

where $\boldsymbol{D}^{dev}$ is the deviatoric part of rate of deformation tensor $\boldsymbol{D}$.

In this case hydrostatic pressure p is an additional variable, and represents the Lagrange multiplier associated with the additional kinematic constraint

$$\mathrm{tr}[\nabla \boldsymbol{v}] = 0. \tag{4.3}$$

In the initial configuration the constitutive equation for incompressible fluid and associated kinematic constraint have the expressions

$$\boldsymbol{P} = -p\boldsymbol{F}^{-T} + 2\ \mu\ \boldsymbol{D}^{dev}\boldsymbol{F}^{-T}, \tag{4.4}$$

$$J := \det[\boldsymbol{F}\,] = 1. \tag{4.5}$$

Assume that the boundary $\partial\Omega_0$ is composed of two parts that satisfy

$$\partial\Omega_0 = \partial\Omega_0^{\varphi} \cup \partial\Omega_0^{\sigma} \quad \text{and} \quad \partial\Omega_0^{\varphi} \cap \partial\Omega_0^{\sigma} = \emptyset, \tag{4.6}$$

where $\partial\Omega_0^{\varphi}$ is the part of $\partial\Omega_0$ where the deformations are assumed prescribed as $\boldsymbol{\varphi}(\boldsymbol{X}, t)|_{\partial\Omega_0^{\varphi}} = \overline{\boldsymbol{\varphi}}(\boldsymbol{X}, t)$ and $\partial\Omega_0^{\sigma}$ is the part in which the traction vector is assumed to be prescribed $\boldsymbol{S}(\boldsymbol{X}, t)|_{\partial\Omega_0^{\sigma}} = \overline{\boldsymbol{S}}(\boldsymbol{X}, t)$.

The essential boundary condition is provided by

$$\boldsymbol{\varphi}(\boldsymbol{X},t) = \overline{\boldsymbol{\varphi}}(\boldsymbol{X},t) \quad \forall \boldsymbol{\varphi}(\boldsymbol{X},t) \in \boldsymbol{\varphi}(\partial\Omega_0^{\boldsymbol{\varphi}},t). \tag{4.7}$$

Boundary condition at the free surface requires that the stress tangential to the surface must vanish and the stress normal to the surface must exactly balance any applied normal stress [31, 30]. These conditions can be expressed as

$$\begin{aligned} (\boldsymbol{PN})\cdot\boldsymbol{N} &= \overline{\boldsymbol{S}}^{N} \\ (\boldsymbol{PN})\cdot\boldsymbol{T} &= 0 \end{aligned} \quad \text{on} \quad \partial\Omega_0^{\boldsymbol{\sigma}} \times \mathscr{I}, \tag{4.8}$$

where $\overline{\boldsymbol{S}}^{N}$ is the applied normal stress and $\boldsymbol{T}$ is the tangential vector.

To render the initial boundary-value problem well possed, an initial condition on material velocity field $\dot{\boldsymbol{\varphi}}$ must be specified

$$\dot{\boldsymbol{\varphi}}(\boldsymbol{X},0) = \dot{\boldsymbol{\varphi}}_0(\boldsymbol{X}) \quad \boldsymbol{X} \in \Omega_0, \tag{4.9}$$

$$\boldsymbol{\varphi}(\boldsymbol{X},0) = \boldsymbol{\varphi}_0(\boldsymbol{X}) \quad \boldsymbol{X} \in \Omega_0. \tag{4.10}$$

The strong form of initial boundary value problem for Lagrangian free surface flow in reference configuration can now be summarized as follows

Given $\boldsymbol{b}_0 : \Omega_0 \times \mathscr{I} \to \mathscr{V}$, $\overline{\boldsymbol{\varphi}} : \partial\Omega_0^{\boldsymbol{\varphi}} \times \mathscr{I} \to \mathscr{V}$ and $\overline{\boldsymbol{S}} : \partial\Omega_0^{\boldsymbol{\sigma}} \times \mathscr{I} \to \mathscr{V}$, find the deformation field $\boldsymbol{\varphi} : \overline{\Omega}_0 \times \mathscr{I} \to \mathscr{V}$ and the pressure field $p : \overline{\Omega}_n \times \mathscr{I} \to \mathscr{R}$ such that

$$\mathrm{DIV}[\boldsymbol{P}] + \boldsymbol{b}_0 = \rho_0 \ddot{\boldsymbol{\varphi}} \quad \text{in} \quad \Omega_0 \times \mathscr{I} \tag{4.11}$$

$$\det[\boldsymbol{F}] = 1 \quad \text{in} \quad \Omega_0 \times \mathscr{I} \tag{4.12}$$

$$\boldsymbol{\varphi}(\boldsymbol{X},t) = \overline{\boldsymbol{\varphi}}(\boldsymbol{X},t) \quad \text{on} \quad \partial\Omega_0^{\boldsymbol{\varphi}} \times \mathscr{I} \tag{4.13}$$

$$(\boldsymbol{P}(\boldsymbol{X},t)\boldsymbol{N}(\boldsymbol{X}))\cdot\boldsymbol{N}(\boldsymbol{X}) = \overline{\boldsymbol{S}}^{N}(\boldsymbol{X},t) \quad \text{on} \quad \partial\Omega_0^{\boldsymbol{\sigma}} \times \mathscr{I} \tag{4.14}$$

$$(\boldsymbol{P}(\boldsymbol{X},t)\boldsymbol{N}(\boldsymbol{X}))\cdot\boldsymbol{T}(\boldsymbol{X}) = 0 \quad \text{on} \quad \partial\Omega_0^{\boldsymbol{\sigma}} \times \mathscr{I} \tag{4.15}$$

$$\dot{\boldsymbol{\varphi}}(\boldsymbol{X},0) = \dot{\boldsymbol{\varphi}}_0(\boldsymbol{X}) \quad \text{in} \quad \Omega_0 \tag{4.16}$$

$$\boldsymbol{\varphi}(\boldsymbol{X},0) = \boldsymbol{\varphi}_0(\boldsymbol{X}) \quad \text{in} \quad \Omega_0 \tag{4.17}$$

where $\boldsymbol{P}(\boldsymbol{X},t)$ is given by Equation (4.4). The spatial version of the strong form of initial boundary value problem for Lagrangian free surface flow is presented in Box 1.

Box 1. Strong form of Lagrangian free surface flow in spatial configuration

Given $\boldsymbol{b} : \Omega_t \times \mathscr{I} \to \mathscr{V}$, $\overline{\boldsymbol{u}} : \partial\Omega_t^{\varphi} \times \mathscr{I} \to \mathscr{V}$, and $\overline{\boldsymbol{t}} : \partial\Omega_t^{\sigma} \times \mathscr{I} \to \mathscr{V}$
Find $\boldsymbol{u} : \overline{\Omega}_t \times \mathscr{I} \to \mathscr{V}$ and $p : \overline{\Omega}_t \times \mathscr{I} \to \mathscr{R}$ such that

$$\operatorname{div}[\boldsymbol{\sigma}] + \rho\boldsymbol{b} = \rho\ddot{\boldsymbol{u}} \quad \text{in} \quad \Omega \times \mathscr{I}$$

$$\operatorname{div}[\dot{\boldsymbol{u}}] = 0 \quad \text{in} \quad \Omega \times \mathscr{I}$$

$$\boldsymbol{u}(\boldsymbol{x}, t) = \overline{\boldsymbol{u}}(\boldsymbol{x}, t) \quad \forall \boldsymbol{x} \in \partial\Omega_t^{\varphi} \text{ and } t \in \mathscr{I}$$

$$\boldsymbol{\sigma}(\boldsymbol{x}, t)\boldsymbol{n}(\boldsymbol{x}, t) = \overline{\boldsymbol{t}}(\boldsymbol{x}, t) \quad \forall \boldsymbol{x} \in \partial\Omega_t^{\sigma} \text{ and } t \in \mathscr{I}$$

$$\dot{\boldsymbol{u}}(\boldsymbol{x}, 0) = \boldsymbol{v}_0(\boldsymbol{x}) \quad \forall \boldsymbol{x} \in \Omega_t$$

$$\boldsymbol{u}(\boldsymbol{x}, 0) = \boldsymbol{u}_0(\boldsymbol{x}) \quad \forall \boldsymbol{x} \in \Omega_t$$

where $\boldsymbol{\sigma}$ is given by

$$\boldsymbol{\sigma} = -p\boldsymbol{I} + 2\,\mu\,\boldsymbol{D}^{dev}$$

and

$$\boldsymbol{D}^{dev} = [\mathbb{I} - \tfrac{1}{3}\boldsymbol{I} \otimes \boldsymbol{I}] : \boldsymbol{D}$$

4.1.2 Weak formulation of initial boundary value problem

The strong form of the initial boundary value problem requires that the solution has regularity properties, usually expressed by a certain degree of smoothness. However, there are many physical problems in which solutions of the governing equations do not satisfy this requirement. For this class of problems the required regularity can be relaxed by writing the governing equations in a *weak form* with consequent broadening the set of the candidates for solution. In this way, the question of existence and regularity are separated and mathematically helpful in the study of existence and uniqueness of the solution [21]. The weak form of initial boundary value problem

is also more convenient for numerical computation.

Let the set of kinematically admissible deformation of $\mathscr{B}$ is defined by

$$\mathscr{K} = \{\boldsymbol{\varphi}(\boldsymbol{X},t) | \boldsymbol{\varphi}(\boldsymbol{X},t) = \overline{\boldsymbol{\varphi}}(\boldsymbol{X},t) \quad \text{on} \quad \boldsymbol{X} \in \partial\Omega_{\boldsymbol{\varphi}}\},$$

and the space of virtual displacements of $\mathscr{B}$ is defined by

$$\mathscr{U} = \{\boldsymbol{w} : \overline{\Omega}_0 \times \mathscr{I} \to \mathscr{V} |\ \boldsymbol{w}(\boldsymbol{X},t) = \boldsymbol{0} \quad \text{on} \quad \boldsymbol{X} \in \partial\Omega_{\boldsymbol{\varphi}}\}$$

Given $\boldsymbol{b}_0$, $\overline{\boldsymbol{\varphi}}$, $\overline{\boldsymbol{S}}$, $\boldsymbol{\varphi}_0$ and $\dot{\boldsymbol{\varphi}}_0$, find $\boldsymbol{\varphi}(\cdot,t) \in \mathscr{K}$ and $p(\cdot,t) \in \mathscr{P}, \forall t \in \mathscr{I}$ such that $\forall\ \boldsymbol{w} \in \mathscr{U}$, $\zeta \in \mathscr{P}$

$$\int_{\Omega_0} \rho_0 \ddot{\boldsymbol{\varphi}} \cdot \boldsymbol{w}\, \mathrm{d}V + \int_{\Omega_0} \left[-p\boldsymbol{F}^{-T} + 2\mu \boldsymbol{D}^{dev}\boldsymbol{F}^{-T}\right] : \nabla_0 \boldsymbol{w}\, \mathrm{d}V + \int_{\Omega_0} \left(\det[\boldsymbol{F}] - 1\right) \zeta\, \mathrm{d}V = \int_{\Omega_0} \rho_0 \boldsymbol{b}_0 \cdot \boldsymbol{w}\, \mathrm{d}V + \int_{\partial\Omega_0^{\boldsymbol{\sigma}}} \overline{\boldsymbol{S}} \cdot \boldsymbol{w}\, \mathrm{d}A \quad (4.18)$$

$$\int_{\Omega_0} \rho_0 \dot{\boldsymbol{\varphi}}|_{t=0} \cdot \boldsymbol{w}\, \mathrm{d}V = \int_{\Omega_0} \rho_0 \dot{\boldsymbol{\varphi}}_0 \cdot \boldsymbol{w}\, \mathrm{d}V \quad (4.19)$$

$$\int_{\Omega_0} \rho_0 \boldsymbol{\varphi}|_{t=0} \cdot \boldsymbol{w}\, \mathrm{d}V = \int_{\Omega_0} \rho_0 \boldsymbol{\varphi}_0 \cdot \boldsymbol{w}\, \mathrm{d}V \quad (4.20)$$

The spatial version of the weak formulation of initial boundary value problem for free-surface Lagrangian flow is obtained by performing push forward operation on Equations (4.18) - (4.20). The space of kinematically admissible displacements $\mathscr{K}$ and the space of virtual displacements $\mathscr{U}$ now are defined, respectively, as

$$\mathscr{K} = \{\boldsymbol{u}(\boldsymbol{x},t) | \boldsymbol{u}(\boldsymbol{x},t) = \overline{\boldsymbol{u}}(\boldsymbol{x},t) \quad \text{on} \quad \boldsymbol{x} \in \partial\Omega_t^{\boldsymbol{\varphi}},\ \forall t \in \mathscr{I}\},$$

$$\mathscr{U} = \{\boldsymbol{w} : \overline{\Omega}_t \times \mathscr{I} \to \mathscr{V} |\ \boldsymbol{w}(\boldsymbol{x},t) = \boldsymbol{0} \quad \text{on} \quad \boldsymbol{x} \in \partial\Omega_t^{\boldsymbol{\varphi}},\ \forall t \in \mathscr{I}\},$$

and the *space of pressures* $\mathscr{P}$ is given by

$$\mathscr{P} = \{p(\boldsymbol{x},t) |\ p(\boldsymbol{x},t) \in \mathcal{L}^2(\overline{\Omega}_t),\ \forall t \in \mathscr{I}\},$$

where $\mathcal{L}^2(\overline{\Omega}_t)$ denotes the space of square integrable functions defined over $\overline{\Omega}_t$. Because the boundary condition for pressure is not given explicitly p and ζ belong to the same space [16]. The weak formulation now reads:

Given $\boldsymbol{b}$, $\bar{\boldsymbol{t}}$, $\boldsymbol{u}_0$ and $\dot{\boldsymbol{u}}_0$, find $\boldsymbol{u}(\boldsymbol{x},t) \in \mathscr{K}$ and $p(\boldsymbol{x},t) \in \mathscr{P}$, $\forall t \in \mathscr{I}$ such that $\forall\, \boldsymbol{w} \in \mathscr{U}$, $\zeta \in \mathscr{P}$

$$\int_{\Omega_t} \rho\, \ddot{\boldsymbol{u}} \cdot \boldsymbol{w}\, \mathrm{d}v + \int_{\Omega_t} \left[-p\boldsymbol{I} + 2\mu \boldsymbol{D}^{dev}\right] : \nabla \boldsymbol{w}\, \mathrm{d}v + \int_{\Omega_t} \mathrm{div}[\dot{\boldsymbol{u}}]\zeta\, \mathrm{d}v = \int_{\Omega_t} \rho\, \boldsymbol{b} \cdot \boldsymbol{w}\, \mathrm{d}v + \int_{\partial\Omega_t^{\sigma}} \bar{\boldsymbol{t}} \cdot \boldsymbol{w}\, \mathrm{d}a \quad (4.21)$$

$$\int_{\Omega_t} \rho \dot{\boldsymbol{u}}|_{t=0} \cdot \boldsymbol{w}\, \mathrm{d}v = \int_{\Omega_0} \rho \dot{\boldsymbol{u}}_0 \cdot \boldsymbol{w}\, \mathrm{d}v \quad (4.22)$$

$$\int_{\Omega_t} \rho \boldsymbol{u}|_{t=0} \cdot \boldsymbol{w}\, \mathrm{d}v = \int_{\Omega_0} \rho \boldsymbol{u}_0 \cdot \boldsymbol{w}\, \mathrm{d}v \quad (4.23)$$

where $\boldsymbol{b}$, $\bar{\boldsymbol{t}}$, $\boldsymbol{u}_0$, and $\dot{\boldsymbol{u}}_0$ are body forces, tractions, initial displacements field and initial velocity fields, respectively.

This weak formulation is used as a starting point for numerical solution procedure such as finite element method.

Box 2. Weak form of Lagrangian free surface flow in spatial configuration

Given $\boldsymbol{b} : \Omega_t \times \mathscr{I} \to \mathscr{V}$, $\overline{\boldsymbol{u}} : \partial\Omega_t^{\varphi} \times \mathscr{I} \to \mathscr{V}$, and $\bar{\boldsymbol{t}} : \partial\Omega_t^{\sigma} \times \mathscr{I} \to \mathscr{V}$
Find displacement field $\boldsymbol{u} \in \mathscr{K}$, and pressure field $p \in \mathscr{P}$
such that $\forall\, \boldsymbol{\eta} \in \mathscr{U}$ and $\zeta \in \mathscr{P}$

$$\int_{\Omega_t} \rho \ddot{\boldsymbol{u}} \cdot \boldsymbol{\eta}\, \mathrm{d}v + \int_{\Omega_t} \boldsymbol{\sigma} : \nabla \boldsymbol{\eta}\, \mathrm{d}v + \int_{\Omega_t} \mathrm{div}[\dot{\boldsymbol{u}}]\, \zeta\, \mathrm{d}v = \int_{\Omega_t} \rho \boldsymbol{b} \cdot \boldsymbol{\eta}\, \mathrm{d}v + \int_{\partial\Omega_t^{\sigma}} \bar{\boldsymbol{t}} \cdot \boldsymbol{\eta}\, \mathrm{d}a$$

$$\int_{\Omega_t} \dot{\boldsymbol{u}}|_{t=0} \cdot \boldsymbol{\eta}\, \mathrm{d}v = \int_{\Omega_t} \boldsymbol{v}_0 \cdot \boldsymbol{\eta}\, \mathrm{d}v$$

$$\int_{\Omega_t} \boldsymbol{u}|_{t=0} \cdot \boldsymbol{\eta}\, \mathrm{d}v = \int_{\Omega_t} \boldsymbol{u}_0 \cdot \boldsymbol{\eta}\, \mathrm{d}v$$

where

$$\boldsymbol{\sigma} = -p\boldsymbol{I} + 2\mu\, \boldsymbol{D}^{dev}$$

4.1.3 Penalty method

Solution of the weak form of Lagrangian free surface flow for incompressible Newtonian fluid is in fact a two-field variational problem. This is due to the presence of pressure p as a field variable in addition to displacement $\boldsymbol{u}$. In the so-called *penalty method* this weak form, however, can be written so that its solution renders a single-field variational problem, involving only displacement as field variable. This amounts to relaxing slightly the incompressibility constraint. To achieve this the incompressible Newtonian fluid is modeled as a nearly incompressible one by using a very large bulk modulus. In this way an incompressible Newtonian fluid can be obtained by taking the infinity limit for the bulk modulus. Note that from the numerical point of view the incompressible limit can never be achieved.

As has been mentioned in section 3.1 the Cauchy stress tensor can be additively decomposed into an equilibrium part (from now on will be called hydrostatic part) $\boldsymbol{\sigma}^{hydr}$ and a nonequilibrium part (in the case of linear viscous fluid this will be the viscous part) $\boldsymbol{\sigma}^{visc}$

$$\boldsymbol{\sigma} = \boldsymbol{\sigma}^{hydr} + \boldsymbol{\sigma}^{visc} \tag{4.24}$$

From the Clausius-Duhem inequality, it is required that the hydrostatic stress is obtained from the Helmholtz free energy function $\psi(J)$ through

$$\boldsymbol{\sigma}^{hydr} = -p(J)\boldsymbol{I} \tag{4.25}$$

where the pressure $p(J)$ is given by

$$p(J) = \frac{\partial \psi}{\partial J} \tag{4.26}$$

Here, the Helmholtz free energy function can be considered to have similar expression as the volumetric strain energy function used in incompressible elasticity. Different kind of volumetric strain energy functions have been proposed in the literature for nearly incompressible materials [32, 33, 20, 8]. The paper by Doll and Schweizerhof [8] is particularly interesting because it gives some physical conditions that have to be satisfied by an energy function as well as discussion on several energy functions.

Consider a free energy function of the form

$$\psi(J) = \frac{1}{2}K(J-1)^2 \tag{4.27}$$

where K is a very large penalty parameter. Then the hydrostatic part of the Cauchy stress tensor has the expression

$$\boldsymbol{\sigma}^{hydr} \equiv -p\boldsymbol{I} = -K(J-1)\boldsymbol{I}. \tag{4.28}$$

The viscous part of Cauchy stress tensor is said to be derived from a potential if there exists a function $\phi(\boldsymbol{F}, \boldsymbol{D})$, called *viscous potential*, such that

$$\boldsymbol{\sigma}^{visc} = \frac{\partial \phi}{\partial \boldsymbol{D}}. \tag{4.29}$$

It can easily be proved that the viscous part of Cauchy stress for temperature independent linear viscous fluid such that

$$\boldsymbol{\sigma}^{visc} = 2\mu\, \boldsymbol{D}^{dev},$$

can be derived from a viscous potential of the form

$$\phi(\boldsymbol{F}, \boldsymbol{D}) = \mu\, \boldsymbol{D}^{dev} : \boldsymbol{D}^{dev}. \tag{4.30}$$

The expression for the Cauchy stress tensor for temperature-independent linear viscous fluid can then be written as

$$\boldsymbol{\sigma} = -K(J-1)\boldsymbol{I} + 2\mu\, \boldsymbol{D}^{dev}. \tag{4.31}$$

4.2 Lagrangian free-surface flow: incremental formulation

The incremental flow formulation has initially been developed in the context of metal forming by Bonet [3] for plane stress problems, where displacements are used as main solution variables. Later Bonet and Bhargava [5] made an extension to 3-D problem and recently Bonet [4] showed that by using logarithmic stretches as a strain measure more accurate incremental approach can be obtained. In this formulation the constitutive equations are approximated by time integration, in contrast with the standard Lagrangian description of Newtonian flows where the kinematics variables are approximated by time integration. The resulting material equations relate stresses to incremental changes in geometry.

4.2.1 Incremental kinematics

Incremental motion relates the spatial coordinates of a material point $\boldsymbol{p}$ at time t_n to its spatial coordinates at time t_{n+1}

$$\boldsymbol{x}_{n+1} = \boldsymbol{\varphi}(\boldsymbol{x}_n). \tag{4.32}$$

Assuming that incremental displacement $\boldsymbol{u}$ is given and $\boldsymbol{\varphi}(\boldsymbol{x}_n)$ has the expression

$$\boldsymbol{\varphi}(\boldsymbol{x}_n) = \boldsymbol{x}_n + \boldsymbol{u}, \tag{4.33}$$

the incremental deformation gradient can be evaluated through

$$\begin{aligned} \boldsymbol{F} &= \frac{\partial \boldsymbol{\varphi}(\boldsymbol{x}_n)}{\partial \boldsymbol{x}_n} \\ &= \boldsymbol{I} + \nabla_n \boldsymbol{u}. \end{aligned} \tag{4.34}$$

The incremental left Cauchy-Green tensor can be written in term of incremental principal stretches and their directions as

$$\boldsymbol{B} = \boldsymbol{F}\boldsymbol{F}^T = \sum_{l=1}^{3} \left(\lambda_{(l)}\right)^2 \boldsymbol{n}_{(l)} \otimes \boldsymbol{n}_{(l)}. \tag{4.35}$$

Having the incremental principal stretches the incremental logarithmic stretches can be computed as

$$\ln[\boldsymbol{V}] = \sum_{l=1}^{3} \ln[\lambda_{(l)}]\, \boldsymbol{n}_{(l)} \otimes \boldsymbol{n}_{(l)}. \tag{4.36}$$

The incremental rate of deformation tensor can be expressed in terms of the time rate of incremental logarithmic stretches as

$$\boldsymbol{D} = \sum_{l=1}^{3} \frac{d \ln[\lambda_{(l)}]}{dt}\, \boldsymbol{n}_{(l)} \otimes \boldsymbol{n}_{(l)}. \tag{4.37}$$

By assuming that the rate of change of the incremental logarithmic stretches is constant through the time step an approximate expression for the rate of deformation tensor at the end of increment can be obtained as

$$\widetilde{\boldsymbol{D}} = \frac{1}{\Delta t} \sum_{l=1}^{3} \ln[\lambda_{(l)}]\, \boldsymbol{n}_{(l)} \otimes \boldsymbol{n}_{(l)}. \tag{4.38}$$

It has been proved in [3] that as $\Delta t \to 0$ tensor $\widetilde{\boldsymbol{D}}$ converges to $\boldsymbol{D}$. The deviatoric part of the incremental rate of deformation tensor is given by

$$\widetilde{\boldsymbol{D}}^{dev} = \frac{1}{\Delta t}\sum_{l=1}^{3}\left[\ln[\lambda_{(l)}] - \frac{1}{3}\left(\sum_{k=1}^{3}\ln[\lambda_{(k)}]\right)\right]\boldsymbol{n}_{(l)}\otimes\boldsymbol{n}_{(l)}. \tag{4.39}$$

The incremental kinematics employed in this thesis is summerized in Box. 3.

4.2.2 Incremental constitutive equation

Substituting the expression for incremental deviatoric rate of deformation tensor $\widetilde{\boldsymbol{D}}^{dev}$ into Equation (4.30), the incremental version of the viscous potential has the expression as follows

$$\begin{aligned}\tilde{\phi} &= \mu\widetilde{\boldsymbol{D}}^{dev} : \widetilde{\boldsymbol{D}}^{dev} \\ &= \frac{\mu}{\Delta t^2}\left[\sum_{l=1}^{3}\left(\ln[\lambda_{(l)}]\right)^2 - \frac{1}{3}\left(\ln[J]\right)^2\right].\end{aligned} \tag{4.40}$$

Differentiating Equation (4.40) with respect to the incremental rate of deformation tensor $\widetilde{\boldsymbol{D}}$, gives the viscous component of the Cauchy stress tensor $\boldsymbol{\sigma}^{visc}$,

$$\begin{aligned}\boldsymbol{\sigma}^{visc} &= \frac{\partial\tilde{\phi}}{\partial\widetilde{\boldsymbol{D}}} \\ &= \frac{2\mu}{\Delta t}\sum_{l=1}^{3}\left[\ln[\lambda_{(l)}] - \frac{1}{3}\ln[J]\right]\left(\boldsymbol{n}_{(l)}\otimes\boldsymbol{n}_{(l)}\right) \\ &= 2\mu\widetilde{\boldsymbol{D}}^{dev}\end{aligned} \tag{4.41}$$

In the original incremental flow formulation [5] the rate of deformation tensor $\boldsymbol{D}$ is approximated by $\widetilde{\boldsymbol{D}} = \frac{1}{2\Delta t}(\boldsymbol{C} - \boldsymbol{I})$, i.e., $\widetilde{\boldsymbol{D}}$ is defined at the previous configuration V_n. Therefore, differentiation of the potential with respect to $\widetilde{\boldsymbol{D}}$ gives the second Piola-Kirchhoff stress tensor. In the current approach, the use of logarithmic strain allows $\widetilde{\boldsymbol{D}}$ to be approximated at the current configuration V_{n+1}. This results in a more accurate approach [4] and differentiation of the potential with respect to $\widetilde{\boldsymbol{D}}$ gives the Cauchy stress tensor.

The hydrostatic part of the Cauchy stress is only a function of J. Thus, it takes the same expression as in equation (4.28). The expression for the Cauchy stress tensor then has the form

Box 3. Incremental kinematics

- Update configuration

$$\boldsymbol{x}_{n+1} = \boldsymbol{x}_n + \boldsymbol{u}$$

- Compute current incremental deformation gradient

$$\boldsymbol{F} = \boldsymbol{I} + \nabla_n \boldsymbol{u}$$

- Compute incremental left Cauchy-Green tensor

$$\boldsymbol{B} = \boldsymbol{F}\,\boldsymbol{F}^T$$

- Perform spectral decomposition on $\boldsymbol{B}$

$$\boldsymbol{B} = \sum_{l=1}^{3} B_{(l)}\, \boldsymbol{n}_{(l)} \otimes \boldsymbol{n}_{(l)}$$

- Evaluate the incremental principal stretches

$$\lambda_{(l)} = \left(B_{(l)}\right)^{\frac{1}{2}}$$

- Obtain the logarithmic incremental stretches

$$\ln[\boldsymbol{V}] = \sum_{l=1}^{3} \ln[\lambda_{(l)}]\, \boldsymbol{n}_{(l)} \otimes \boldsymbol{n}_{(l)}$$

- Compute incremental rate of deformation gradient

$$\widetilde{\boldsymbol{D}} = \frac{1}{\Delta t} \sum_{l=1}^{3} \ln[\lambda_{(l)}]\, \boldsymbol{n}_{(l)} \otimes \boldsymbol{n}_{(l)}$$

$$\boldsymbol{\sigma} = -K\,(J-1)\boldsymbol{I} + 2\mu \widetilde{\boldsymbol{D}}^{dev} \tag{4.42}$$

4.2.3 Weak formulation of incremental initial boundary value problem

The weak formulation of incremental Lagrangian free surface flow in current configuration is obtained by substituting the incremental constitutive equation (4.42) into equation (4.21) and taking the current volume as the domain of integration in equations (4.21)-(4.23).

$$\int_{V_{n+1}} \rho \ddot{\boldsymbol{u}} \cdot \boldsymbol{w} \, \mathrm{d}v + \int_{V_{n+1}} \left[2\mu \widetilde{\boldsymbol{D}}^{dev} - K(J-1)\boldsymbol{I} \right] : \nabla_{n+1} \boldsymbol{w} \, \mathrm{d}v = \int_{V_{n+1}} \rho \boldsymbol{b} \cdot \boldsymbol{w} \, \mathrm{d}v + \int_{\partial V_{n+1}} \bar{\boldsymbol{t}} \cdot \boldsymbol{w} \, \mathrm{d}a, \quad (4.43)$$

with initial conditions

$$\int_{V_{n+1}} \dot{\boldsymbol{u}}|_{t=0} \cdot \boldsymbol{w} \, \mathrm{d}v = \int_{V_{n+1}} \dot{\boldsymbol{u}}_0 \cdot \boldsymbol{w} \, \mathrm{d}v, \quad (4.44)$$

$$\int_{V_{n+1}} \boldsymbol{u}|_{t=0} \cdot \boldsymbol{w} \, \mathrm{d}v = \int_{V_{n+1}} \boldsymbol{u}_0 \cdot \boldsymbol{w} \, \mathrm{d}v. \quad (4.45)$$

4.2.4 Consistent linearization

Although the temperature-independent linear viscous model is employed, the weak form of incremental Lagrangian free surface flow is nonlinear with respect to the geometry. Its solution is given in the current configuration which is in a state of dynamic equilibrium. In order to obtain the solution using a Newton-Raphson iterative procedure, equation (4.43) has to be linearized in the direction of incremental displacement $\Delta \boldsymbol{u}$.

Assuming that the inertial and external virtual work are independent of deformation, only the second integrand on the left hand side of equation (4.43)

$$\begin{aligned} G^{\text{int}}(\boldsymbol{u}, \boldsymbol{w}) &= \int_{V_{n+1}} \left[-K(J-1)\boldsymbol{I} + 2\mu \widetilde{\boldsymbol{D}}^{dev} \right] : \nabla_{n+1} \boldsymbol{w} \, \mathrm{d}v \\ &= \int_{V_{n+1}} \left[\boldsymbol{\sigma}^{hydr} + \boldsymbol{\sigma}^{visc} \right] : \nabla_{n+1} \boldsymbol{w} \, \mathrm{d}v \end{aligned} \quad (4.46)$$

needs to be linearized and this linearization gives

$$G^{\text{int}}(\boldsymbol{u}, \boldsymbol{w}) + \mathrm{D}\left\{\int_{V_{n+1}} \left[\boldsymbol{\sigma}^{hydr} + \boldsymbol{\sigma}^{visc}\right] : \nabla_{n+1}\boldsymbol{w}\, \mathrm{d}v\right\}[\Delta\boldsymbol{u}] = 0 \qquad (4.47)$$

Pull back of the second term on the left hand-side to the previous configuration gives

$$\mathrm{D}\left\{\int_{V_{n+1}} \left[\boldsymbol{\sigma}^{hydr} + \boldsymbol{\sigma}^{visc}\right] : \nabla_{n+1}\boldsymbol{w}\, \mathrm{d}v\right\}[\Delta\boldsymbol{u}] = \mathrm{D}\left\{\int_{V_n} \left[\boldsymbol{\tau}^{hydr} + \boldsymbol{\tau}^{visc}\right] : \nabla_{n+1}\boldsymbol{w}\, \mathrm{d}v\right\}[\Delta\boldsymbol{u}] \qquad (4.48)$$

where $\boldsymbol{\tau}^{hydr}$ and $\boldsymbol{\tau}^{visc}$ are the hydrostatic and viscous incremental Kirchhoff stress tensor, respectively. The derivative on the right hand side of equation (4.48) can be decomposed as

$$\mathrm{D}\left\{\int_{V_n} \boldsymbol{\tau}^{hydr} : \nabla_{n+1}\boldsymbol{w}\, \mathrm{d}v\right\}[\Delta\boldsymbol{u}] = \int_{V_n} \mathrm{D}\,\boldsymbol{\tau}^{hydr}[\Delta\boldsymbol{u}] : \nabla_{n+1}\boldsymbol{w}\, \mathrm{d}v + \int_{V_n} \boldsymbol{\tau}^{hydr} : \mathrm{D}\,\nabla_{n+1}\boldsymbol{w}\,[\Delta\boldsymbol{u}]\, \mathrm{d}v, \qquad (4.49)$$

where

$$\mathrm{D}\,\boldsymbol{\tau}^{hydr}[\Delta\boldsymbol{u}] = \frac{\partial \boldsymbol{\tau}^{hydr}}{\partial \boldsymbol{F}} \boldsymbol{F}^T : \nabla_{n+1}\Delta\boldsymbol{u}, \qquad (4.50)$$

and

$$\mathrm{D}\,\nabla_{n+1}\boldsymbol{w}\,[\Delta\boldsymbol{u}] = -\nabla_{n+1}\boldsymbol{w}\nabla_{n+1}\Delta\boldsymbol{u}. \qquad (4.51)$$

By substituting equations (4.50) and (4.51) into (4.49), it follows pushing forward the domain of integration and rearranging

$$\mathrm{D}\int_{V_{n+1}} \boldsymbol{\sigma}^{hydr} : \nabla_{n+1}\boldsymbol{w}\, \mathrm{d}v\,[\Delta\boldsymbol{u}] = \int_{V_{n+1}} \nabla_{n+1}\boldsymbol{w} : \left[\frac{1}{J}\frac{\partial \boldsymbol{\tau}^{hydr}}{\partial \boldsymbol{F}}\boldsymbol{F}^T - \boldsymbol{\sigma}^{hydr}\tilde{\mathbb{I}}\right] : \nabla_{n+1}\Delta\boldsymbol{u}\, \mathrm{d}v, \qquad (4.52)$$

where $\tilde{\mathbb{I}}_{ijkl} = \delta_{il}\delta_{jk}$ is the fourth-order transpose identity tensor with the property $\boldsymbol{a}^T = \tilde{\mathbb{I}}\boldsymbol{a}$. The term in the square brackets is the hydrostatic part

of the *spatial elasticity tensor* and for the specific expression (4.42) it takes the form

$$\begin{aligned}\mathbb{A}^{hydr} &= \left[\frac{1}{J}\frac{\partial \boldsymbol{\tau}^{hydr}}{\partial \boldsymbol{F}}\boldsymbol{F}^T - \boldsymbol{\sigma}^{hydr}\tilde{\mathbb{I}}\right] \\ &= -K(2J-1)\,(\boldsymbol{I}\otimes\boldsymbol{I}) + K(J-1)\tilde{\mathbb{I}}. \end{aligned} \tag{4.53}$$

Following the same procedure the viscous part of equation (4.48) has the expression

$$\mathrm{D}\left\{\int_{V_{n+1}} \boldsymbol{\sigma}^{visc} : \nabla_{n+1}\boldsymbol{w}\,\mathrm{d}v\right\}[\Delta\boldsymbol{u}] = \int_{V_{n+1}} \nabla_{n+1}\boldsymbol{w} : \left[\frac{1}{J}\frac{\partial \boldsymbol{\tau}^{visc}}{\partial \boldsymbol{F}}\boldsymbol{F}^T - \boldsymbol{\sigma}^{visc}\tilde{\mathbb{I}}\right] : \nabla_{n+1}\Delta\boldsymbol{u}\,\mathrm{d}v, \tag{4.54}$$

with the *viscous part of the spatial elasticity tensor* $\mathbb{A}^{visc}$ given by

$$\begin{aligned}\mathbb{A}^{visc} &= \left[\frac{1}{J}\frac{\partial \boldsymbol{\tau}^{visc}}{\partial \boldsymbol{F}}\boldsymbol{F}^T - \boldsymbol{\sigma}^{visc}\tilde{\mathbb{I}}\right] \\ &= \frac{\partial \boldsymbol{\sigma}^{visc}}{\partial \boldsymbol{F}}\boldsymbol{F}^T + \frac{1}{J}\left[\boldsymbol{\sigma}^{visc}\otimes\frac{\partial J}{\partial \boldsymbol{F}}\right]\boldsymbol{F}^T - \boldsymbol{\sigma}^{visc}\tilde{\mathbb{I}} \\ &= \left[\frac{\partial \boldsymbol{\sigma}^{visc}}{\partial \widetilde{\boldsymbol{D}}} : \frac{\partial \widetilde{\boldsymbol{D}}}{\partial \boldsymbol{B}} : \frac{\partial \boldsymbol{B}}{\partial \boldsymbol{F}}\right]\boldsymbol{F}^T + \boldsymbol{\sigma}^{visc}\otimes\boldsymbol{I} - \boldsymbol{\sigma}^{visc}\tilde{\mathbb{I}} \end{aligned} \tag{4.55}$$

By substituting the expression for $\boldsymbol{\sigma}^{visc}$, $\widetilde{\boldsymbol{D}}$, and $\boldsymbol{B}$ in terms of $\widetilde{\boldsymbol{D}}$, $\boldsymbol{B}$, and $\boldsymbol{F}$, respectively the viscous spatial elasticity tensor, in its Cartesian components, can be obtained as

$$\mathbb{A}^{visc}_{ijkl} = \frac{2\mu}{\Delta t}\left[\delta_{im}\delta_{jn} - \frac{1}{3}\delta_{ij}\delta_{mn}\right]\left[\frac{\partial \ln \boldsymbol{B}}{\partial \boldsymbol{B}}\right]_{mnko} B_{ol} + \sigma^{visc}_{ij}\delta_{kl} - \sigma^{visc}_{il}\delta_{jk} \tag{4.56}$$

The fourth order tensor

$$\frac{\partial \ln[\boldsymbol{B}]}{\partial \boldsymbol{B}},$$

is the derivative of the tensor logarithm function. The tensor logarithm is a member of the class of isotropic tensor functions and the computation of its derivative follows the procedure described in appendix B.

4.3 Finite element semi-discretization

The finite element semi-discretization is obtained by replacing the space of kinematically admissible displacement $\mathscr{K}$ and the space of virtual displacement $\mathscr{U}$ by their finite dimensional subspaces $\mathscr{K}^h$ and $\mathscr{U}^h$, respectively, generated by the standard procedure described in finite element textbooks [16, 36, 2], the resulting equations can be written as

$$\mathbb{R}(\mathbb{U}) := \mathbb{M}\ddot{\mathbb{U}} + \mathbb{F}^{\text{INT}} - \mathbb{F}^{\text{EXT}} = 0, \tag{4.57}$$

where $\ddot{\mathbb{U}}$ is the global acceleration vector and $\mathbb{M}$, $\mathbb{F}^{\text{INT}}$, and $\mathbb{F}^{\text{EXT}}$ are, respectively, the global mass matrix, internal and external global force vectors resulting from the assemblage

$$\mathbb{M} = \mathop{\mathsf{A}}_{e=1}^{\text{NEL}} (\mathbb{M}_e), \qquad \mathbb{F}^{\text{INT}} = \mathop{\mathsf{A}}_{e=1}^{\text{NEL}} (\mathbb{F}_e^{\text{INT}}), \qquad \mathbb{F}^{\text{EXT}} = \mathop{\mathsf{A}}_{e=1}^{\text{NEL}} (\mathbb{F}_e^{\text{EXT}}), \tag{4.58}$$

of the element mass matrix $\mathbb{M}_e$, element internal force vector $\mathbb{F}_e^{\text{INT}}$ and element external force vector $\mathbb{F}_e^{\text{EXT}}$ defined by

$$\begin{aligned}
\mathbb{M}_e &= \int_{V_{n+1}^e} \rho \mathbb{N}^T \mathbb{N} \, \mathrm{d}v \\
\mathbb{F}_e^{\text{INT}} &= \int_{V_{n+1}^e} \mathbb{B}^T \{\boldsymbol{\sigma}\} \mathrm{d}v \\
\mathbb{F}_e^{\text{EXT}} &= \int_{V_{n+1}^e} \mathbb{N}^T \{\boldsymbol{b}\} \mathrm{d}v + \int_{\partial V_{n+1}^e} \mathbb{N}^T \{\boldsymbol{t}\} \mathrm{d}a,
\end{aligned} \tag{4.59}$$

where $\mathbb{B}$ and $\mathbb{N}$ are, respectively, the standard discrete symmetric gradient operator and the interpolation matrix of the element e in the configuration defined by $\boldsymbol{\varphi}$, and $\{\boldsymbol{\sigma}\}$ is the six dimensional vector containing the components of the Cauchy stress.

4.4 Temporal discretization

Throughout this thesis the Newmark method [23] will be used for temporal discretization of the semi-discrete equation (4.57) resulting from finite element discretization of the weak form of initial boundary value problem. The stability, accuracy, and convergence analyses of this method can be found in standard finite element textbooks [2, 16]. The Newmark method gives

$$\mathbb{U}_{n+1} = \mathbb{U}_n + \Delta t\,\dot{\mathbb{U}}_n + (1-2\beta)\frac{\Delta t}{2}\,\ddot{\mathbb{U}}_n + \beta\Delta t^2\,\ddot{\mathbb{U}}_{n+1} \tag{4.60}$$

$$\dot{\mathbb{U}}_{n+1} = \dot{\mathbb{U}}_n + (1-\delta)\Delta t\ddot{\mathbb{U}}_n + \delta\Delta t\ddot{\mathbb{U}}_{n+1} \tag{4.61}$$

where β and δ are parameters that can be determined in order to control accuracy and stability. From the stability analysis it is found that the method is unconditionally stable as long as the parameter β and δ are chosen to satisfy the conditions $\delta \geq \frac{1}{2}$ and $\beta \geq \frac{1}{4}(\delta + \frac{1}{2})^2$, and conditionally stable if β and δ are chosen to be $\delta \geq \frac{1}{2}$ and $\beta < \frac{\delta}{2}$. Two members of the Newmark family will be used in this thesis; the first one with $\beta = \frac{1}{4}$ and $\delta = \frac{1}{2}$ is associated with *average acceleration* method which is implicit in nature, and the second one with $\beta = 0$ and $\delta = \frac{1}{2}$ is associated with *central difference* method which is explicit in nature.

For cases where $\beta \neq 0$, solving equation (4.60) for $\ddot{\mathbb{U}}_{n+1}$ in terms of $\mathbb{U}_{n+1}$ gives

$$\ddot{\mathbb{U}}_{n+1} = \frac{1}{\beta\Delta t^2}(\mathbb{U}_{n+1} - \mathbb{U}_n) - \frac{1}{\beta\Delta t}\dot{\mathbb{U}}_n - \frac{1}{2}(\frac{1}{\beta} - 2)\ddot{\mathbb{U}}_n \tag{4.62}$$

By substituting equation (4.62) into equation (4.61) the expression for $\dot{\mathbb{U}}_{n+1}$ now does not involve $\ddot{\mathbb{U}}_{n+1}$

$$\dot{\mathbb{U}}_{n+1} = \frac{\delta}{\beta\Delta t}(\mathbb{U}_{n+1} - \mathbb{U}_n) - (\frac{\delta}{\beta} - 1)\dot{\mathbb{U}}_n - (\frac{\delta}{\beta} - 2)\frac{\Delta t}{2}\ddot{\mathbb{U}}_n \tag{4.63}$$

Finally, by substituting equation (4.62) into equation (4.57), the discretization of the weak form of incremental initial boundary value problem governing the free surface flow in Lagrangian coordinates is completed which renders a system of nonlinear algebraic equations.

$$\mathbb{R}(\mathbb{U}_{n+1}) := \frac{1}{\beta\Delta t^2}\mathbb{M}\,\Delta\mathbb{U} - \frac{1}{\beta\Delta t}\mathbb{M}\,\dot{\mathbb{U}}_n - \frac{1}{2}(\frac{1}{\beta} - 2)\mathbb{M}\,\ddot{\mathbb{U}}_n + \\ + \mathbb{F}^{\text{INT}}_{n+1} - \mathbb{F}^{\text{EXT}}_{n+1} = 0 \tag{4.64}$$

4.5 Solution procedures

An effective and efficient way to solve the system of nonlinear algebraic equation resulting from discretization process is to use the standard Newton-Rhapson iterative procedure. The standard Newton-Rhapson procedure replaces iteratively $\mathbb{R}(\mathbb{U}_{n+1})$ by its first order expansion around the point $\mathbb{U}^{(k)}_{n+1}$

$$\mathbb{R}(\mathbb{U}_{n+1}^{(k)}) + \widehat{\mathbb{K}}(\mathbb{U}_{n+1}^{(k)})[\mathbb{U}_{n+1}^{(k+1)} - \mathbb{U}_{n+1}^{(k)}] = 0 \tag{4.65}$$

where the *effective tangent stiffness* $\widehat{\mathbb{K}}$ is defined by the directional derivative formula

$$\widehat{\mathbb{K}}(\mathbb{U}_{n+1}^{(k)})[\Delta\mathbb{U}^{(k+1)}] = \frac{\mathrm{d}}{\mathrm{d}\varepsilon}\bigg|_{\varepsilon=0} \mathbb{R}(\mathbb{U}_{n+1}^{(k)} + \varepsilon\Delta\mathbb{U}^{(k+1)}) \tag{4.66}$$

Assume that the external force vector $\mathbb{F}_{n+1}^{\mathrm{EXT}}$ is independent of the displacement. By substituting Equation (4.64) into Equation (4.65) and arranging, the resulting equation takes the form

$$\begin{aligned}\widehat{\mathbb{K}}(\mathbb{U}_{n+1}^{(k)})[\Delta\mathbb{U}^{(k+1)}] &= \mathbb{F}_{n+1}^{\mathrm{EXT}} - \mathbb{F}_{n+1}^{\mathrm{INT}(k)} - \\ &- \mathbb{M}\left\{\frac{1}{\beta\Delta t^2}(\mathbb{U}_{n+1}^{(k)} - \mathbb{U}_n) - \frac{1}{\beta\Delta t}\dot{\mathbb{U}}_n - \frac{1}{2}(\frac{1}{\beta} - 2)\ddot{\mathbb{U}}_n\right\}\end{aligned} \tag{4.67}$$

$$\widehat{\mathbb{K}}(\mathbb{U}_{n+1}^{(k)})[\Delta\mathbb{U}^{(k+1)}] = \left\{\frac{1}{\beta\Delta t^2}\mathbb{M} + \mathbb{K}\right\}\Delta\mathbb{U}^{(k+1)} \tag{4.68}$$

where

$$\mathbb{K}(\mathbb{U}_{n+1}^{(k)})[\Delta\mathbb{U}^{(k+1)}] = \frac{\mathrm{d}}{\mathrm{d}\varepsilon}\bigg|_{\varepsilon=0} \mathbb{F}^{\mathrm{INT}}(\mathbb{U}_{n+1}^{(k)} + \varepsilon\Delta\mathbb{U}^{(k+1)}) \tag{4.69}$$

is the usual tangent stiffness matrix used in static analysis and given by the formula

$$\mathbb{K}_e = \int_{V_{n+1}^e} \mathbb{G}^T[\mathbb{A}]\mathbb{G}\,\mathrm{d}v \tag{4.70}$$

where $\mathbb{G}$ is the standard discrete spatial gradient operator and $[\mathbb{A}]$ denotes the matrix form of the *spatial elasticity tensor.*

4.6 Adaptive Strategy

The use of Lagrangian finite element analysis in free-surface flow naturally represents the moving boundaries. However, in certain cases, convection and large fluid distortions induce mesh entanglement and/or over-distorted element which in turn cause rapid solution degradation and preclude achievement of any solution for the flows of practical interest. This problem can be

avoided by employing adaptive solution strategy in the finite element analysis [1, 22, 28].

The early works on Lagrangian finite element analysis of free surface flow [31, 30] do not deal with the adaptive strategy simply because the presented numerical examples do not experience severe deformation. The first work on Lagrangian free-surface flow that employed remeshing to avoid entanglement and over distorted element is by Bach and Hassager [1]. The authors devise a measure of element deformation and use it as a remeshing indicator. If maximum element deformation exceeds the allowable value a new mesh is generated and the old solution is interpolated onto the new mesh. Later Muttin *et. al.* [22] used similar geometric criteria to decide whether to remesh or not. Recently Radovitzky and Ortiz [28] used the bounded deformation norm of the velocity field as a refinement indicator following the success of similar approach used by Ortiz and Quigley [24] for solving the problem of strain localization in solids.

The key components of an adaptive strategy adopted in this work are the estimation of the solution error, prediction of the new mesh density, mesh regeneration, and transfer of material and process data to the new mesh.

4.6.1 Error indicator

In this work the estimation of the solution error is carried out by using an *a posteriori* error indicator based on the dissipation functional proposed by Perić *et al.* [27]. This type of error indicator was developed initially for elastoplastic solids by considering the error based on plastic dissipation. For the free surface problem under consideration the error is based on viscous dissipation.

From Clausius-Duhem inequality (3.39), the local viscous dissipation is given by

$$\mathscr{D}^{visc} = \boldsymbol{\sigma}^{visc} : \boldsymbol{D}^{dev}, \tag{4.71}$$

where $\boldsymbol{\sigma}^{visc}$ and $\boldsymbol{D}^{dev}$ are viscous part of Cauchy stress and deviatoric part of rate of deformation tensor, respectively. The viscous dissipation over the entire domain is then given by

$$\mathscr{D}^{visc}_{V_{n+1}} = \langle \boldsymbol{\sigma}^{visc}, \boldsymbol{D}^{dev} \rangle := \int_{V_{n+1}} \boldsymbol{\sigma}^{visc} : \boldsymbol{D}^{dev} \, dv. \tag{4.72}$$

Denote the error corresponding to viscous part of Cauchy stress and the deviatoric part of rate of deformation tensor, respectively, by

$$\boldsymbol{e}_{\boldsymbol{\sigma}^{visc}} := \boldsymbol{\sigma}_{ex}^{visc} - \boldsymbol{\sigma}_{h}^{visc} \qquad \text{and} \qquad \boldsymbol{e}_{\boldsymbol{D}^{dev}} := \boldsymbol{D}_{ex}^{dev} - \boldsymbol{D}_{h}^{dev},$$

where $\boldsymbol{\sigma}_{ex}^{visc}$, $\boldsymbol{\sigma}_{h}^{visc}$, $\boldsymbol{D}_{ex}^{dev}$ and $\boldsymbol{D}_{ex}^{dev}$ are the exact viscous Cauchy stress, approximate viscous Cauchy stress, exact deviatoric rate of deformation and approximate deviatoric rate of deformation, respectively. It can be observed that

$$\begin{aligned}
|\langle \boldsymbol{e}_{\boldsymbol{\sigma}^{visc}}, \boldsymbol{e}_{\boldsymbol{D}^{dev}} \rangle| &= \left| \sum_{e=1}^{\text{NEL}} \int_{V_{n+1}^e} \left(\boldsymbol{\sigma}_{ex}^{visc} - \boldsymbol{\sigma}_{h}^{visc} \right) : \left(\widehat{\boldsymbol{D}}_{ex}^{dev} - \widehat{\boldsymbol{D}}_{h}^{dev} \right) \, \mathrm{d}v \right| \\
&\leq \sum_{e=1}^{\text{NEL}} \left| \int_{V_{n+1}^e} \left(\boldsymbol{\sigma}_{ex}^{visc} - \boldsymbol{\sigma}_{h}^{visc} \right) : \left(\widehat{\boldsymbol{D}}_{ex}^{dev} - \widehat{\boldsymbol{D}}_{h}^{dev} \right) \, \mathrm{d}v \right| \\
&\leq \sum_{e=1}^{\text{NEL}} \int_{V_{n+1}^e} \left| \left(\boldsymbol{\sigma}_{ex}^{visc} - \boldsymbol{\sigma}_{h}^{visc} \right) : \left(\widehat{\boldsymbol{D}}_{ex}^{dev} - \widehat{\boldsymbol{D}}_{h}^{dev} \right) \right| \mathrm{d}v. \quad (4.73)
\end{aligned}$$

The error based on the viscous dissipation for an element (e) may be defined as

$$|e_{\mathscr{D}}^e|^2 = \int_{V_{n+1}^e} \left| \left(\boldsymbol{\sigma}_{ex}^{visc} - \boldsymbol{\sigma}_{h}^{visc} \right) : \left(\widehat{\boldsymbol{D}}_{ex}^{dev} - \widehat{\boldsymbol{D}}_{h}^{dev} \right) \right| \, \mathrm{d}v. \qquad (4.74)$$

Following Zienkiewicz and Zhu [37] the exact viscous stress $\boldsymbol{\sigma}_{ex}^{visc}$ and exact incremental deviatoric rate of deformation tensor $\widehat{\boldsymbol{D}}_{ex}^{dev}$ may be represented by the smoothed viscous stress $\boldsymbol{\sigma}_{*}^{visc}$ and smoothed incremental deviatoric rate of deformation tensor $\widehat{\boldsymbol{D}}_{*}^{dev}$, respectively. This smoothed quantities are obtained by suitable projection of approximate viscous stress $\boldsymbol{\sigma}_{h}^{visc}$ and deviatoric rate of deformation tensor $\widehat{\boldsymbol{D}}_{h}^{dev}$ which satisfy

$$\begin{aligned}
\int_{V_{n+1}} \boldsymbol{\Pi} \left(\boldsymbol{\sigma}_{*}^{visc} - \boldsymbol{\sigma}_{h}^{visc} \right) \, \mathrm{d}v &= \mathbf{0}, \\
\int_{V_{n+1}} \boldsymbol{\Pi} \left(\widehat{\boldsymbol{D}}_{*}^{dev} - \widehat{\boldsymbol{D}}_{h}^{dev} \right) \, \mathrm{d}v &= \mathbf{0},
\end{aligned}$$

where $\boldsymbol{\Pi}$ is a projection matrix.
The associated *a posteriori* error indicator for an element (e) is then given by

$$(\varepsilon_{\mathscr{D}}^e)^2 = \int_{V_{n+1}^e} \left| \left(\boldsymbol{\sigma}_{*}^{visc} - \boldsymbol{\sigma}_{h}^{visc} \right) : \left(\widehat{\boldsymbol{D}}_{*}^{dev} - \widehat{\boldsymbol{D}}_{h}^{dev} \right) \right| \mathrm{d}v. \qquad (4.75)$$

The corresponding global quantities are obtained, in a standard way, as

$$|e_{\mathscr{D}}|^2 = \sum_{e=1}^{\text{NEL}} |e^e_{\mathscr{D}}|^2 \tag{4.76}$$

$$|\varepsilon_{\mathscr{D}}|^2 = \sum_{e=1}^{\text{NEL}} |\varepsilon^e_{\mathscr{D}}|^2 \tag{4.77}$$

respectively. In addition, the element *relative error* $\eta^e_{\mathscr{D}}$ is defined as

$$\eta^e_{\mathscr{D}} = \frac{|e^e_{\mathscr{D}}|}{\left(\frac{\mathscr{D}+|e_{\mathscr{D}}|^2}{\text{NEL}}\right)^{1/2}} \approx \frac{\varepsilon^e_{\mathscr{D}}}{\left(\frac{\mathscr{D}^h+(\varepsilon^h_{\mathscr{D}})^2}{\text{NEL}}\right)^{1/2}}. \tag{4.78}$$

The ideal mesh requires an equal distribution of the element relative errors.

After the element relative errors are obtained a certain criteria is required to decide whether to remesh or not. Let η^e be the target error. The *error index* is then obtained by comparing the target error with the current element relative error

$$\xi^e_{\mathscr{D}} = \frac{\eta^e_{\mathscr{D}}}{\eta^e}. \tag{4.79}$$

The remeshing procedure is required whenever $\xi^e_{\mathscr{D}} > 1$.

4.6.2 Mesh density prediction

In view of *h-adaptivity* employed in this work, a new element size needs to be predicted over all the domain so that the error of the finite element solution carried out on new mesh is less then the target error. There are several ways of predicting the element size [37, 11, 19]. Here, the element size prediction is due to [37] which is based on the assumption of asymptotic convergence rate of error.

By assuming the convergence rate of the error to be $O(h^p)$, the new mesh size h^{new}_e can be computed using the following formula

$$h^{new}_e = \frac{h^{old}_e}{(\xi^e_{\mathscr{D}})^{1/p}} \tag{4.80}$$

where h^{old}_e is the previous mesh size and p is the degree of polynomial of the interpolation function. The information on the new element size is then fed into the mesh generator to generate the new mesh.

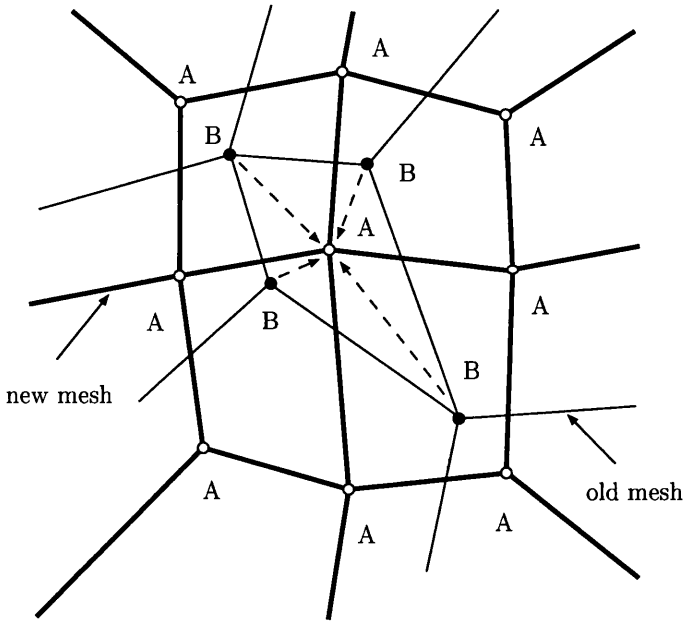

Figure 4.1: Transfer operator.

4.6.3 Mesh regeneration

For the mesh generation and subsequent mesh adaptation, an unstructured meshing approach is used employing the advancing front technique due to its relatively simple way of controlling the mesh density and recovering geometric features of the deformed surface [9].

4.6.4 Transfer operator

After mesh has been regenerated to carry on the analysis some of the information from the previous increment must be transferred to the new mesh using a transfer operator. The issue of transfer operator has been addressed, among others, by Ortiz and Quigley [24], Lee and Bathe [18], Perić *et al.* [25], Dutko *et al.* [9], and Perić *et al.* [26] in which various transfer operator are designed for history dependent materials with application to strain localization problems or manufacturing processes.

In general, information that needs to be transfer can be put into two categories. The first category represents the nodal variables and the second one represents the state variables at the quadrature points. However, for history independent materials, such as Newtonian fluids, the stresses depend solely on the Jacobian of deformation J and the current rate of deformation

$\boldsymbol{D}$. For the incremental flow formulation approach that is adopted in this work the dependence on both quantities reduces to the dependence on the incremental displacement $\boldsymbol{u}$ which is a nodal data. Therefore, no need to transfer any state variables from the quadrature points of the old mesh onto the quadrature points of the new one.

The transfer procedure of nodal variables from the old mesh h onto the new mesh $h+1$ (see, Figure 4.1) can be subdivided into three stages [25].

i.) *Construction of the background mesh*

For each node A of the new mesh $h+1$ with known coordinates ${}^{h+1}\boldsymbol{x}_{n,A}$ the so-called background element ${}^{h}\Omega_e$ is found in the old mesh h for which ${}^{h+1}\boldsymbol{x}_{n,A} \in {}^{h}\Omega_e$.

ii.) *Evaluation of the local coordinates*

The local coordinates $\left({}^{h}\xi_A, {}^{h}\eta_A\right)$ of the node A of the new mesh within the background element ${}^{h}\Omega_e$ can be evaluated by solving the following equation

$$ {}^{h+1}\boldsymbol{x}_{n,A} = \sum_{B=1}^{4} {}^{h}\mathbb{N}_B \left({}^{h}\xi_A, {}^{h}\eta_A\right) {}^{h}\boldsymbol{x}_{n,B}, \tag{4.81} $$

where $\mathbb{N}$ are the interpolation functions.

iii.) *Mapping of the nodal values*

By using the shape functions ${}^{h}\mathbb{N}_B \left({}^{h}\xi_A, {}^{h}\eta_A\right)$ the nodal values ${}^{h}\Lambda_{n,B}$ are mapped from the nodes B of the old mesh h to the nodes A of the new mesh $h+1$. This mapping may be expressed as

$$ {}^{h+1}\boldsymbol{\Lambda}_{n,A} = \sum_{B=1}^{4} {}^{h}\mathbb{N}_B \left({}^{h}\xi_A, {}^{h}\eta_A\right) {}^{h}\boldsymbol{\Lambda}_{n,B}. \tag{4.82} $$

where ${}^{h}\boldsymbol{\Lambda}_n$ denotes the array containing all nodal information at given time step t_n and mesh h, that are going to be transferred.

Table 4.1: Density and viscosity of the liquid employed in the numerical examples of Lagrangian free-surface flows.

density ρ $(unit)$	1.0
viscosity μ $(unit)$	1.0×10^{-2}

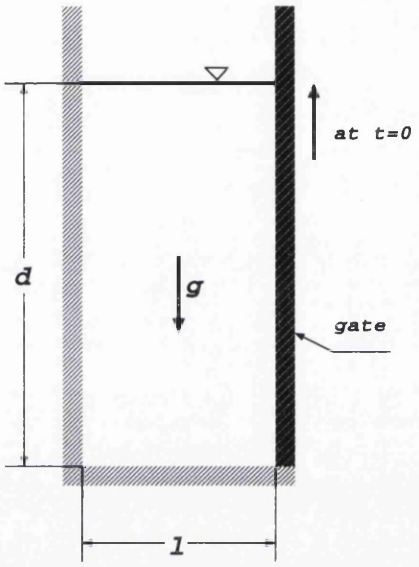

Figure 4.2: Breaking dam problem: problem definition and geometry.

4.7 Numerical examples

The ability of the present formulation to solve free surface flow problems is illustrated in this section for some benchmark problems that frequently appear in the literatures [31, 30, 28]. The first example corresponds to broken dam problem. In the second example, a sloshing tank problem is chosen to demonstrate the validity of the incremental formulation with highly nonlinear effects. The third example considers free oscillation of viscous liquid in a rectangular tank and finally, the fourth example deal with propagation of a solitary wave in a rectangular channel of uniform depth. All examples are carried out in two dimension and the properties of the liquid employed is given in table4.1.

4.7.1 Broken dam problem

In this example, a rectangular column of water in hydrostatic equilibrium is confined between two vertical walls. The geometry is shown in Figure 4.2 in which the width l is 3.5 units and depth d is 7.0 units. Gravity g is acting downward with magnitude of 1.0 unit. The dam holding the water vanishes at time $t = 0$ and the water falls away under the action of gravity force. Slip boundary condition is applied on both vertical and horizontal wall. The total number of nodes and bilinear quadrilateral F-bar elements used in computation are 289 and 256 respectively. Time integration is carried out implicitly by taking Newmark integration parameters $\beta = 0.25$ and $\delta = 0.5$. Time step size is taken to be $\Delta t = 0.02$ unit. To enforce the incompressibility the penalty parameter is chosen $K = 0.5 \times 10^7$. Figure 4.3 shows a sequence of mesh configurations at different time instants. Comparison of the finite element solution with the experimental data obtained by Martin and Moyce [15] is shown in Figure 4.4. For this particular example the finite element solution of incremental Lagrangian free surface flow, in general, shows a good agreement with the experimental result except for time $t = 1$ due to the difficulty to make the dam disappear instantaneously in the experiment.

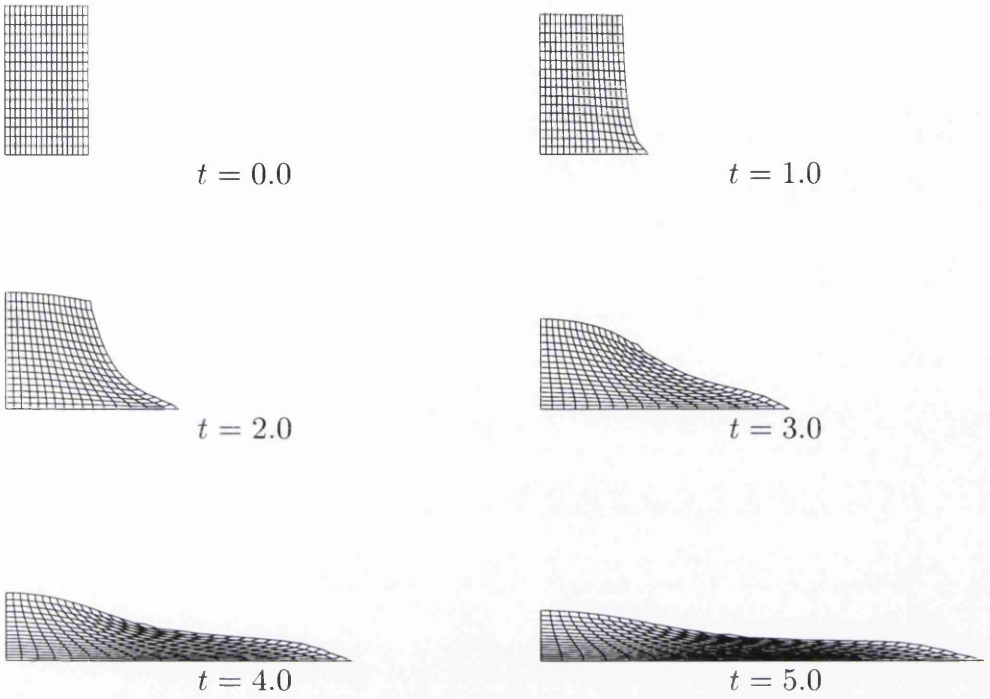

Figure 4.3: Breaking dam problem: finite element meshes at different time instants.

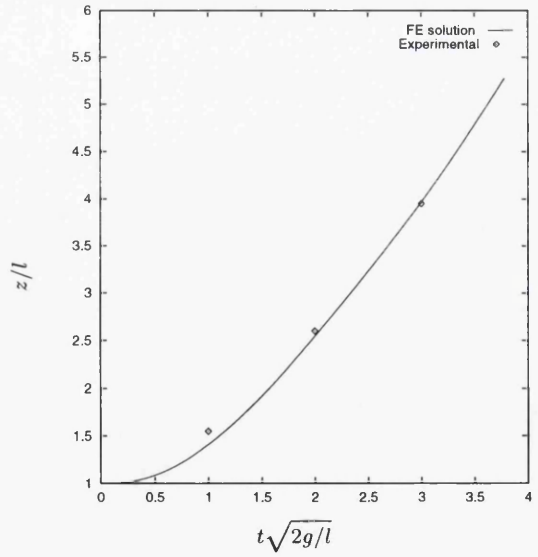

Figure 4.4: Breaking dam problem: comparison of finite element solution with experimental data.

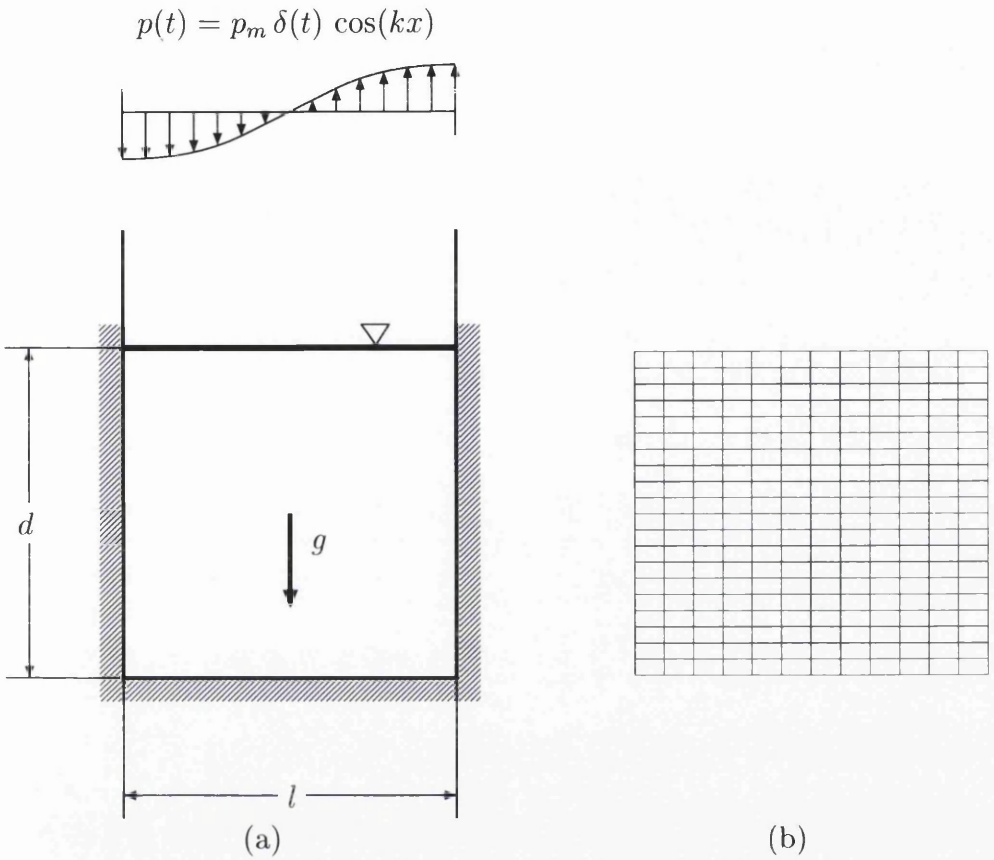

Figure 4.5: Sloshing tank problem: problem definition. (a) geometry and (b) finite element mesh.

4.7.2 Sloshing tank problem

The example considered in this subsection is nonlinear oscillation of fluid in a rectangular tank. The fluid is initially at rest and occupies a region 4.8 units wide and 4.0 units high. The oscillation is obtained by impulsively applying a cosine pressure pulse given by

$$p(t) = p_m\,\delta(t)\,\cos(kx) \tag{4.83}$$

at the free surface. Here p_m is the maximum applied pressure, $\delta(t)$ is the Dirac delta function, and $k = 2\pi/\lambda$, where λ is the disturbance wavelength. The geometry of the problem and the finite element mesh used are shown in Figure 4.5(a) and Figure 4.5(b), respectively. This example is associated with half-wave impulsive loading ($\lambda = 2$) with the maximum applied pressure $p_m = 1$ and gravitational acceleration of one unit acting downward. Slip

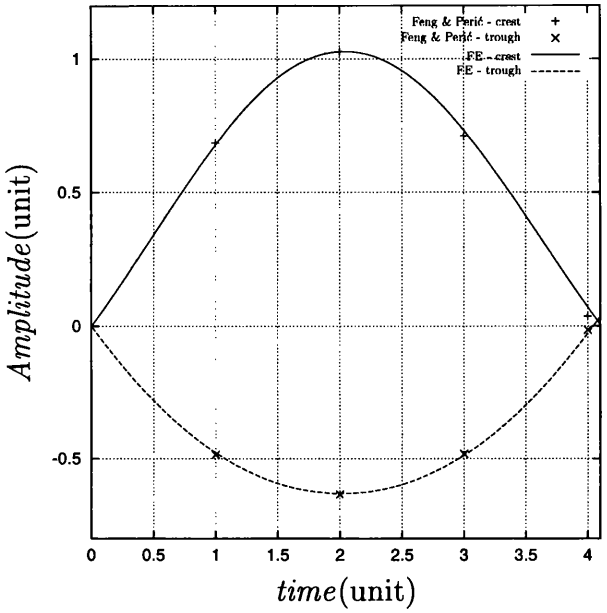

Figure 4.6: Sloshing tank problem: comparison of finite element solution with the results obtained by Feng and Perić [10].

boundary condition is imposed on all walls. Total number of finite element used is 240 bilinear quadrilateral F-bar elements and the time step size is $\Delta t = 0.005$ unit. As in previous example implicit time integration is used with Newmark integration parameters $\beta = 0.25$ and $\delta = 0.5$ and penalty parameter $K = 0.5 \times 10^7$ is chosen to enforce incompressibility. To asses the accuracy of the present work the finite element solution is compared with the one obtained by Feng and Perić [10] using a *space-time* finite element method. This comparison is shown in Figure 4.6. Figure 4.7 shows the finite element mesh at different time instants.

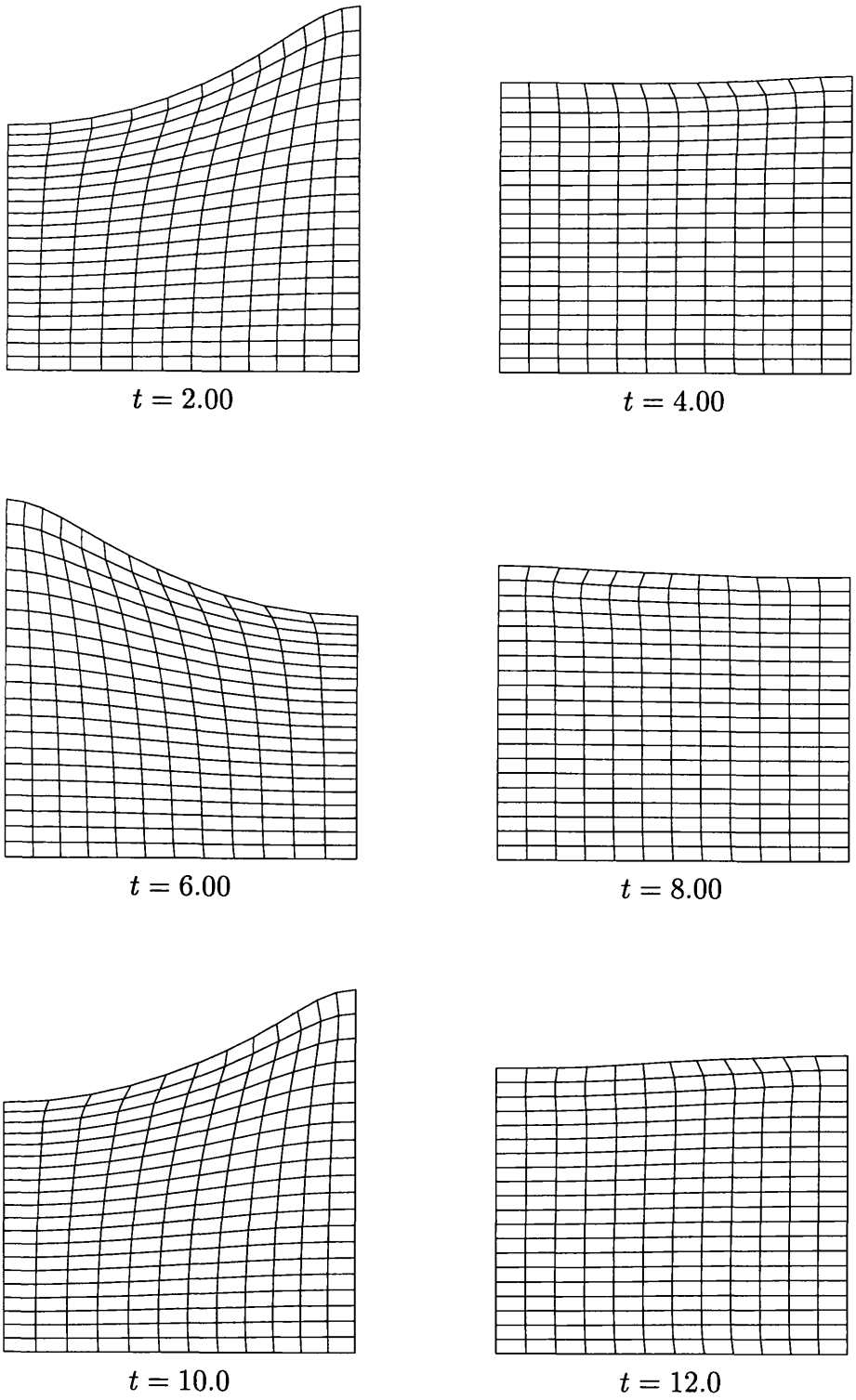

Figure 4.7: Sloshing tank problem: Finite element meshes at different time instants.

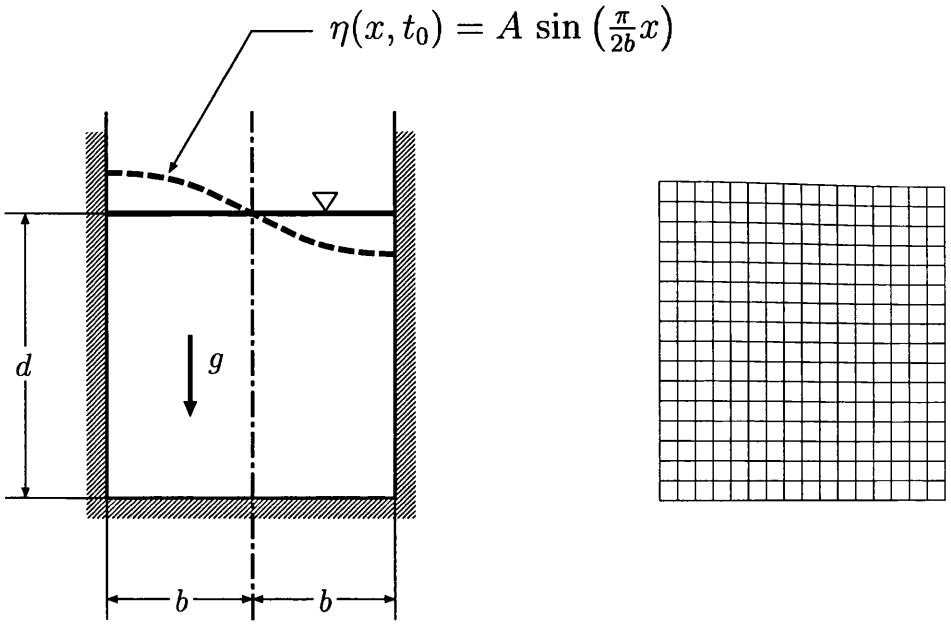

Figure 4.8: Free oscillation of a viscous liquid: problem definition. (a) geometry and (b) finite element mesh

4.7.3 Free oscillation of viscous liquid

This example consider small amplitude free oscillation of viscous liquid in a rectangular tank with depth d of 1.0 units and width $2b$ of 1.0 units as shown in Figure 4.8. Gravity acts downward with magnitude g of 1.0 unit. The first antisymmetric natural mode is taken as the initial profile of the free surface and is given as

$$\eta(x, t_0) = A \sin\left(\frac{\pi}{2b}x\right) \tag{4.84}$$

where A is the amplitude of the antisymmetric natural mode, which is assumed to be 0.01 units. For the finite element computation 289 nodes and 256 bilinear quadrilateral F-bar elements are used. The time step is taken to be $\Delta t = 0.02$ unit and the penalty parameter is $K = 0.5 \times 10^7$. As in previous examples the boundary condition on the walls are considered to be slip boundary condition.

Figure 4.9 shows the time history of surface elevation amplitude of both contact point. This result is in agreement with the results obtained by Ramaswamy [29], Radovitzky and Ortiz [28] (i.e. our analysis gives the same frequency as their analyses). We note that in the present simulation a small

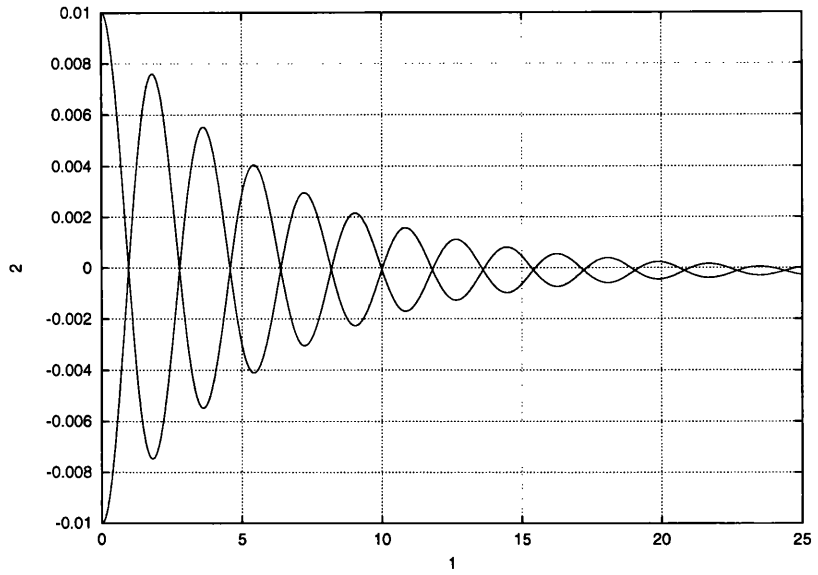

Figure 4.9: Free oscillation of viscous liquids: time history of the amplitude

volume loss of 0.0125 % has been recorded as a result of employing penalty method to impose incompressibility constraint. The time history of kinetic energy is shown in Figure 4.10.

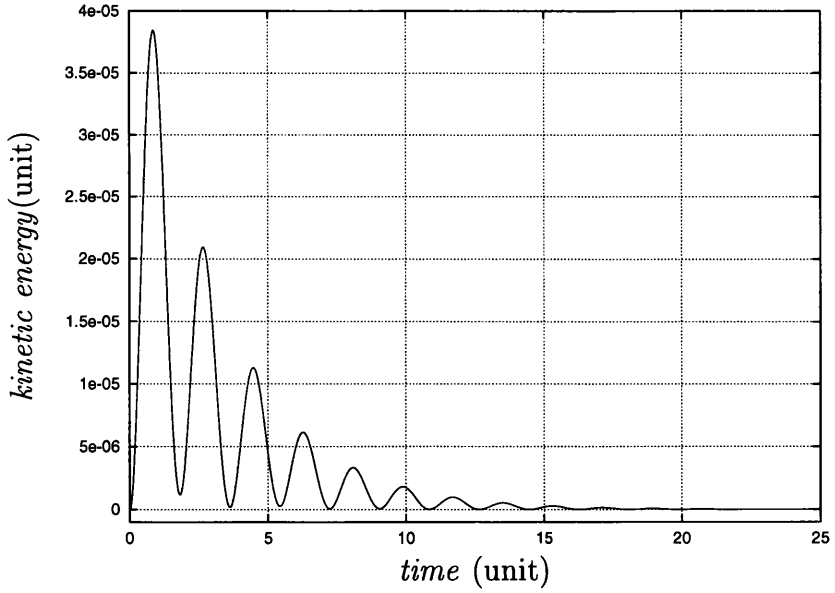

Figure 4.10: Free oscillation of viscous liquids: time history of kinetic energy

4.8 Closure

A Lagrangian free surface flow solver has been presented in this chapter based on the finite element methodology. Using the incremental flow formulation the rate type of constitutive equation characterizing the Newtonian fluid is approximated by integration over finite time steps. As a consequence the viscous stresses are obtained by measuring changes in geometry over a time interval. In this work the incompressibility constraint is imposed using penalty method resulting in a nearly incompressible fluid.

Three numerical examples commonly used as benchmarks for the free surface flow problems have been considered to test the performance of the approach adopted in this work. For these examples the solver gives a good agreement with either experimental or numerical results obtained by other authors. Based on these benchmark results we are confident that this free surface flow solver can be used as a finite element framework to implement surface tension effect on the free surface.

The next chapter deals with a technique to incorporate surface tension into finite element simulation of free surface flow including also the contact angle condition at the contact line. Surface tension force vector and its consistent linearization associated with Newton-Raphson iterative procedure are presented for both two dimensional and axisymmetric cases.

Bibliography

[1] P. Bach and O. Hassager. An algorithm for the use of the lagrangian specification in newtonian fluid mechanics and applications to free-surface flow. *J. Fluid Mech.*, 152:173 – 190, 1985.

[2] K.J. Bathe. *Finite Element Procedures.* Prentice-Hall, Englewood Cliffs, New Jersey, 1996.

[3] J. Bonet. The incremental flow formulation for the numerical analysis of plane stress and thin sheet viscous forming proceses. *Comput. Methods Appl. Mech. Engrg.*, 114:103–122, 1994.

[4] J. Bonet. Recent developments in the incremental flow formulation for the numerical simulation of metal forming processes. *Engng. Comp.*, 15:345–356, 1998.

[5] J. Bonet and P. Bhargava. The incremental flow formulation for the numerical analysis of 3-dimensional viscous deformation processes: Continuum formulation and computational aspects. *Comput. Methods Appl. Mech. Engrg.*, 122:51–68, 1995.

[6] J. U. Brackbill, D. B. Kothe, and C. Zemach. A continuum method for modelling surface tension. *J. Comp. Physics*, 100:335 – 354, 1992.

[7] B.J. Daly. A technique for including surface tension effects in hydrodynamics calculations. *J. Comp. Physics.*, 4:97–117, 1969.

[8] S. Doll and K. Schweizerhof. On the development of volumetric strain energy functions. *J. Appl. Mech.*, 67:17 – 21, 2000.

[9] M. Dutko, D. Perić, D.R.J. Owen, A.J.L. Crook, Z. Wei, and J. Yu. Bulk forming simulation by adaptive explicit fem. In D.R.J. Owen, E. Oñate, and E. Hinton, editors, *Proceedings of the Fifth International Conference on Computational Plasticity: Fundamentals and Applications – Barcelona, April 1997*, pages 1305–1312, Barcelona, 1997. CIMNE.

[10] Y.T. Feng and D. Perić. A time-adaptive space-time finite element method for incompresible lagrangian flows with free surfaces: Computational issues. *Comput. Methods Appl. Mech. Engrg*, 190:499 – 518, 2000.

[11] L. Fourment and J.L. Chenot. Error estimators for viscoplastic materials: Application to forming processes. *Engng. Comp.*, 12:469 – 490, 1995.

[12] F.H. Harlow and J.E. Welch. Numerical calculation of time-dependent viscous incompressible flow of fluid with free surface. *Phys. Fluids*, 8:2182 – 2189, 1965.

[13] C.W. Hirt, A.A. Amsden, and J.L. Cook. An arbitrary Eulerian-Lagrangian computing method for all flow speeds. *J. Comp. Physics.*, 14:227 – 253, 1974.

[14] C.W. Hirt, J.L. Cook, and T.D. Butler. A Lagrangian method for calculating the dynamics of an incompressible fluid with free surfaces. *J. Comp. Physics.*, 5:103 – 124, 1970.

[15] C.W. Hirt and B.D. Nichols. Volume of fluid (VOF) method for the dynamics of free boundaries. *J. Comp. Physics.*, 39:201 – 225, 1981.

[16] T.J.R. Hughes. *The Finite Element Method. Linear Static and Dynamic Finite Element Analysis.* Prentice-Hall, Englewood Cliffs, New Jersey, 1987.

[17] B. Lafaurie, C. Nardone, R. Scardovelli, S. Zaleski, and G. Zanetti. Modelling merging and fragmentation in multiphase flows with SURFER. *J. Comp. Physics.*, 113:134 – 147, 1994.

[18] N.S. Lee and K.J. Bathe. Error indicator and adaptive remeshing in large deformation finite element analysis. *Finite Elem. Anal. Des.*, 16:99 – 139, 1994.

[19] L.Y. Li and P. Bettes. Notes on optimal criteria in adaptive finite element computations. *Comm. Num. Meth. Engng.*, 11:911 – 915, 1995.

[20] C.H. Liu, G. Hofstetter, and H.A. Mang. 3d finite element analysis of rubber–like materials at finite strains. *Engng. Comp.*, 11:111 – 128, 1994.

[21] J.E. Marsden and T.J.R. Hughes. *Mathematical Foundations of Elasticity.* Prentice-Hall, Englewood Cliffs, New Jersey, 1983.

[22] F. Muttin, T. Coupez, M. Bellet, and J. L. Chenot. Lagrangian finite-element analysis of time-dependent viscous free-surface flow using an automatic remeshing technique: Application to metal casting flow. *Int. J. Num. Meth. Engng*, 36:2001 – 2015, 1993.

[23] N.M. Newmark. A method of computation for structural dynamics. *ASCE J. Engg. Mech. Div.*, 85:67–74, 1959.

[24] M. Ortiz and J.J. Quigley IV. Adaptive mesh refinement in strain localization problems. *Comput. Methods Appl. Mech. Engrg.*, 90:781 – 804, 1991.

[25] D. Perić, Ch. Hochard, M. Dutko, and D.R.J. Owen. Transfer operator for evolving meshes in small strain elasto-plasticity. *Comput. Methods Appl. Mech. Engrg.*, 137:331 – 344, 1996.

[26] D. Perić, M. Vaz Jr, and D.R.J. Owen. On adaptive strategies for large deformations of elasto-plastic solids at finite strains: Computational issues and industrial applications. *Comput. Methods Appl. Mech. Engrg.*, 176:279 – 312, 1999.

[27] D. Perić, J. Yu, and D.R.J. Owen. On error estimates and adaptivity in elastoplastic solids: Application to the numerical simulation of strain localization in classical and cosserat continua. *Int. J. Num. Meth. Engng.*, 37:1351–1379, 1994.

[28] R. Radovitzky and M. Ortiz. Lagrangian finite element analysis of Newtonian fluid flows. *Int. J. Num. Meth. Engng.*, 43:607 – 619, 1998.

[29] B. Ramaswamy. Numerical simulation of unsteady viscous free surface flow. *J. Comp. Physics*, 90:396–430, 1990.

[30] B. Ramaswamy and M. Kawahara. Lagrangian finite element analysis applied to viscous free surface fluid flow. *Int. J. Num. Meth. Fluids*, 7:953 – 984, 1987.

[31] B. Ramaswamy, M. Kawahara, and T. Nakayama. Lagrangian finite element method for the analysis of two-dimensional sloshing problems. *Int. J. Num. Meth. Fluids*, 6:659 – 670, 1986.

[32] J.C. Simo and R.L. Taylor. Penalty function formulations for incompressible nonlinear elastostatics. *Comput. Methods Appl. Mech. Engrg.*, 35:107 – 118, 1982.

[33] T. Sussman and K.-J. Bathe. A finite element formulation for nonlinear incompressible elastic and inelastic analysis. *Comp. Struct.*, 26:357–409, 1987.

[34] P. Szabo and O. Hassager. Simulation of free surfaces in 3-d with the arbitrary Lagrange-Euler method. *Int. J. Num. Meth. Engng*, 38:717 – 734, 1995.

[35] J. Wu, S.T. Yu, and B.N. Jiang. Simulation of two-fluid flows by the least-squares finite element method using a continuum surface tension model. *Int. J. Num. Meth. Engng*, 42:583 – 600, 1998.

[36] O.C. Zienkiewicz and R.L. Taylor. *The Finite Element Method – Vol.1: Basic Formulation and Linear Problems.* McGraw-Hill, 1989.

[37] O.C. Zienkiewicz and J.Z. Zhu. A simple error estimator and adaptive procedure for practical engineering analysis. *Int. J. Num. Meth. Engng.*, 24:337 – 357, 1987.

Chapter 5

Formulation and Implementation of the Surface Tension

In numerical computations, the surface tension effect can be included in two equivalent ways [5]. The first approach is to include it as boundary condition at the fluid interfaces, which is most appropriate if the interface evolution is described explicitly. The second approach is to include the surface tension effect as forces that act at the fluid interfaces. The latter approach can be applied to situations where the evolution of interfaces is described either explicitly or implicitly.

A procedure for incorporating surface tension effects in numerical simulation of fluid flows has been first described by Daly and Pracht [6] for the purpose of numerical study of the density-current surges. Using *marker and cell* (MAC) method as a surface tracking procedure in conjunction with finite difference method, the authors used additional set of particles called *interface particles* and cubic spline interpolation to curve fit the fluid interface in order to resolve its orientation and in turn determine the surface tension force in each grid cell through which it passes. Later Daly [4, 5] extended the procedure to axisymmetric problem to study the interface stability.

The first procedure that describes modelling of free surfaces with surface tension by using finite elements was described by Ruschak [13]. The author pointed out that using the surface divergence theorem the continuity requirement on the fluid-fluid interface can be lowered and as a result the interface can be approximated by piecewise linear functions. This finding significantly simplified the problem at hand and is incorporated in this work.

In the Eulerian framework Brackbill *et al.* [3] introduced *continuum surface force* (CSF) model as a method for modelling surface tension by con-

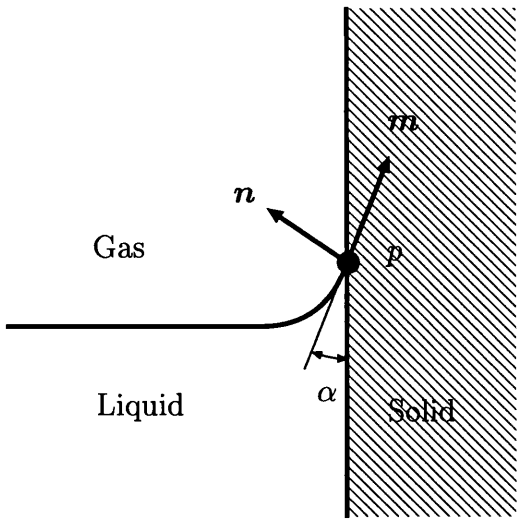

Figure 5.1: Condition at the contact line.

sidering surface tension as a continuous, three-dimensional effect across the interface. Since then combinations of CSF model and VOF become very popular to solve numerically free surface problem in Eulerian framework [8, 9, 14].

Recently some attempts were also carried out to use other numerical methods, such as boundary elements, to solve surface tension driven problems [12, 11, 10].

This chapter is concerned with a technique to incorporate the surface tension effects in the framework of Lagrangian finite element method. The fact that Lagrangian description represents the free-surface boundary explicitly, makes the approach in which surface tension is included as boundary condition a natural choice. This technique is implemented for two dimensional, as well as axisymmetric problem in conjunction with a bilinear finite element.

The surface tension model considered is based on the Laplace-Young equation in which the surface tension coefficient is assumed constant over the surface. At the three-phase contact-line the contact angle is also regarded as constant. As an additional assumption, the second fluid in the system is assumed to be in gaseous state so that its viscosity can be neglected an their pressure is taken as a datum.

5.1 Continuum Formulation

In the presence of surface tension on the free surface boundaries, the weak form of the initial boundary value problem, (4.21)-(4.23), in its spatial ver-

sion, can be written in the form

$$G(\boldsymbol{u},\boldsymbol{w}) := \int_{\Omega_t} (\boldsymbol{\sigma}:\nabla\boldsymbol{w} - \rho(\boldsymbol{b}-\ddot{\boldsymbol{u}})\cdot\boldsymbol{w})\,\mathrm{d}v - \int_{\partial\Omega_t^{\sigma}} \bar{\boldsymbol{t}}\cdot\boldsymbol{w}\,\mathrm{d}a - \\ - \int_{\partial\Omega_t^{\gamma}} (-p_{\mathrm{ext}}\boldsymbol{n}\cdot\boldsymbol{w} + 2H\gamma\boldsymbol{n}\cdot\boldsymbol{w})\,\mathrm{d}a = 0, \quad \forall\boldsymbol{w}\in\mathscr{U} \quad (5.1)$$

where $\boldsymbol{b}$ and $\bar{\boldsymbol{t}}$ are respectively the body force and surface traction fields referred to the current configuration and $\mathscr{U}$ is the space of virtual displacements of $\mathscr{B}$ defined by

$$\mathscr{U} = \{\boldsymbol{w} : \overline{\Omega}_t \times \mathscr{I} \to \mathscr{V} \mid \boldsymbol{w}(\boldsymbol{x},t) = \boldsymbol{0} \quad \text{on} \quad \boldsymbol{x}\in\partial\Omega_t^{\varphi}\}.$$

It is well known that a straightforward finite element discretization of Equation (5.1) requires elements with boundaries given by polynomials of at least second order and C^1 continuity across the element boundaries [13, 1], due to the fact that the mean curvature, H, involves second derivatives of the surface location. This requirement can be reduced by employing surface divergence theorem on the third integral on the right-hand side of Equation (5.1), which states that for arbitrary vector field $\boldsymbol{w}$ on the surface

$$\int_{\partial\Omega_t^{\gamma}} \nabla_s\cdot\boldsymbol{w}\,\mathrm{d}a = \int_{\partial\Omega_t^{c}} \boldsymbol{w}\cdot\boldsymbol{m}\,\mathrm{d}s - \int_{\partial\Omega_t^{\gamma}} 2H\boldsymbol{w}\cdot\boldsymbol{n}\,\mathrm{d}a. \quad (5.2)$$

where $\partial\Omega_t^c$ is the boundary curve of the surface $\partial\Omega_t^{\gamma}$ and $\boldsymbol{m}\in\mathscr{T}_{\boldsymbol{p}}$ is a unit vector that lies on the tangent plane of the surface $\partial\Omega_t^{\gamma}$ at point $\boldsymbol{p}$ and is orthogonal to the curve $\partial\Omega_t^c$ (Fig.5.1).

The weak form (5.1) may then be expressed as

$$G(\boldsymbol{u},\boldsymbol{w}) := \int_{\Omega_t} (\boldsymbol{\sigma}:\nabla\boldsymbol{w} - \rho(\boldsymbol{b}-\ddot{\boldsymbol{u}})\cdot\boldsymbol{w})\ \mathrm{d}v - \int_{\partial\Omega_t^{\sigma}} \bar{\boldsymbol{t}}\cdot\boldsymbol{w}\,\mathrm{d}a - \\ - \int_{\partial\Omega_t^{\gamma}} (-p_{\mathrm{ext}}\,\boldsymbol{n}\cdot\boldsymbol{w})\ \mathrm{d}a + \\ + \int_{\partial\Omega_t^{\gamma}} (\gamma\nabla_s\cdot\boldsymbol{w})\ \mathrm{d}a - \int_{\partial\Omega_t^{c}} (\gamma\boldsymbol{w}\cdot\boldsymbol{m})\ \mathrm{d}s = 0 \quad \forall\boldsymbol{w}\in\mathscr{U}. \quad (5.3)$$

Hence the finite element formulation of the surface tension results in two additional integrals which need to be evaluated over the fluid-gas interface and along the three-phase contact line, respectively.

5.2 Finite Element Formulation

Following procedure described in previous chapter, the finite element approximation of the expression (5.3) is obtained by introducing the finite dimensional subspaces, $\mathscr{K}^h$ and $\mathscr{U}^h$, of the space of kinematically admissible deformation $\mathscr{K}$ of $\mathscr{B}$ and the space of virtual displacements of $\mathscr{B}$, respectively. Thus, the discrete counterparts of (5.3) become

$$
\begin{aligned}
G(\boldsymbol{u}^h, \boldsymbol{w}^h) := & \int_{(\Omega_{n+1})^h} \left(\boldsymbol{\sigma}(\boldsymbol{u}^h, p^h) : \nabla \boldsymbol{w}^h - \rho(\boldsymbol{b} - \ddot{\boldsymbol{u}}^h) \cdot \boldsymbol{w}^h\right) \mathrm{d}v - \\
& - \int_{(\partial\Omega^{\sigma}_{n+1})^h} \bar{\boldsymbol{t}}(\boldsymbol{u}^h) \cdot \boldsymbol{w}^h \, \mathrm{d}a - \int_{(\partial\Omega^{\gamma}_{n+1})^h} \left(-p_{\text{ext}} \boldsymbol{n}(\boldsymbol{u}^h) \cdot \boldsymbol{w}^h\right) \mathrm{d}a + \\
& + \int_{(\partial\Omega^{\gamma}_{n+1})^h} \left(\gamma \nabla_s \cdot \boldsymbol{w}^h\right) \mathrm{d}a - \int_{(\partial\Omega^{c}_{n+1})^h} \left(\gamma \boldsymbol{w}^h \cdot \boldsymbol{m}(\boldsymbol{u}^h)\right) \mathrm{d}s = 0 \quad (5.4)
\end{aligned}
$$

Notice that the surface gradient ∇_s depends on $\boldsymbol{u}^h$ as well, and its discretized form can be expressed as $\nabla_s := \left(\boldsymbol{I} - \boldsymbol{n}(\boldsymbol{u}^h) \otimes \boldsymbol{n}(\boldsymbol{u}^h)\right) \nabla$.

The resulting system of nonlinear ordinary differential equations then can be discretized in time using either implicit or explicit temporal discretization procedures. If implicit time discretization procedure is used, as in Chapter 4, this renders a set of nonlinear algebraic equations and Newton-Raphson iterative procedure is usually used to speed up the convergence. Additional contributions to the stiffness matrix come from the surface tension and contact angle terms, due to the fact that at time t_{n+1} they depend nonlinearly on the nodal point displacements at time t_{n+1}. This is analog to nonconservative external force case.

Expression (5.4) can be simplified by assuming the ambient fluid is air and its pressure is considered as a datum, so that the third integral on the right-hand side of equation (5.4) can be eliminated. Therefore, the element force vector contributed by the surface tension has the following expression

$$
\mathbb{F}_e^{\text{SURF}} = \int_{(\partial\Omega^{c}_{n+1})^e} \gamma \mathbb{N}^T \boldsymbol{m} \, \mathrm{d}s - \int_{(\partial\Omega^{\gamma}_{n+1})^e} \gamma \nabla_s \mathbb{N} \, \mathrm{d}a \quad (5.5)
$$

with $\mathbb{N}$ being the interpolation matrix of the boundary of element (e).

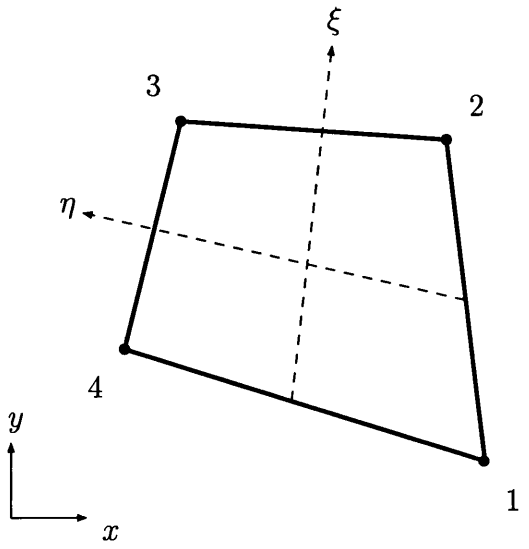

Figure 5.2: Bilinear quadrilateral element.

5.3 Two-dimensional problem

5.3.1 The force vector

Consider an isoparametric bilinear quadrilateral element with the interpolation functions [7, 15, 2] given by

$$N_1(\xi,\eta) = \tfrac{1}{4}(1-\xi)(1-\eta),$$

$$N_2(\xi,\eta) = \tfrac{1}{4}(1+\xi)(1-\eta),$$

$$N_3(\xi,\eta) = \tfrac{1}{4}(1+\xi)(1+\eta),$$

$$N_4(\xi,\eta) = \tfrac{1}{4}(1-\xi)(1+\eta).$$

First Procedure

The position vector of any point and virtual displacements vector can be expressed as a linear combination of N_1, N_2, N_3, and N_4

$$\begin{aligned}\{\boldsymbol{x}^h\} &= [\mathbb{N}]\{\hat{\boldsymbol{x}}\} \\ &= \left\{ \begin{array}{l} N_1\hat{x}_1 + N_2\hat{x}_2 + N_3\hat{x}_3 + N_4\hat{x}_4 \\ \\ N_1\hat{y}_1 + N_2\hat{y}_2 + N_3\hat{y}_3 + N_4\hat{y}_4 \end{array} \right\}. \end{aligned} \tag{5.6}$$

$$\begin{aligned}\{\boldsymbol{w}^h\} &= [\mathbb{N}]\{\hat{\boldsymbol{w}}\} \\ &= \left\{ \begin{array}{l} N_1\hat{w}_x^1 + N_2\hat{w}_x^2 + N_3\hat{w}_x^3 + N_4\hat{w}_x^4 \\ \\ N_1\hat{w}_y^1 + N_2\hat{w}_y^2 + N_3\hat{w}_y^3 + N_4\hat{w}_y^4 \end{array} \right\}. \end{aligned} \tag{5.7}$$

The matrix of the jacobian of coordinate transformation is given by

$$\mathbb{J} = \left[\begin{array}{cc} \frac{\partial x}{\partial \xi} & \frac{\partial x}{\partial \eta} \\ \\ \frac{\partial y}{\partial \xi} & \frac{\partial y}{\partial \eta} \end{array} \right]. \tag{5.8}$$

The gradient vector is given by

$$\nabla = \frac{1}{\det[\mathbb{J}]} \left[\begin{array}{cc} \frac{\partial y}{\partial \eta} & -\frac{\partial x}{\partial \eta} \\ \\ -\frac{\partial y}{\partial \xi} & \frac{\partial x}{\partial \xi} \end{array} \right] \left\{ \begin{array}{c} \frac{\partial}{\partial \xi} \\ \\ \frac{\partial}{\partial \eta} \end{array} \right\}. \tag{5.9}$$

By assuming that a surface tension acts on the set in which $\eta = -1$, the unit normal $\boldsymbol{n}$ at any point on this side is given by

$$\{\boldsymbol{n}\} = \frac{1}{L_e} \left\{ \begin{array}{c} -(y_2 - y_1) \\ \\ (x_2 - x_1) \end{array} \right\}, \tag{5.10}$$

where $L_e = [(x_2 - x_1)^2 + (y_2 - y_1)^2]^{\frac{1}{2}}$, is the length of the side of the element. The projection tensor $\boldsymbol{P}$ in the matrix form has the expression

$$\begin{aligned} \boldsymbol{P} &= \boldsymbol{I} - \boldsymbol{n} \otimes \boldsymbol{n} \\ &= \frac{1}{L_e^2} \begin{bmatrix} (x_2 - x_1)^2 & (x_2 - x_1)(y_2 - y_1) \\ (x_2 - x_1)(y_2 - y_1) & (y_2 - y_1)^2 \end{bmatrix}. \end{aligned} \tag{5.11}$$

The surface gradient is defined as

$$\nabla_s = \boldsymbol{P} \nabla. \tag{5.12}$$

Substituting equations (5.7) and (5.12) into the two dimensional version of the third integral in the equation (5.4) gives

$$\int_{(\partial\Omega^{\gamma}_{n+1})^e} \left(\gamma \nabla_s \cdot \boldsymbol{w}^h\right) \, \mathrm{d}s = \int_{(\partial\Omega^{\gamma}_{n+1})^e} \left(\gamma \boldsymbol{P} \nabla \cdot \boldsymbol{w}^h\right) \, \mathrm{d}s. \tag{5.13}$$

Based on the assumption that the surface tension acts on the side $\eta = -1$, the integrand in equation (5.13) has to be evaluated at $\eta = -1$ and integrated with respect to ξ with the limits of integral from $\xi = -1$ to $\xi = 1$. The surface tension virtual work for an element can be expressed as

$$\int_{(\partial\Omega^{\gamma}_{n+1})^e} \left(\gamma \nabla_s \cdot \boldsymbol{w}^h\right) \, \mathrm{d}s = \int_{-1}^{1} \gamma \left[\det[\mathbb{J}] \boldsymbol{P} \nabla \cdot \boldsymbol{w}^h\right]_{\eta=-1} \mathrm{d}\xi. \tag{5.14}$$

Evaluation of integral on the right-hand side of equation (5.14) is difficult. Thus, this integration can be carried out numerically using Gauss quadrature or using commercial symbolic operation mathematical software to obtain an explicit expression. The advantage of having explicit expression is its computational efficiency. By using commercial symbolic operation mathematical software the surface tension virtual work for an element has the expression

$$\int_{(\partial\Omega^{\gamma}_{n+1})^e} \left(\gamma \nabla_s \cdot \boldsymbol{w}^h\right) \, \mathrm{d}s = \{\bar{\boldsymbol{w}}\}^T \frac{\gamma}{L_e} \begin{Bmatrix} -(x_2 - x_1) \\ -(y_2 - y_1) \\ (x_2 - x_1) \\ (y_2 - y_1) \end{Bmatrix}, \tag{5.15}$$

where $\{\bar{\boldsymbol{w}}\}^T = [\bar{w}_x^1 \quad \bar{w}_y^1 \quad \bar{w}_x^2 \quad \bar{w}_y^2]$ is the reduced form of $\{\hat{\boldsymbol{w}}\}^T$ due to the fact that interior node 3 and 4 do not contribute to the surface tension virtual work. The element surface force vector for two dimensional problem is then given by

$$\mathbb{F}_e^{\text{SURF}} = \frac{\gamma}{L_e} \begin{Bmatrix} -(x_2 - x_1) \\ -(y_2 - y_1) \\ (x_2 - x_1) \\ (y_2 - y_1) \end{Bmatrix}. \tag{5.16}$$

Second Procedure

Expression (5.16) can be obtained in a much simpler way by considering the side where the surface tension acts as a line parameterized by arc length $\xi \in [-1, 1]$. Hence the second integral on the right-hand side of equation (5.5) can be written as

$$\int_{(\partial\Omega_{n+1}^{\gamma})^e} \gamma \nabla_s \mathbb{N} \, \mathrm{d}a = \int_{\xi_0}^{\xi_1} \gamma \boldsymbol{t} \cdot \frac{\mathrm{d}\mathbb{N}}{\mathrm{d}\xi} \, \mathrm{d}\xi, \tag{5.17}$$

where $\boldsymbol{t}$ is a unit tangent vector at any point on the side where the surface tension act. Let the surface tension acts on the side in which $\eta = -1$ (see Figure 5.2), the shape function matrix $\mathbb{N}$ for this side is given by

$$[\mathbb{N}] = \begin{bmatrix} \frac{1}{2}(1-\xi) & 0 & \frac{1}{2}(1+\xi) & 0 \\ 0 & \frac{1}{2}(1-\xi) & 0 & \frac{1}{2}(1+\xi) \end{bmatrix}, \tag{5.18}$$

and the position vector of any point on that side is given by

$$\{\boldsymbol{x}\} = [\mathbb{N}]\{\hat{\boldsymbol{x}}\}$$

$$= \begin{bmatrix} \frac{1}{2}(1-\xi) & 0 & \frac{1}{2}(1+\xi) & 0 \\ 0 & \frac{1}{2}(1-\xi) & 0 & \frac{1}{2}(1+\xi) \end{bmatrix} \begin{Bmatrix} x_1 \\ y_1 \\ x_2 \\ y_2 \end{Bmatrix}. \quad (5.19)$$

The unit tangent vector is given by

$$\boldsymbol{t} = \frac{1}{L_e} \begin{Bmatrix} (x_2 - x_1) \\ (y_2 - y_1) \end{Bmatrix}, \quad (5.20)$$

and $\mathrm{d}\mathbb{N}/\mathrm{d}\xi$ is given by

$$\frac{\mathrm{d}\mathbb{N}}{\mathrm{d}\xi} = \begin{bmatrix} -\frac{1}{2} & 0 & \frac{1}{2} & 0 \\ 0 & -\frac{1}{2} & 0 & \frac{1}{2} \end{bmatrix}. \quad (5.21)$$

By substituting equations (5.20) and (5.21) into equation (5.17) and taking the limits of integral $\xi_0 = -1$ and $\xi_1 = 1$ expression (5.16) can be recovered as

$$\int_{-1}^{1} \frac{\gamma}{L_e} \begin{bmatrix} -\frac{1}{2} & 0 \\ 0 & -\frac{1}{2} \\ \frac{1}{2} & 0 \\ 0 & \frac{1}{2} \end{bmatrix} \begin{Bmatrix} (x_2 - x_1) \\ (y_2 - y_1) \end{Bmatrix} \mathrm{d}\xi = \frac{\gamma}{L_e} \begin{Bmatrix} -(x_2 - x_1) \\ -(y_2 - y_1) \\ (x_2 - x_1) \\ (y_2 - y_1) \end{Bmatrix} \quad (5.22)$$

5.3.2 The stiffness matrix

The element surface tension stiffness matrix is obtained by taking the directional derivative of the element surface tension force in the direction of the incremental displacement, i.e.

$$\mathbb{K}^{\text{SURF}}(\mathbb{U})\,[\Delta\mathbb{U}] = \frac{\mathrm{d}}{\mathrm{d}\varepsilon}\bigg|_{\varepsilon=0} \mathbb{F}^{\text{SURF}}(\mathbb{U} + \varepsilon\Delta\mathbb{U}). \tag{5.23}$$

For two dimensional problem the element surface tension stiffness matrix is given by

$$\mathbb{K}_e^{\text{SURF}} = \frac{\gamma}{L_e}\begin{bmatrix} 1 & 0 & -1 & 0 \\ 0 & 1 & 0 & -1 \\ -1 & 0 & 1 & 0 \\ 0 & -1 & 0 & 1 \end{bmatrix} - \frac{\gamma}{L_e^3}\begin{Bmatrix} -(x_2 - x_1) \\ -(y_2 - y_1) \\ (x_2 - x_1) \\ (y_2 - y_1) \end{Bmatrix}\begin{Bmatrix} -(x_2 - x_1) \\ -(y_2 - y_1) \\ (x_2 - x_1) \\ (y_2 - y_1) \end{Bmatrix}^T . \tag{5.24}$$

5.3.3 Contact angle contribution

Lets node 1 in figure 5.2 is a contact point and the unit vector $\boldsymbol{m}$ is a function of the prescribed contact angle α. The vector $\boldsymbol{m}$ is given as

$$\boldsymbol{m} = \left\{ \begin{array}{c} \cos\alpha \\ -\sin\alpha \end{array} \right\} \tag{5.25}$$

For two dimensional problem, the last integral in equation (5.4) become an end condition. By substituting equations (5.18) and (5.25) into equation (5.4) gives

$$\begin{aligned} \int_{(\partial\Omega^e_{n+1})^e} \gamma\, \mathbb{N}^T \boldsymbol{m}\, \mathrm{d}s &= \gamma \left[\begin{array}{cc} \frac{1}{2}(1-\xi) & 0 \\ 0 & \frac{1}{2}(1-\xi) \\ \frac{1}{2}(1+\xi) & 0 \\ 0 & \frac{1}{2}(1+\xi) \end{array} \right] \left\{ \begin{array}{c} \cos\alpha \\ -\sin\alpha \end{array} \right\} \\ &= \gamma \left\{ \begin{array}{c} \frac{1}{2}(1-\xi)\cos\alpha \\ -\frac{1}{2}(1-\xi)\sin\alpha \\ \frac{1}{2}(1+\xi)\cos\alpha \\ -\frac{1}{2}(1+\xi)\sin\alpha \end{array} \right\}. \end{aligned} \tag{5.26}$$

Evaluating equation (5.26) for $\xi = -1$ and considering only the non-zero term, gives the contact angle contribution to the force vector as follows

$$\mathbb{F}_e^{\mathrm{CONT}} = \gamma \left\{ \begin{array}{c} \cos\alpha \\ -\sin\alpha \end{array} \right\}. \tag{5.27}$$

The fact that both γ and α are assumed to be constant, means that there is no contact angle contribution to the stiffness matrix for two-dimensional case.

5.4 Axisymmetric case

5.4.1 The force vector

Consider an axisymmetric bilinear quadrilateral element, shown in Figure 5.3 and assume that one of its side is being subjected to surface tension boundary condition.

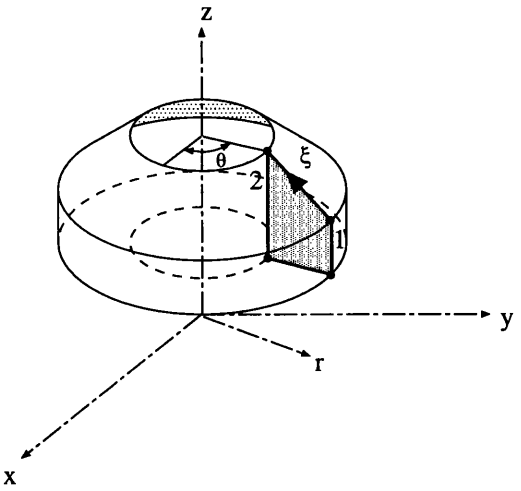

Figure 5.3: Axisymmetric bilinear quadrilateral element.

The shape function matrix for the surface of revolution generated by line $1-2$ take the form

$$\mathbb{N} = \begin{bmatrix} \frac{1}{2}(1-\xi)\cos\theta & 0 & \frac{1}{2}(1+\xi)\cos\theta & 0 \\ \frac{1}{2}(1-\xi)\sin\theta & 0 & \frac{1}{2}(1+\xi)\sin\theta & 0 \\ 0 & \frac{1}{2}(1-\xi) & 0 & \frac{1}{2}(1+\xi) \end{bmatrix}. \tag{5.28}$$

Then, the position vector of a point on the line 1 - 2 can be expressed as

$$\boldsymbol{x}(\xi,\theta) = \begin{Bmatrix} \frac{1}{2}(1-\xi)r_1\cos\theta + \frac{1}{2}(1+\xi)r_2\cos\theta \\ \frac{1}{2}(1-\xi)r_1\sin\theta + \frac{1}{2}(1+\xi)r_2\sin\theta \\ \frac{1}{2}(1-\xi)z_1 + \frac{1}{2}(1+\xi)z_2 \end{Bmatrix} \tag{5.29}$$

where r_i and z_i are the nodal coordinates of a line element. The first fundamental form then have the expression

$$
\begin{aligned}
A &\equiv \frac{\partial \boldsymbol{x}(\xi,\theta)}{\partial \xi} \cdot \frac{\partial \boldsymbol{x}(\xi,\theta)}{\partial \xi} = \frac{1}{4}\left[(r_1 - r_2)^2 + (z_1 - z_2)^2\right] \\
B &\equiv \frac{\partial \boldsymbol{x}(\xi,\theta)}{\partial \theta} \cdot \frac{\partial \boldsymbol{x}(\xi,\theta)}{\partial \theta} = \frac{1}{4}\left[(1-\xi)r_1 + (1+\xi)r_2\right]^2
\end{aligned} \tag{5.30}
$$

and the elemental area $\mathrm{d}a$ is given as

$$
\mathrm{d}a = \sqrt{AB}\mathrm{d}\xi\mathrm{d}\theta \tag{5.31}
$$

The surface gradient of the shape function matrix is given by

$$
\nabla_s \mathbb{N} = \frac{1}{A}\frac{\partial \mathbb{N}^T}{\partial \xi}\frac{\partial \boldsymbol{x}(\xi,\theta)}{\partial \xi} + \frac{1}{B}\frac{\partial \mathbb{N}^T}{\partial \theta}\frac{\partial \boldsymbol{x}(\xi,\theta)}{\partial \theta} \tag{5.32}
$$

Substituting equations (5.28), (5.31) and (5.32) into the second integral on the right-hand side of equation (5.5), gives

$$
\gamma \int_{(\partial\Omega^{\gamma}_{n+1})^e} \nabla_s \mathbb{N}\, \mathrm{d}a = \gamma \int_{-1}^{1}\int_{0}^{2\pi} \frac{\sqrt{AB}}{A}\frac{\partial \mathbb{N}^T}{\partial \xi}\frac{\partial \boldsymbol{x}(\xi,\theta)}{\partial \xi}\,\mathrm{d}\xi\mathrm{d}\theta + \gamma \int_{-1}^{1}\int_{0}^{2\pi} \frac{\sqrt{AB}}{B}\frac{\partial \mathbb{N}^T}{\partial \theta}\frac{\partial \boldsymbol{x}(\xi,\theta)}{\partial \theta}\,\mathrm{d}\xi\mathrm{d}\theta
$$

After some algebraic manipulation the above expression takes the form

$$
\begin{aligned}
\gamma \int_{(\partial\Omega^{\gamma}_{n+1})^e} \nabla_s \mathbb{N}\, \mathrm{d}a = {} & \frac{\pi\gamma(r_1 + r_2)}{\left[(r_1 - r_2)^2 + (z_1 - z_2)^2\right]^{\frac{1}{2}}} \begin{Bmatrix} r_1 - r_2 \\ z_1 - z_2 \\ r_2 - r_1 \\ z_2 - z_1 \end{Bmatrix} + \\
& \pi\gamma\left[(r_1 - r_2)^2 + (z_1 - z_2)^2\right]^{\frac{1}{2}} \begin{Bmatrix} 1 \\ 0 \\ 1 \\ 0 \end{Bmatrix}
\end{aligned} \tag{5.33}
$$

5.4.2 The stiffness matrix

The element surface tension stiffness matrix for axisymmetric case has the following expression

$$\mathbb{K}_e^{\text{SURF}} = \mathbb{K}_{\text{I}}^{\text{SURF}} + \mathbb{K}_{\text{II}}^{\text{SURF}} + \mathbb{K}_{\text{III}}^{\text{SURF}} \tag{5.34}$$

where

$$\mathbb{K}_{\text{I}}^{\text{SURF}} = \frac{\pi\gamma}{L_e}\begin{bmatrix} 2r_1 & 0 & -2r_2 & 0 \\ (z_1 - z_2) & (r_1 + r_2) & (z_1 - z_2) & -(r_1 + r_2) \\ -2r_1 & 0 & 2r_2 & 0 \\ -(z_1 - z_2) & -(r_1 + r_2) & -(z1 - z_2) & (r_1 + r_2) \end{bmatrix}$$

$$\mathbb{K}_{\text{II}}^{\text{SURF}} = -\frac{\pi\gamma}{L_e^3}\begin{Bmatrix} (r_1 + r_2)(r_1 - r_2) \\ (r_1 + r_2)(z_1 - z_2) \\ (r_1 + r_2)(r_2 - r_1) \\ (r_1 + r_2)(z_2 - z_1) \end{Bmatrix}\begin{Bmatrix} (r_1 - r_2) \\ (z_1 - z_2) \\ (r_2 - r_1) \\ (z_2 - z_1) \end{Bmatrix}^T$$

$$\mathbb{K}_{\text{III}}^{\text{SURF}} = \frac{\pi\gamma}{L_e}\begin{Bmatrix} 1 \\ 0 \\ 1 \\ 0 \end{Bmatrix}\begin{Bmatrix} (r_1 - r_2) \\ (z_1 - z_2) \\ (r_2 - r_1) \\ (z_2 - z_1) \end{Bmatrix}^T$$

and $L_e = [(r_1 - r_2)^2 + (z_1 - z_2)^2]^{\frac{1}{2}}$

5.4.3 Contact angle contribution

The force vector

Assume that line generated by node 1 in figure 5.3 is the contact line and consider the unit vector $\boldsymbol{m}$ as a function of the prescribed contact angle α and is independent of displacement. The shape function matrix for this line is

$$\mathbb{N} = \begin{bmatrix} \frac{1}{2}(1-\xi)\cos\theta & 0 \\ \frac{1}{2}(1-\xi)\sin\theta & 0 \\ 0 & \frac{1}{2}(1-\xi) \end{bmatrix} \tag{5.35}$$

and the vector $\boldsymbol{m}$ as a function of contact angle α is given as

$$\boldsymbol{m} = \begin{Bmatrix} \cos\theta\cos\alpha \\ \sin\theta\cos\alpha \\ -\sin\alpha \end{Bmatrix} \tag{5.36}$$

Substituting equations (5.35) and (5.36) into the first integral in equation (5.5), using the relation $\mathrm{d}s = \frac{1}{2}(1-\xi)r_1\mathrm{d}\theta$ and evaluating expressions for $\xi = -1$ gives

$$\begin{aligned} \int_{(\partial\Omega^c_{n+1})^e} \gamma\,\mathbb{N}^T\boldsymbol{m}\,\mathrm{d}s &= \int_0^{2\pi} \gamma \begin{bmatrix} \cos\theta & \sin\theta & 0 \\ & & \\ 0 & 0 & 1 \end{bmatrix} \begin{Bmatrix} \cos\theta\cos\alpha \\ \sin\theta\cos\alpha \\ -\sin\alpha \end{Bmatrix} r_1\mathrm{d}\theta \\ &= 2\pi\gamma r_1 \begin{Bmatrix} \cos\alpha \\ \\ -\sin\alpha \end{Bmatrix} \end{aligned} \tag{5.37}$$

The stiffness matrix

Contribution from the contact line to the tangent stiffness matrix is obtained by taking the directional derivative of the contact line force equation (5.37) in the direction of displacement and has the expression

$$\mathbb{K}_e^{\mathrm{CONT}} = 2\pi\gamma \begin{bmatrix} \cos\alpha & 0 \\ & \\ -\sin\alpha & 0 \end{bmatrix} \tag{5.38}$$

Table 5.1: Physical properties of water.

density ρ (gr/cm^3)	0.998
viscosity μ (dyne s/cm^2)	1.01×10^{-2}
surface tension γ (dyne/cm)	73.0

5.5 Numerical example

As mentioned previously in section 2.4, in the absence of external forces the sum of the principal curvatures must be constant over any surface of separation of an unsupported drop if it is in mechanical equilibrium. In other words, the drop must be of the spherical shape for three dimensional or axisymmetric case or circular one in two dimensional case. The first test carried out to see whether the numerical technique described in this chapter is applicable is based on this simple fact. Here, a drop of water of arbitrary initial shape under influence of surface tension is left to deform until mechanical equilibrium is reached. In this particular example, the initial shape is taken to be square of 1 cm width. Starting from this example water will be used as the liquid in all examples throughout the rest of this thesis. Its mechanical properties are assumed to be constant and are listed in the table 5.1. The surface tension is taken to be constant and the value describe water-air interface.

Figure 5.4 shows evolution of finite element mesh for several different increment steps.

Although the result from this example agrees with what is predicted by the theory further tests need to be carried out to ensure the accuracy, reliability and robustness of the proposed technique.

5.6 Closure

A numerical technique to incorporate the surface tension effects into a finite element analysis of free surface flows has been discussed in this chapter. The approach adopted in this work is based on the use of the surface divergence theorem to reduce the C^1 continuity requirement across the element boundary to the simpler C^0 requirement. The derivation of the expression for element surface tension force vector for two dimensional and axisymmetric problems was given in detail. For the bilinear quadrilateral element the expression for the element surface tension force vector is relatively simple,

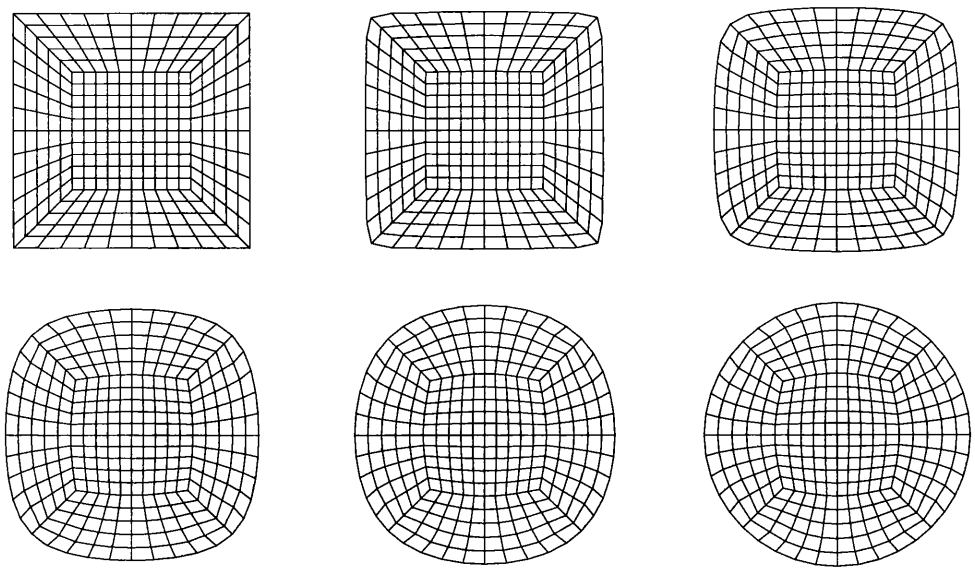

Figure 5.4: Evolution of equilibrium shapes of unsupported drop under no external force at different increment steps.

and the explicit form can be obtained. In addition the expression for contact angle force vector was also derived. The explicit expression of the stiffness matrix associated with the Newton-Raphson iterative procedure was also presented.

In the next chapter the performance of the technique to incorporate surface tension effect into a finite element analysis developed in this chapter together with the finite element procedure for solving Lagrangian free surface flow problem developed in Chapter 4 will be validated for quasi-static condition. The numerical examples that will be carried out belong to a class of problems known as the *generalized Plateau problem.* For some simpler situations certain problems from this class can be solved analytically, thus providing a means to assess the accuracy of the finite elements solution.

Bibliography

[1] P. Bach and O. Hassager. An algorithm for the use of the lagrangian specification in newtonian fluid mechanics and applications to free-surface flow. *J. Fluid Mech.*, 152:173 – 190, 1985.

[2] K.J. Bathe. *Finite Element Procedures.* Prentice-Hall, Englewood Cliffs, New Jersey, 1996.

[3] J. U. Brackbill, D. B. Kothe, and C. Zemach. A continuum method for modelling surface tension. *J. Comp. Physics*, 100:335 – 354, 1992.

[4] B. J. Daly. Numerical study of the effect of surface tension on interface stability. *Phys. Fluids*, 12:1340 – 1354, 1969.

[5] B. J. Daly. A technique for including surface tension effects in hydrodynamic calculation. *J. Comp. Physics*, 4:97 – 117, 1969.

[6] B. J. Daly and W. E. Pracht. Numerical study of density-current surges. *Phys. Fluids*, 11:15 – 30, 1968.

[7] T.J.R. Hughes. *The Finite Element Method. Linear Static and Dynamic Finite Element Analysis.* Prentice-Hall, Englewood Cliffs, New Jersey, 1987.

[8] D. B. Kothe and R. C. Mjolsness. RIPPLE: A new model for incompressible flows with free surfaces. *AIAA J.*, 30:2694–2700, 1992.

[9] B. Lafaurie, C. Nardone, R. Scardovelli, S. Zaleski, and G. Zanetti. Modelling merging and fragmentation in multiphase flows with SURFER. *J. Comp. Physics.*, 113:134 – 147, 1994.

[10] C. Pozrikidis. Interfacial dynamics for stokes flow. *J. Comp. Phys.*, 169:250 – 301, 2001.

[11] C. Pozrikidis. Three-dimensional oscillations of inviscid drops induced by surface tension. *Comp. Fluids*, 30:417 – 444, 2001.

[12] A.R.M. Primo, L.C. Wrobel, and H. Power. Low reynolds number deformation of vicous drops in a bounded flow region under surface tension. *Math. Comp. Model.*, 31:99 – 118, 2000.

[13] K. J. Ruschak. A method for incorporating free boundaries with surface tension in finite element fluid-flow simulators. *Int. J. Num. Meth. Engng.*, 15:639 – 648, 1980.

[14] J. Wu, S.T. Yu, and B.N. Jiang. Simulation of two-fluid flows by the least-squares finite element method using a continuum surface tension model. *Int. J. Num. Meth. Engng*, 42:583 – 600, 1998.

[15] O.C. Zienkiewicz and R.L. Taylor. *The Finite Element Method – Vol.1: Basic Formulation and Linear Problems.* McGraw-Hill, 1989.

Chapter 6

Validation I: Quasi-static Problems

In this chapter some numerical examples will be presented. These examples are intended for further validation of the techniques that have been used to include surface tension into finite element analysis and the incremental flow formulation presented in previous chapters. Examples in this chapter are limited to equilibrium problems in which the inertial forces can be neglected.

A class of capillary problems, known as the *generalized Plateau problem*, has been selected. This problem is governed by the Laplace-Young equation and basically consists of finding the shape of a drop of liquid for a given volume under surface tension, gravity and geometrical constraints. Attention is focused to axisymmetric case and the geometrical constraints involved can be prescribed either at the bottom, at the top, or at both ends of the drop which relate to, respectively, *sessile drops*, *pendent drops*, and *liquid bridges*.

The reason for the choice of this particular problem is based on two considerations. The first consideration is that for axisymmetric case the problem can be reduced to an ordinary differential equation (ODE) by employing certain parametrization [10, 2, 12]. The resulting ODE then can be integrated numerically using standard numerical integration schemes for the ordinary differential equations. The second one is that this problem has attracted so much attention from scientific community since the end of nineteenth century. Therefore, a substantial amount of work is available for the comparison purposes. Bashforth and Adams (1883) obtained tables for sessile drops and pendent drops using hand-calculated coefficients of Taylor series and Lord Kelvin (1886) produced a number of profiles of sessile drops and pendent drops using first order graphical integration method. Over the years Bashforth and Adams tables have been extended by a number of authors. With the availability of high speed computer in the early seventies, more advanced

numerical integration procedures were used to give more accurate results [10, 5] and the existing tables were extended to include liquid bridge profiles.

Another approach of solving generalized Plateau problem is through numerically solving the associated variational calculus problem. The numerical methods commonly used are based on finite element methods [4, 7, 3]. In the approach by Brakke [3], the objective is to minimize the total surface energy subject to constraints. The surface is represented as simplicial complex and the finite element is used to approximate the shape of the surface. A surface of somewhat arbitrary shape is given as data. Finally, the surface is evolved towards minimal energy by using an optimization method such as the gradient descent method.

In general, this class of problems does not always have a unique solution [6, 7]. In some situation it also suffers from the non-existence of solution, for example in a square capillary problem solution does not exist in the neighborhood of the corner for contact angle $\alpha < 45°$ [5]. According to Brown [4], the cause of this is a film of liquid that runs up the corner and rise past the point where its thickness is smaller than that allowed for a bulk phase. This makes the Laplace-Young equation invalid. Moreover, the existence of equilibrium of meniscus in physical sense implies mathematically not only equilibrium but also stable equilibrium solution [8]. Therefore, the examples are restricted to relatively small volume and certain geometric constraints to avoid the possibility of such difficulties appearing in the analysis.

6.1 Analytical Solution

The Laplace-Young equation that has been described in the previous chapters supplies the condition that has to be met at the interface between two immiscible liquids at the equilibrium. By choosing a certain parametrization for the mean curvature of the Laplace-Young equation, an ordinary differential equation (ODE) describing the shape of stationary interface can be obtained. For axisymmetric interfaces the resulting equation is a second order non-linear ordinary equation involving an unspecified constant. Following the standard practice [12], this equation can be decomposed into a system of two first order differential equation and then solved either analytically or numerically.

6.1.1 Equilibrium shapes of sessile drops

The simplest one among the generalized Plateau problems is the problem of finding the equilibrium shape of a sessile drop of a given volume resting on

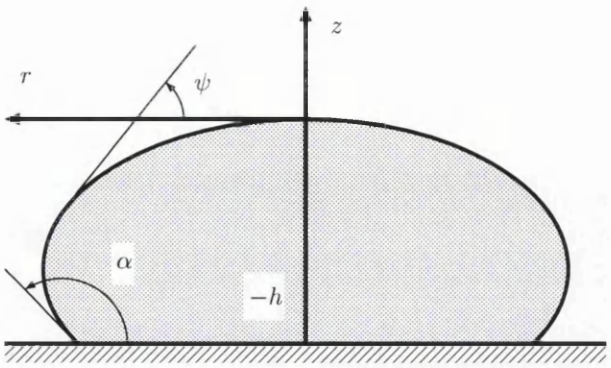

Figure 6.1: Parametrization for sessile drop sitting on a flat surface.

a flat surface, as shown in figure 6.1. The equation governing this particular problem is obtained by using parametric description of the form

$$r = f(z),$$

since z may not be a single valued function of r [12]. The mean curvature associated with the chosen parametrization is

$$H = \frac{1}{2}\frac{1 + f'^2 - ff''}{f(1 + f'^2)^{3/2}}. \tag{6.1}$$

Substituting equation (6.1) into the particular form of the Laplace-Young equation in which the gravitational effect is taken into account

$$2H = \frac{\Delta\rho}{\gamma}\boldsymbol{g} \cdot \boldsymbol{x} + B, \tag{6.2}$$

results in

$$f'' = \left(\frac{z}{l^2} - B\right)(1 + f'^2)^{3/2} + \frac{1 + f'^2}{f}, \tag{6.3}$$

where $l = (\gamma/(\Delta\rho\ g))^{1/2}$ is the capillary length, $\Delta\rho = \rho^{(1)} - \rho^{(2)}$ is the difference between the density of fluid 1 and fluid 2, and B is a constant. The value of B at the origin is equal to twice the mean curvature of the interface at the centreline. This is obtained by evaluating equation (6.2) at the origin.

Following the procedure described in [12] the nonlinear second order ordinary differential equation (6.3) can be decomposed into a set of two ordinary differential equation (ODE) by introducing parameter ψ defined by

$$\cot \psi = -f',$$

where ψ ranges from zero at the centreline of the drop to the value of α at the contact line as depicted in figure 6.1. The variables z and r now can be regarded as functions of ψ along the interface. By this particular choice of parametrization, the contact angle boundary condition is satisfied automatically. This decomposition procedure lead to the following system of two first order ODE

$$\frac{dz}{d\psi} = \frac{\sin\psi}{Q}, \qquad \text{and} \qquad \frac{dr}{d\psi} = -\frac{\cos\psi}{Q}, \tag{6.4}$$

where

$$Q = \left(\frac{\sin\psi}{r} + \frac{z}{l^2} - B\right), \tag{6.5}$$

with the boundary conditions at the centreline of the drop $r(0) = 0$ and $z(0) = 0$. It is also required that the volume of the drop has a specified value V, which gives another condition

$$\int_{-h}^{0} r^2\, dz = \frac{V}{\pi}, \tag{6.6}$$

and at the origin

$$\frac{dz}{d\psi} = 0, \qquad \text{and} \qquad \frac{dr}{d\psi} = \frac{2}{B}. \tag{6.7}$$

The equilibrium shape of a sessile drop can, now, be computed using the shooting method that involves the following steps [12]:

i.) For a given values of l, V and α, guess the value of B

ii.) Integrate equation (6.4) from $\psi = 0$ to α with equation (6.7) as initial conditions

iii.) Check whether equation (6.6) is fulfilled, and, if it is not, the computation is repeated with a new and improved value of B.

For convenience, the procedure is summerized in Box 6.1.

Box 6.1. Computation of Equilibrium Shape of a Sessile Drop

- Given the values of l, α, V and the guessed value of B.
- Integrate equation (6.4) using Euler method over interval $0 \leq \psi \leq \alpha$ (**Box 6.2**).
- Integrate equation (6.6) using trapezoidal rule (**Box 6.3**).
- If $|V - \bar{V}| \geq TOL$ repeat the process with new and improved value of B obtained by *bisection method.*

Box 6.2. Integration of equation (6.4) using Euler method

- Initial condition

$z_0 = 0.0,\ r_0 = 0.0,\ \psi_0 = 0.0,\ \left.\frac{dz}{d\psi}\right|_0 = 0.0,\ \left.\frac{dr}{d\psi}\right|_0 = \frac{2}{B}$

- Integrate equation (6.4) over the interval $0 \leq \psi \leq \alpha$ using Euler method

$\Delta\psi = \frac{\alpha}{N_{step}}$

DO WHILE $[i < N_{step}]$

IF $[i = 0]$ THEN

$z_i = z_0$

$r_i = r_0 + \frac{2}{B}$

ELSE

$$z_i = z_{i-1} + \Delta\psi \frac{\sin\psi_{i-1}}{\frac{\sin\psi_{i-1}}{r_{i-1}} + \frac{z_{i-1}}{l^2} - B}$$

$$r_i = r_{i-1} - \Delta\psi \frac{\cos\psi_{i-1}}{\frac{\sin\psi_{i-1}}{r_{i-1}} + \frac{z_{i-1}}{l^2} - B}$$

ENDIF

$\psi_i = \psi_{i-1} + \Delta\psi$

END DO

6.1.2 Equilibrium shape of a pendent drop

In general, the parametrization previously used to decompose the nonlinear second order ODE governing the equilibrium shape of a sessile drop can not

Box 6.3. Integration of equation (6.6) using trapezoidal rule

- Integrate equation (6.4) over the interval $0 \leq \psi \leq \alpha$ using trapezoidal rule

$\bar{V} = 0.0$

DO WHILE $[i \leq N_{step}]$

IF $[i = N_{step}]$ THEN

$$\bar{V} = \bar{V} + \frac{1}{2} r_i^2 \, \Delta\psi \frac{\sin\psi_{i-1}}{\frac{\sin\psi_{i-1}}{r_{i-1}} + \frac{z_{i-1}}{l^2} - B}$$

ELSE

$$\bar{V} = \bar{V} + r_i^2 \, \Delta\psi \frac{\sin\psi_{i-1}}{\frac{\sin\psi_{i-1}}{r_{i-1}} + \frac{z_{i-1}}{l^2} - B}$$

ENDIF

$\psi_i = \psi_{i-1} + \Delta\psi$

END DO

be used to decompose the one governing the equilibrium shape of a pendent drop. This is due to the fact that both z and r along the interface may not be a single valued function of ψ, in particular for large drops where the point of inflexion may be present.

Following the procedure proposed by Boucher and Evans [2], the parameter ψ employed is of the form

$$f' = \cot \, \psi,$$

and as a consequence the mean curvature has the following expression

$$H = \sin\psi \frac{d\psi}{dz} + \frac{\sin\psi}{r}.$$

The ordinary differential equation governing the equilibrium shape of a pendent drop now has the following expression

$$d\psi = \left(\frac{h - z}{2l^2} - \frac{\sin\psi}{r} \right) \, ds. \tag{6.8}$$

The values of r, z, and ψ for a given value of h and arc length $0 \leq s \leq \bar{s}$, can be obtained by integrating equation (6.8) along s together with

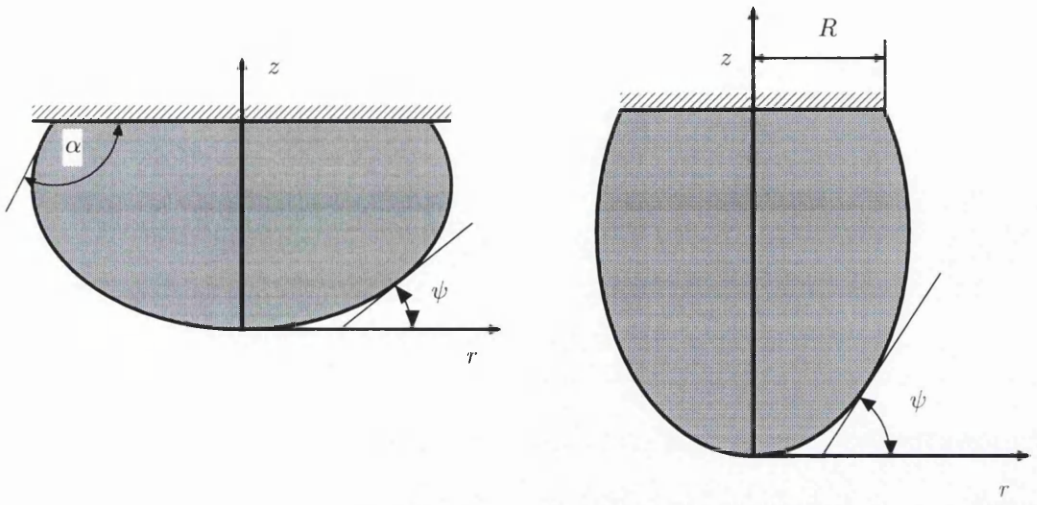

(a) (b)

Figure 6.2: Two types of pendent drops and their parametrization: (a) pendent drop hanging from a flat surface, (b) pendent drop hanging from a tube.

$$dr = \cos\psi \; ds, \tag{6.9}$$

$$dz = \sin\psi \; ds, \tag{6.10}$$

subject to the conditions that at $r = 0,\ z = 0,$

$$s = 0, \qquad \psi = 0 \qquad \text{and} \qquad d\psi = \frac{h}{l^2}\, ds.$$

The value of ψ at $s = \bar{s}$ is then checked against the value of contact angle α. The integration is repeated with new and improved value of either h or $\bar{s}$ if

$$|\psi(\bar{s}) - \alpha| > TOL.$$

In the case of pendent drops hanging from a tube, the check is carried out for the value of r at $s = \bar{s}$ to verify whether it has the same value as the tube radius R. That is, if the condition $|r(\bar{s}) - R| \leq TOL$ satisfied. The volume is obtained as a post processing result and can be used later as a volume of the domain in finite element analysis.

6.1.3 Equilibrium shape of a liquid bridge

The procedure developed for pendent drops can be adapted to obtain the equilibrium shape of liquid bridges by modifying the boundary condition at $z = 0$.

Given the height of the liquid bridge h and the arclength s the boundary conditions required to obtain the equilibrium shape of liquid bridges in which the contact angles at the bottom and the top are prescribed are as follows:

$$r(0) = \bar{r_1}, \qquad \text{and} \qquad \alpha(0) = \bar{\alpha_1},$$

where $\bar{r}$ and $\bar{\alpha_1}$ are prescribed value of radius and contact angle at the bottom, respectively. Using a shooting method the right combinations of h and $\bar{s}$ can be found such that

$$|\bar{\alpha_2} - \alpha(h)| < TOL.$$

is satisfied, where $\bar{\alpha_2}$ represents the prescribed value of contact angle at the top plate. The boundary conditions required for problems with prescribed radius at the bottom and the top plate for a given h and s are

$$r(0) = \bar{r_1}, \qquad \text{and} \qquad \alpha(0) = 0.0.$$

If the value of $|\bar{r_2} - r(h)| > TOL$ either the value of h or $\bar{s}$ is changed, and the analysis is repeated.

6.1.4 Numerical integration

Generally, the set of first order ordinary differential equations governing the three different types of Plateau surfaces, mentioned in the subsections (6.1.1-6.1.3), can only be solved numerically. Different kind of numerical methods have been used even long before digital computer become common. The numerical methods used mostly of the multistep types, such as the Adams-Bashforth [10], or a single step fourth order Runge-Kutta [2] to obtain a better accuracy with less computational effort and limited number of digits. In this thesis, the forward Euler method is used to solve equations (6.4), (6.8), and (6.10). This method is simple and easy to program, and can be expressed as [1]

$$y_{i+1} = y_i + \frac{\mathrm{d}y}{\mathrm{d}x}\Delta x. \tag{6.11}$$

Although the forward Euler method is known to be only conditionally stable, with the computing power of today digital computer, Δx can be made as small as necessary to maintain stability without difficulties.

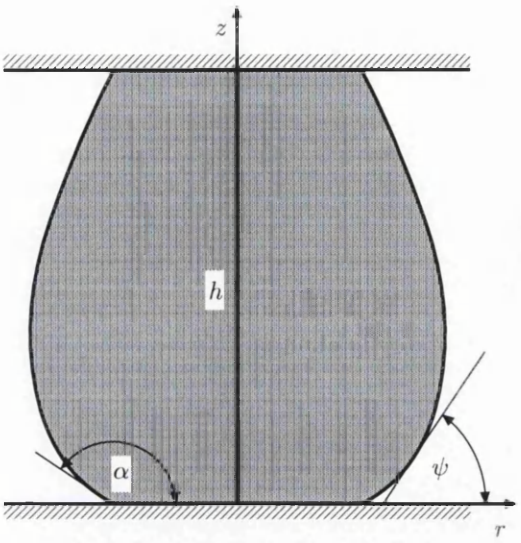

Figure 6.3: Problem description for equilibrium shape of liquid bridges.

The evaluation of equation (6.6), to obtain the volume of liquid drops or bridges is carried out using trapezoidal rule, i.e.

$$\frac{V}{\pi} = \frac{1}{2}\Delta z \left(r_a^2 + 2\sum_{i=1}^{n-1} r_i^2 + r_b^2 \right). \tag{6.12}$$

6.2 Numerical Examples

6.2.1 Sessile Drops

Numerical examples presented in this subsection relate to the equilibrium shapes of liquid sessile drops sitting on rigid flat surfaces under the influence of gravity. These shapes are obtained using finite element procedure described in Chapter 4 and 5. Three drops with different volumes are considered with dimensionless volumes ($E = V/l^3$) $E = 0.01$, $E = 5.0$, and $E = 25.0$, associated with small, medium, and large drops, respectively. These choices are intended to show the effect of gravity on the shape of a drop.

The problem of a sessile drop sitting on a rigid flat surface is the most stable one among the problems related to axisymmetric liquid menisci, except for cases where the surface on which the drop sits is constrained to a certain

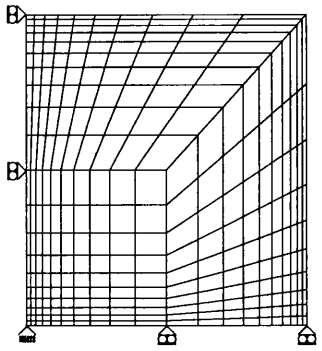

Figure 6.4: Finite element meshes and boundary conditions for sessile drop sitting on a flat surface.

radius. Therefore, there is no possibility of multiple solutions occurring in this problem.

In all examples, a finite element mesh consisting of 300 bilinear quadrilateral F-bar elements is used to discretize half of the domain due to axially symmetric nature of the problem. The initial configurations for the finite element analysis can be chosen arbitrarily and for all examples are taken to be of cylindrical shapes with given volumes. The finite element discretization and the boundary conditions employed for all analyses are depicted in figure 6.4. After the analysis is completed, the finite element results are then compared against the numerical solution of system of ordinary differential equations presented in subsection 6.1.1 by plotting the shapes obtained from both approach in non-dimensional coordinates $R = r/l$ and $Z = z/l$, where l is capillary length.

Figure 6.5 shows the evolution of finite element mesh for sessile drop with $E = 0.01$ and $\alpha = 135°$ during the computation. Finite element results and its comparison with ODE solutions for a sessile drop with $E = 0.01$ and different values of contact angle ($\alpha = 45°$, $\alpha = 60°$, $\alpha = 90°$, and $\alpha = 135°$) are shown in figure 6.6. Figure 6.7 shows finite element results and its comparison with ODE solutions for sessile drop with $E = 5.0$ and contact angles $\alpha = 60°$, $\alpha = 90°$, $\alpha = 120°$, and $\alpha = 135°$. Finally, finite element results for sessile drop with $E = 25.0$ and contact angle $\alpha = 90°$, $\alpha = 120°$, $\alpha = 135°$, and $\alpha = 150°$ are presented in figure 6.8 along with their comparison with ODE solutions.

All finite element solutions show a very good agreement with the numerical solutions of the system of ordinary differential equation resulting from parametrization of Laplace-Young equation.

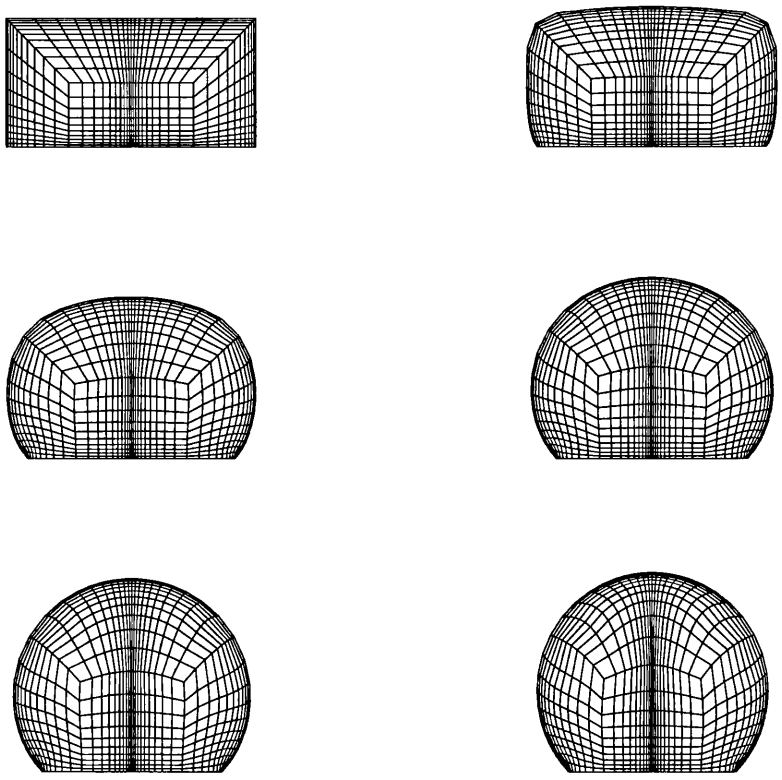

Figure 6.5: Finite element meshes for small sessile drop at different stages of calculation.

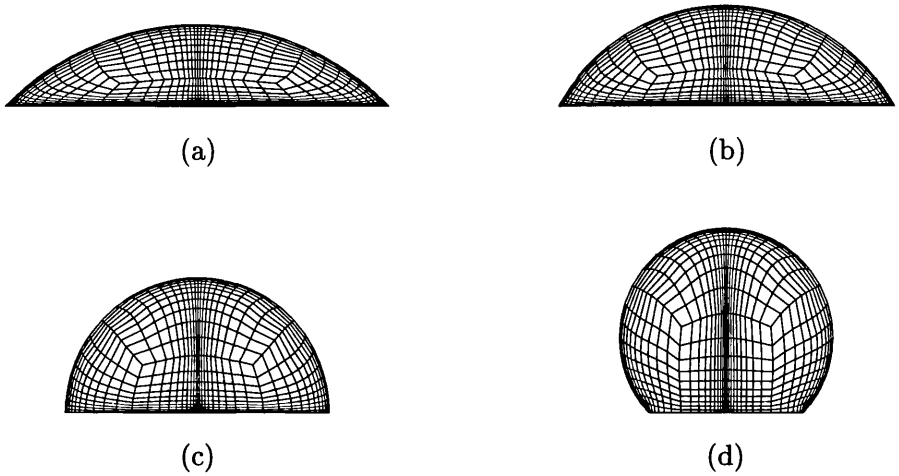

(a) (b)

(c) (d)

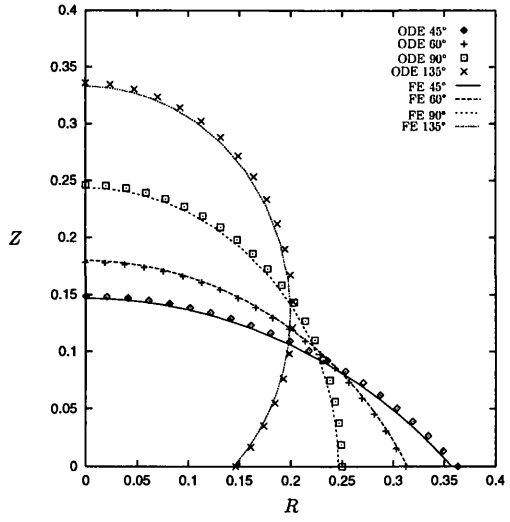

(e)

Figure 6.6: Finite element results for sessile drop sitting on a flat surface with dimensionless volume of $E = 0.01$. Different values of the contact angle (a) $\alpha = 45°$, (b) $\alpha = 60°$, (c) $\alpha = 90°$, (d) $\alpha = 135°$, (e) comparison of finite element and ODE solutions. The axes are in dimensionless units.

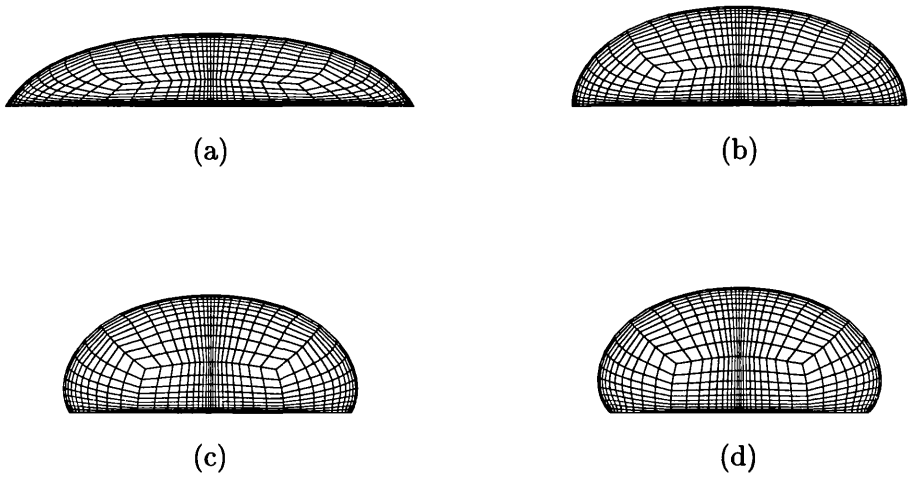

(a) (b)

(c) (d)

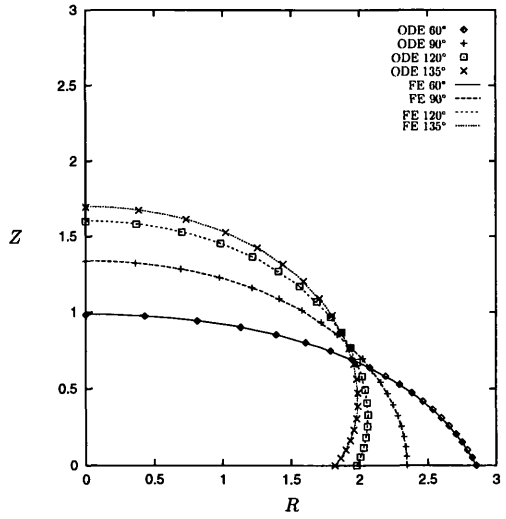

(e)

Figure 6.7: Finite element results for sessile drop sitting on a flat surface with dimensionless volume of $E = 5$. Different values of the contact angle (a) $\alpha = 60°$, (b) $\alpha = 90°$, (c) $\alpha = 120°$, (d) $\alpha = 135°$, (e) comparison of finite element and ODE solutions. The axes are in dimensionless units.

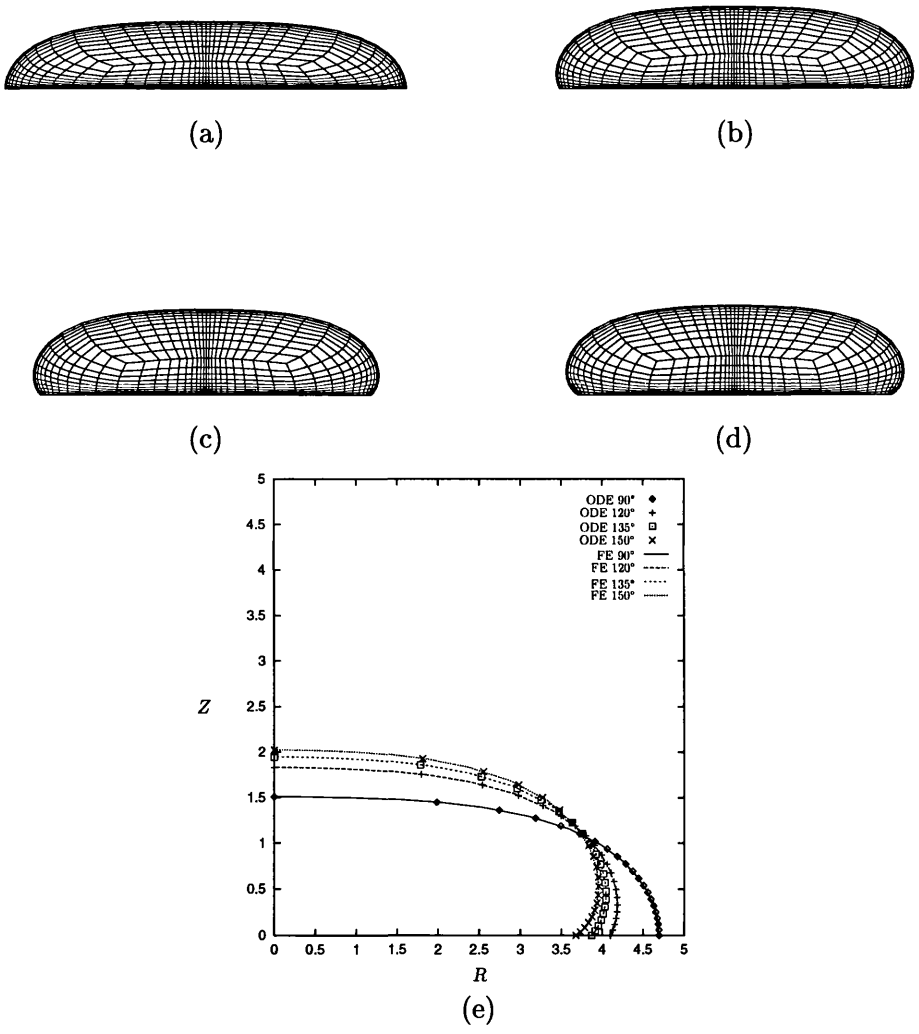

Figure 6.8: Finite element results for sessile drop sitting on a flat surface with dimensionless volume of $E = 25$. Different values of the contact angle (a) $\alpha = 90°$, (b) $\alpha = 120°$, (c) $\alpha = 135°$, (d) $\alpha = 150°$, (e) comparison of finite element and ODE solutions. The axes are in dimensionless units.

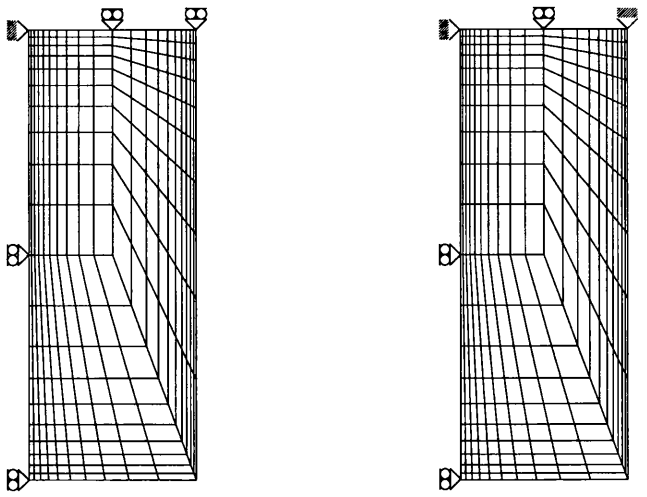

(a) (b)

Figure 6.9: Finite element meshes and boundary conditions for: (a) pendent drop hanging from a flat surface, (b) pendent drop hanging from a tube.

6.2.2 Pendent Drops

In this subsection finite element analysis is carried out to obtain the equilibrium shape of a pendent drop. Two different contact line conditions are considered. The first one is a condition in which the contact angle α is prescribed. This condition represents a pendent drop hanging from a flat surface. The second contact line condition considered is fixed contact line radius associated with a pendent drop hanging from a cylindrical tube. The finite element results are compared with the numerical solution of ordinary differential equation (ODE) resulting from a parametrization of Laplace-Young equation, described in subsection 6.1.2. Unlike the sessile drop case in which volume of the drop is a part of data for numerical solution the system of ODEs, in pendent drop problem the arclength s is taken as a given data and the volume is obtained by postprocessing the solution. This is not a typical situation encountered in finite element analysis where the domain of the problem is a given data. To be able to make the comparison of the results of ODE and finite element solutions, the numerical solution of ODE is obtained first and the associated volume is computed numerically using trapezoidal rule. Then, this volume is used as a volume of the initial finite element mesh.

Precaution has to be taken in selecting the arclength s and the value of pendent drop height due to possibility of existence of multiple solutions. Articles on the stability of pendent drops by Pitts [11], Michael and Williams

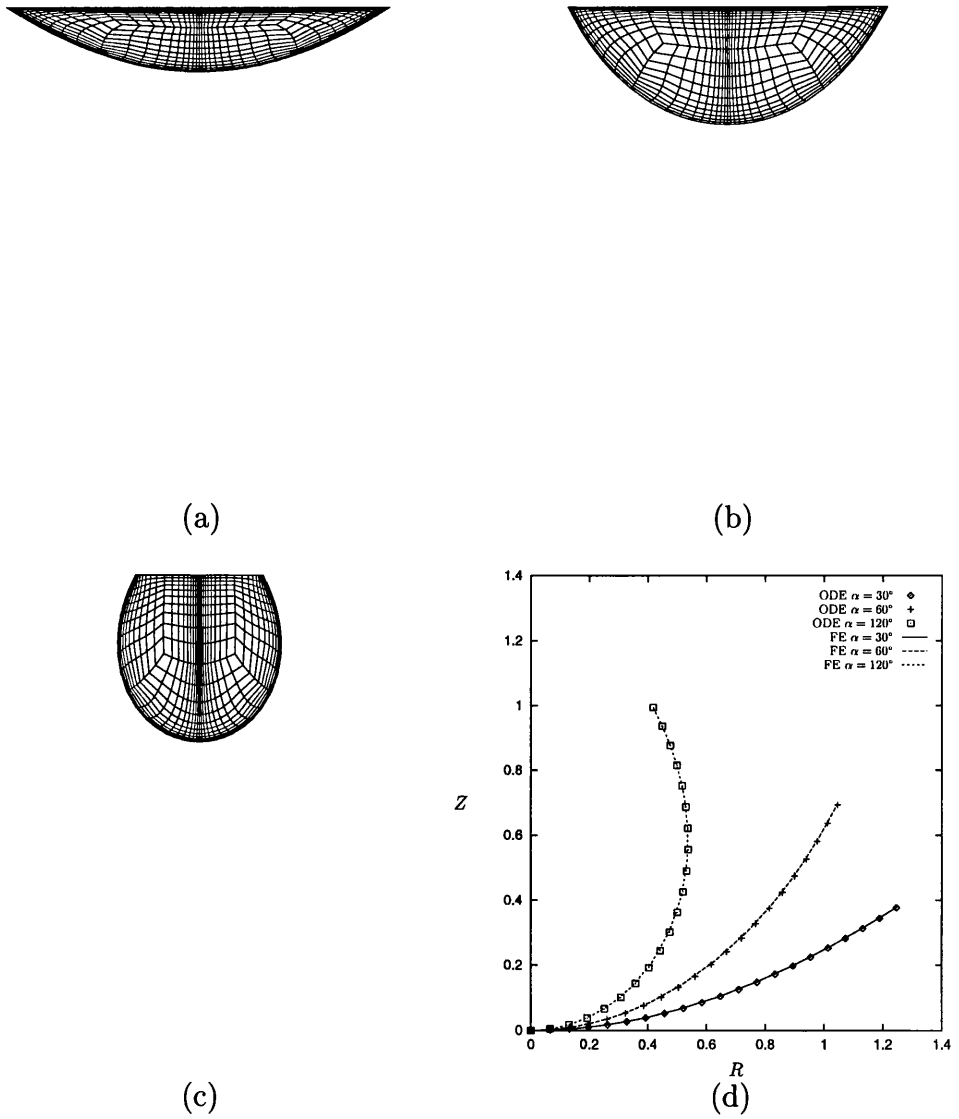

Figure 6.10: Finite element results for pendent drop hanging from a flat surface with non-dimensional arclength $S = 1.3177$. Different contact angle conditions (a) $\alpha = 30°$, (b) $\alpha = 60°$, (c) $\alpha = 120°$, (d) comparison of finite element and ODE solutions. The axes are in dimensionless units.

[9], and Finn [6] discuss some aspects of stability of pendent drops and can be used as a guidance, but the information available has limited practical use.

As for sessile drops examples given in subsection 6.2.1, a finite element mesh consisting of 300 bilinear quadrilateral F-bar elements is employed in all simulations. Figures 6.9(a) and 6.9(b) show, respectively, the initial finite

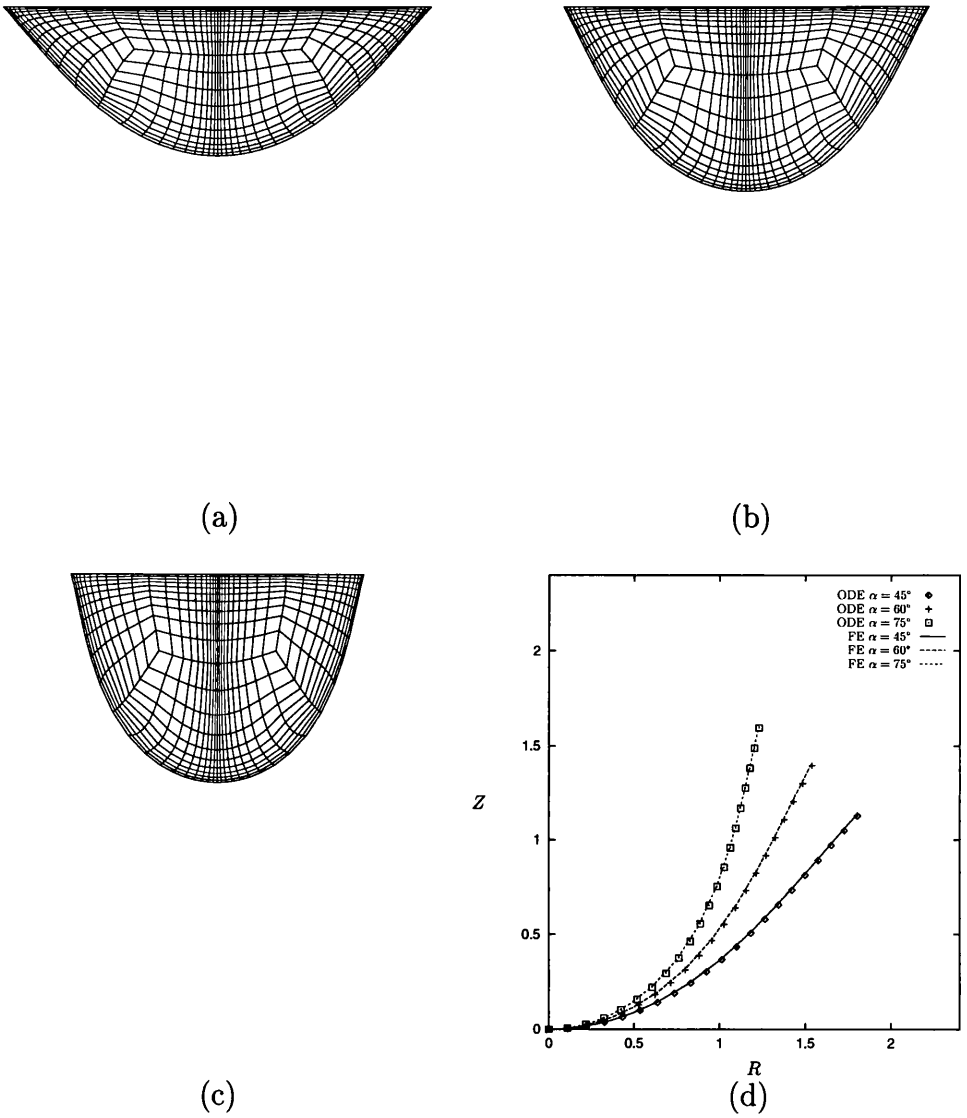

Figure 6.11: Finite element results for pendent drop hanging from a flat surface with non-dimensional arclength $S = 2.1962$. (a) $\alpha = 45°$, (b) $\alpha = 60°$, (c) $\alpha = 75°$, (d) comparison of finite element and ODE solutions. The axes are in dimensionless units.

element meshes and conditions at the contact line for both pendent drop hanging from a flat surface, where contact angle α is prescribed, and for pendent drop hanging from a tube or disk, associated with the condition where the radius of contact line R is fixed. Results from finite element analysis for pendent drop hanging from a flat surface with non-dimensional arclength $S = 1.3177$ and its comparison with numerical solutions of ODE is

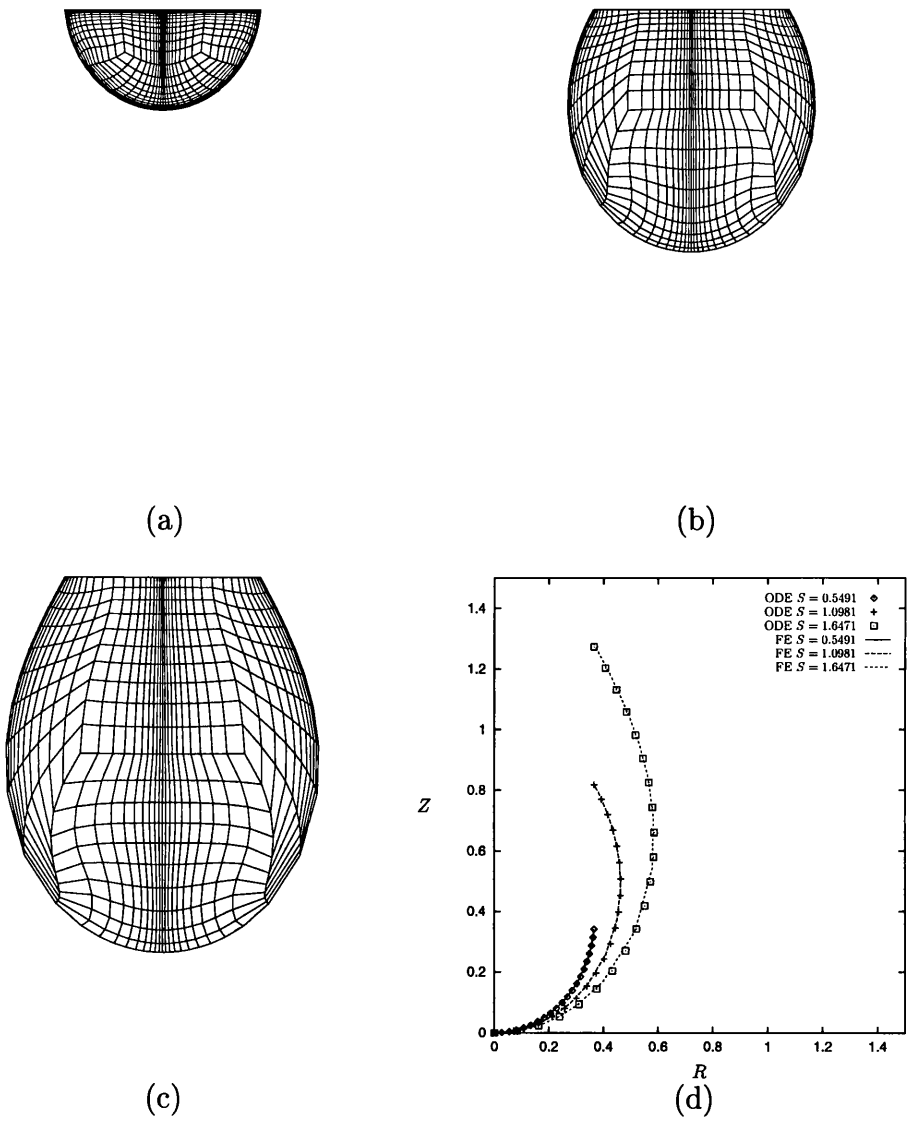

Figure 6.12: Finite element results for pendent drop hanging from a tube/disk with non-dimensional radius $\bar{R} = 0.3660$. Different values of non-dimensional arclength (a) $S = 0.5491$, (b) $S = 1.0981$, (c) $S = 1.6471$, (d) comparison of finite element and ODE solutions. The axes are in dimensionless units.

given in figure 6.10. The shapes of drops obtained by both approach for three different values of contact angle $\alpha = 30°$, $\alpha = 60°$ and $\alpha = 120°$ are plotted in non-dimensional coordinates . Figure 6.11 depicts the finite element results for pendent drop hanging from a flat surface with non-dimensional arclength $S = 2.1962$ for three different values of contact angle $\alpha = 45°$, $\alpha = 60°$ and $\alpha = 75°$ and its comparison with numerical solutions of ODE.

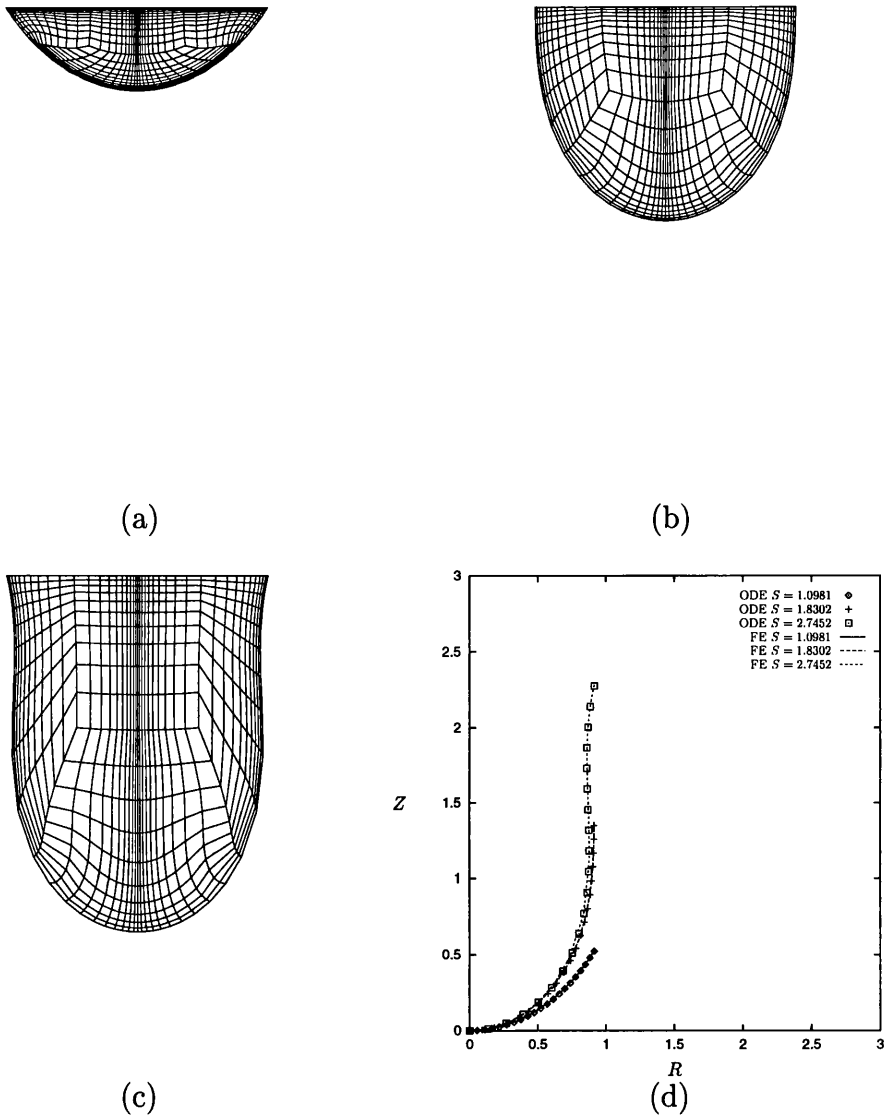

Figure 6.13: Finite element results for pendent drop hanging from a tube/disk with non-dimensional radius $\bar{R} = 0.9151$. Different values of non-dimensional arclength (a) $S = 1.0981$, (b) $S = 1.8302$, (c) $S = 2.7452$, (d) comparison of finite element and ODE solutions. The axes are in dimensionless units.

The finite element results are in good agreement with the numerical solution of ODE. For the case with non-dimensional arclength $S = 2.1962$, due to large volumes associated with it, nonunique solutions appear for contact angle $\alpha \geq 90°$.

Two examples are given for pendent drops hanging from a tube. The first one deals with tube or disk of $R = 0.3660$ non-dimensional radius

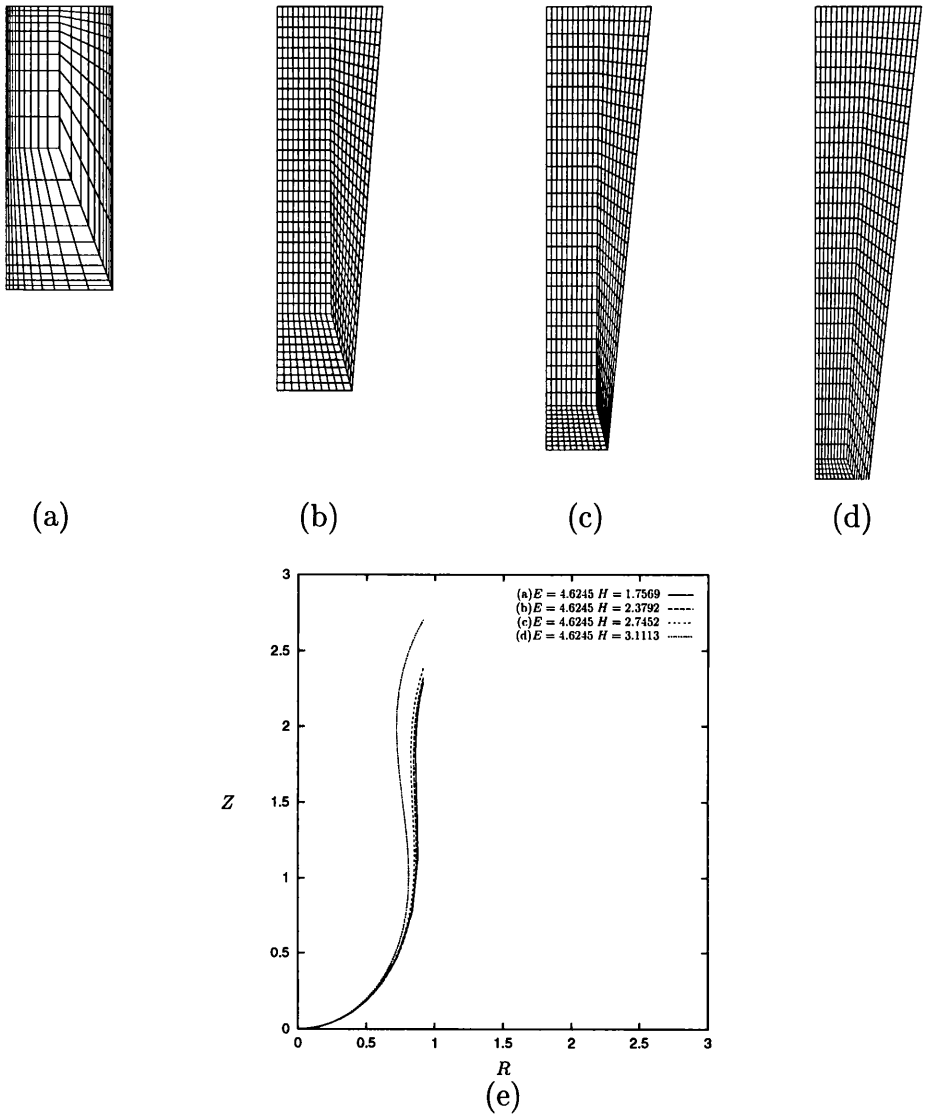

Figure 6.14: Non-uniqueness of the solutions for pendent drop hanging from a tube or disk with non-dimensional radius $R = 0.9151$ and non-dimansional volume $E = 4.6245$. The profile of the drop depends on initial shape.

and in the second example the tube/disk non-dimensional radius is taken as $R = 0.9151$. Results of the first case are shown in figure 6.12 for the non-dimensional arclengths of 0.5491, 1.0981 and 1.6471 along with its comparison with numerical solution of ODE. For the case of $R = 0.9151$ the finite element results together with its comparison with numerical solutions of ODE are presented in figure 6.13. Three drops with different non-dimensional arclength

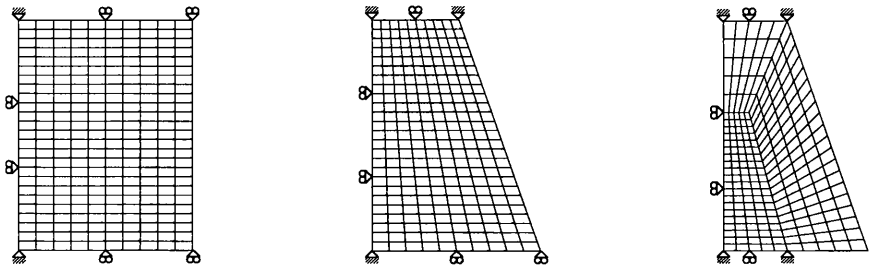

(a) (b) (c)

Figure 6.15: Finite element meshes and boundary conditions for liquid bridges (a) prescribed contact angle on both ends, (b) prescribed radius on top end and contact angle on bottom end, (c) prescribed radius on both ends.

$S = 1.0981, S = 1.8302$ and $S = 2.7452$ are considered in this example. The profiles of equilibrium pendent drops obtained from finite element analysis are in good agreement with the profiles obtained by numerical solution of the system of ODEs associated with the pendent drop profile.

An additional example is given to show a case where multiple solutions are possible. In this example, the equilibrium shape of a pendent drop hanging from a tube/disk with non-dimensional radius dan volume, $R = 0.9151$ and $E = 4.6245$, respectively, is sought using the finite element method. Four different initial finite element meshes are used. These meshes have the same number of elements and topology and represent the same volume. The only difference is related to their initial geometry which is given in figure 6.14(a)-(d). As can be seen in figure 6.14(e) the finite element analyses give four different equilibrium shapes.

6.2.3 Liquid Bridges

While tables of shapes of sessile and pendent drops had been available since the work of Bashforth and Adams (1883), there was no such a table for liquid bridges formed by axially symmetric menisci of liquid held between two parallel horizontal planes of solid surfaces [10]. In fact this situation describes all menisci that do not cross the axis of symmetry. The first tables of liquid bridge shapes are due to Padday (1971) [10].

In this subsection, the equilibrium shapes of axisymmetric liquid bridges held captive between two parallel horizontal surfaces of rigid plates are computed using finite element method. As for pendent drops, the problem of finding the equilibrium shapes of liquid bridges also suffers from possible ex-

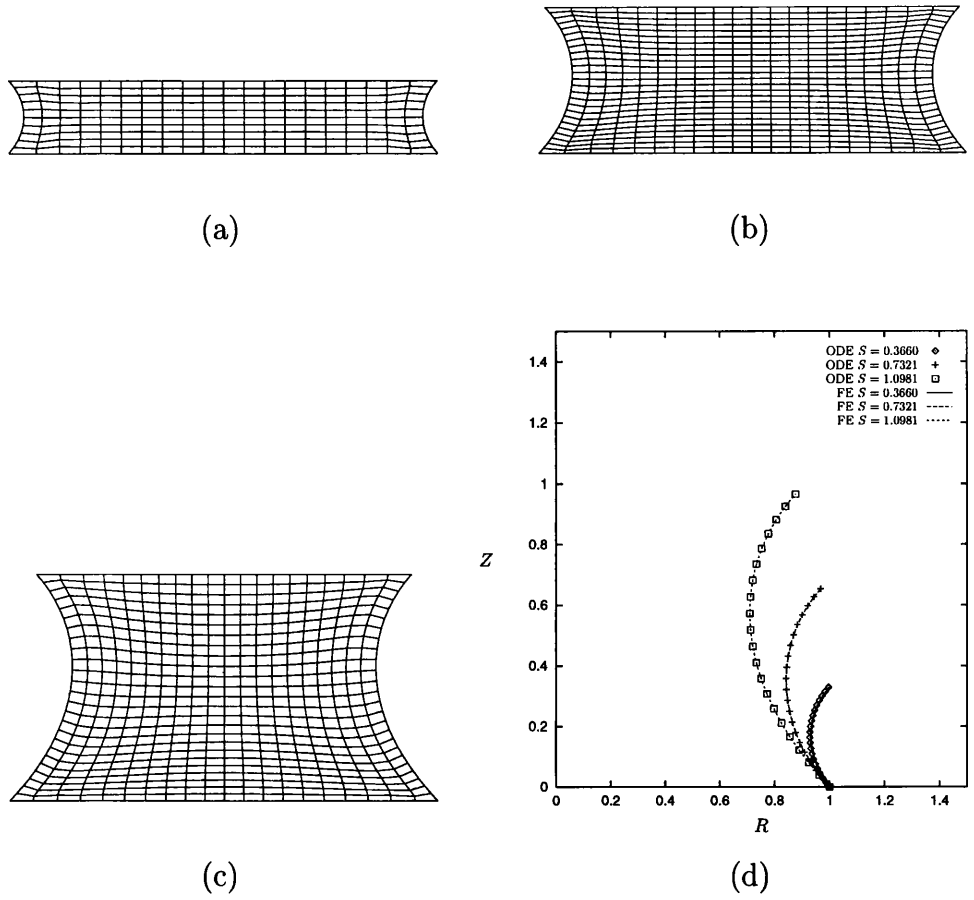

Figure 6.16: The finite element results for liquid bridges with fixed contact angle $\bar{\alpha} = 45°$ at both upper and lower plates, for different non-dimensional arclengths (a) $S = 0.3660$, (b) $S = 0.7321$, (c) $S = 1.0981$, (d) comparison of finite element and ODE solutions. The axes are in dimensionless units.

istence of multiple solutions. For the equilibrium shape to exist in nature it has to be stable. Plateau found that an oil liquid bridge in neutral bouyancy is in stable equilibrium provided the ratio of the length to the diameter did not exceed a critical value. The critical value of this ratio is π.

Three different contact line conditions are considered in this work. The first condition is associated with situation in which the contact angle α is prescribed at both upper and lower plates (figure 6.15(a)). The second condition is related to situation where radius $R = \bar{R}$ is prescribed at the upper plate while contact angle α is prescribed at the lower plate (figure 6.15(b)).

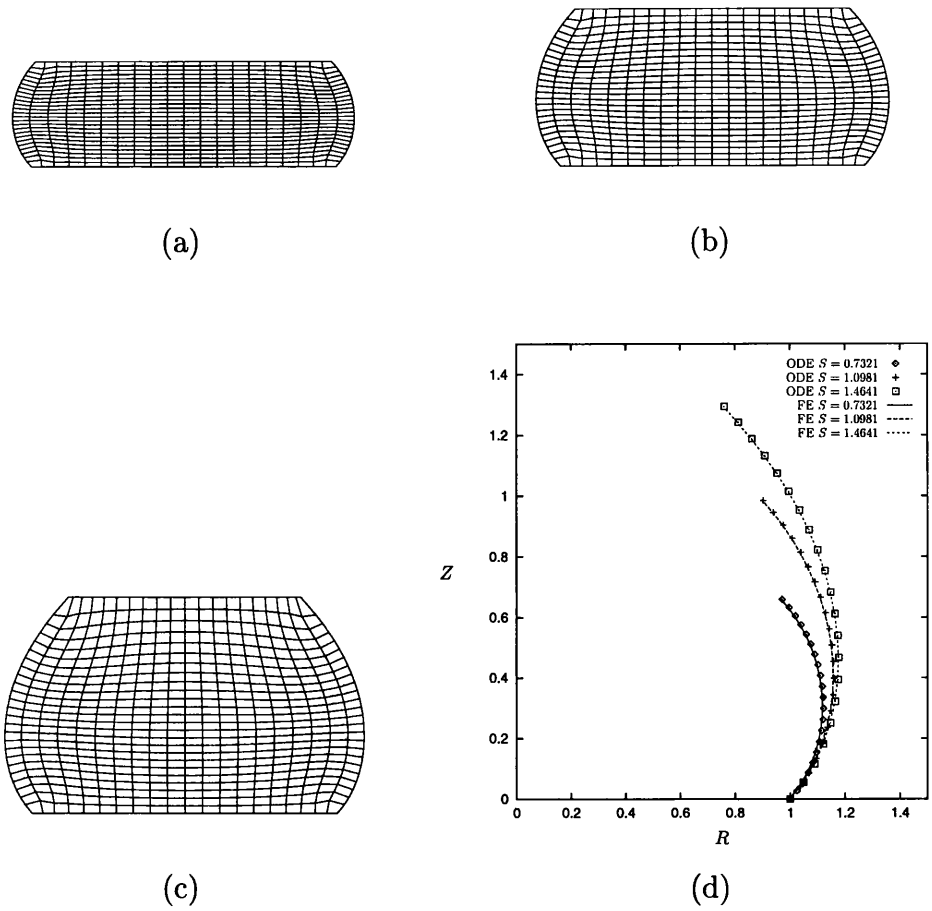

Figure 6.17: The finite element results for liquid bridges with fixed contact angle $\bar{\alpha} = 135°$ at both upper and lower plates, for different non-dimensional arclengths (a) $S = 0.7321$, (b) $S = 1.0981$, (c) $S = 1.4641$, (d) comparison of finite element and ODE solutions. The axes are in dimensionless units.

In the last condition radius $R = \bar{R}$ is prescribed at both upper and lower plates as in figure 6.15(c).

In all examples in this subsection, a mesh consisting of 250 bilinear quadrilateral F-bar elements is used to discretize the domain. The finite element results for each case are compared with results from numerical integration of the set of ordinary differential equations (ODE) governing the same problem, described in section 6.1.3. Figures 6.16 and 6.17 show finite element meshes for cases with contact angle $\alpha = 45°$ and $\alpha = 135°$ prescribed at both the upper and lower plates and different non-dimensional arclengths

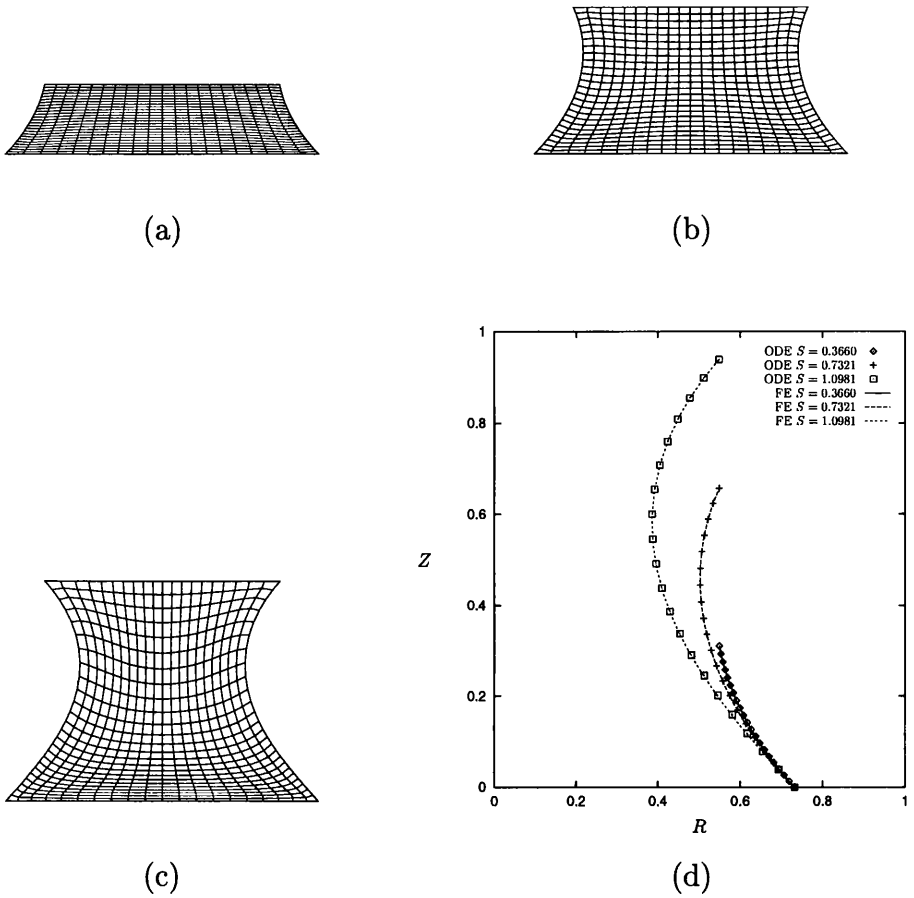

Figure 6.18: The finite element results for liquid bridges with fixed non-dimensional radius $\bar{R} = 0.5491$ at the upper plate and fixed contact angle $\alpha = 45°$ at the lower plate, for different non-dimensional arclengths (a) $S = 0.3660$, (b) $S = 0.7321$, (c) $S = 1.0981$, (d) comparison of finite element and ODE solutions. The axes are in dimensionless units.

S. The finite element results and its comparison with ODE solutions for cases with prescribed non-dimensional radius $\bar{R} = 0.5491$ at the upper plate and contact angles $\alpha = 45°$ and $\alpha = 135°$ at the lower plate for different non-dimensional arclengths S are presented in figures 6.18 and 6.19. Finally, figure 6.20 depicts finite element results for cases where non-dimensional radius $\bar{R} = 0.5491$ is prescribed at both the upper and lower plates. In all examples presented in this subsection the finite element results are in good agreement with the ODE solutions.

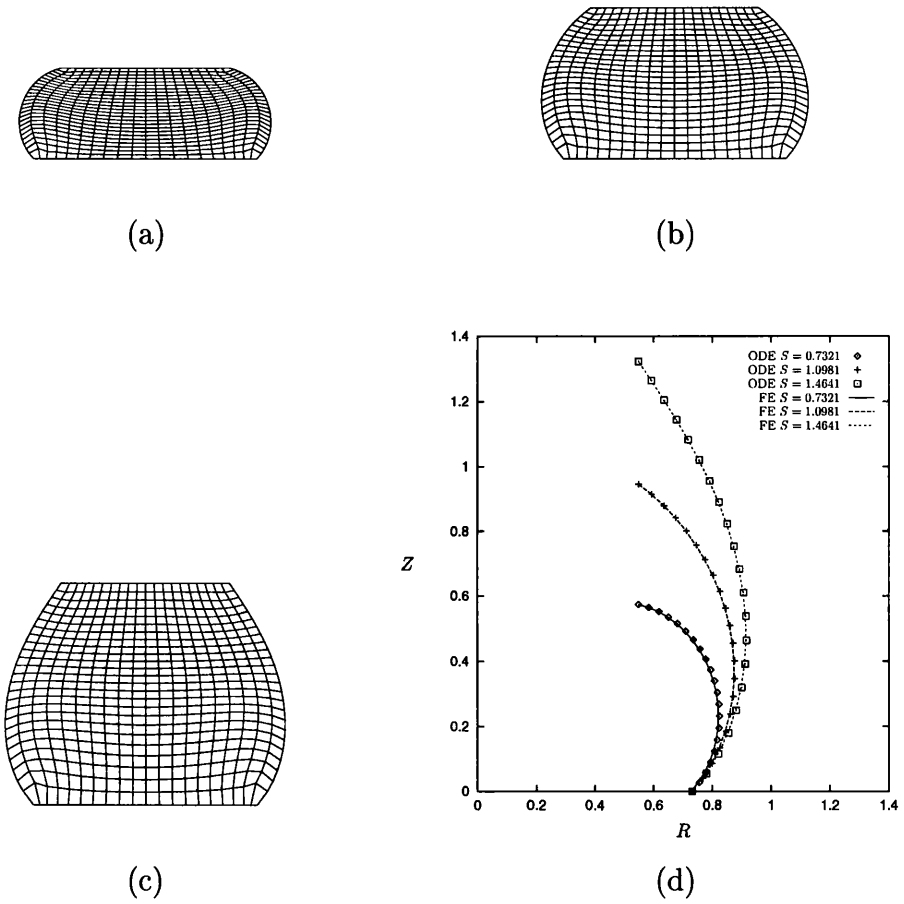

Figure 6.19: The finite element results for liquid bridges with fixed non-dimnesional radius $\bar{R} = 0.5491$ at the upper plate and fixed contact angle $\alpha = 135°$ at the lower plate, for different non-dimensional arclengths (a) $S = 0.7321$, (b) $S = 1.0981$, (c) $S = 1.4641$, (d) comparison of finite element and ODE solutions. The axes are in dimensionless units.

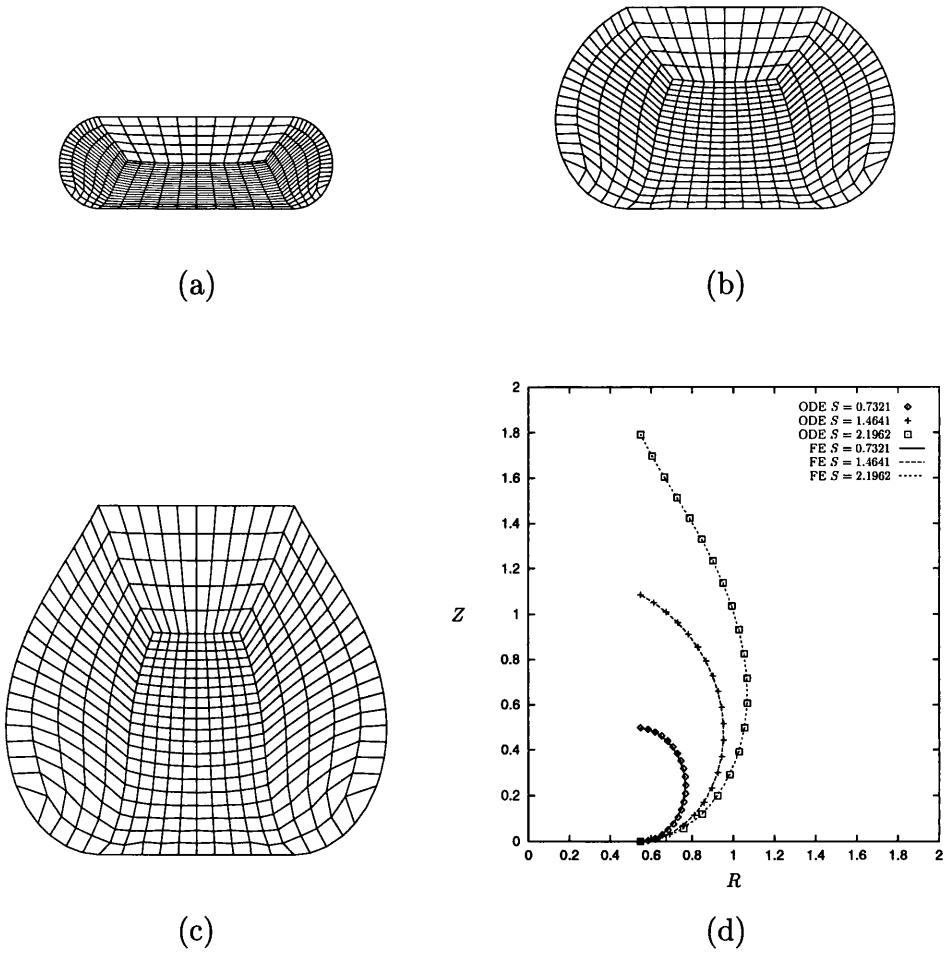

Figure 6.20: The finite element results for liquid bridges with fixed non-dimensional radius $\bar{R} = 0.5491$ at both upper and lower plates, for different non-dimensional arclengths (a) $S = 0.7321$, (b) $S = 1.4641$, (c) $S = 2.1962$, (d) comparison of finite element and ODE solutions. The axes are in dimensionless units.

6.3 Conclusion

Further validation of the Lagrangian finite element formulation incorporating surface tension effects described in the Chapter 5 has been presented in this chapter. The problem of finding the equilibrium shapes of sessile drops, pendent drops and liquid bridges that belong to a class of problems known as the generalized Plateau surface, have been chosen to verify the performance of the technique in quasi-static regime. In general, the equilibrium shapes of liquid menisci obtained by finite element analysis are in a very good agreement with the solution obtained by numerically integrating a system of ordinary differential equations associated with the equilibrium shapes of liquid menisci.

The problems identified relate to possible existence of multiple solutions and instabilities associated with the equilibrium shapes of liquid menisci. It is not directly apparent whether a finite element solution for a given volume of liquid and the boundary conditions is a stable one and whether it can physically exists in nature.

Next chapter will deal with some further aspect of validation. The Lagrangian finite element approach described in Chapter 4 and 5 will be validated against analytical and experimental results available for nonlinear dynamic problems.

Bibliography

[1] G.J. Borse. *FORTRAN 77 and Numerical Methods for Engineers.* PWS-Kent, Boston, 2^{nd} edition, 1991.

[2] E.A. Boucher and M.J.B. Evans. Pendent drop profiles and related capillary phenomena. *Proc. R. Soc. Lond. A.*, 346:349 – 374, 1975.

[3] K.A. Brakke. The surface evolver. *Experiment. Math.*, 1:141 – 165, 1992.

[4] R.A. Brown. Finite element method for the calculation of capillary surfaces. *J. Comp. Physics.*, 33:217 – 235, 1979.

[5] P. Concus and R. Finn. On capillary free surfaces in the absence of gravity. *Acta Math.*, 132:177 – 198, 1974.

[6] R. Finn. *Equilibrium Capillary Surfaces.* Springer-Verlag, New York, 1986.

[7] U. Hornung and H.D. Mittelmann. A finite element method for the calculation of capillary surfaces with volune constraints. *J. Comp. Physics.*, 87:126 – 136, 1990.

[8] D.H. Michael. Meniscus stability. *Ann. Rev. Fluid Mech.*, 13:189 – 215, 1981.

[9] D.H. Michael and P.G. Williams. The equilibrium and stability of axisymmetric pendent drops. *Proc. R. Soc. Lond. A.*, 351:117 – 127, 1976.

[10] J.F. Padday. The profiles of axially symmetric menisci. *Phil. Trans. R. Soc. Lond. A.*, 269:265 – 293, 1971.

[11] E. Pitts. The stability of pendent liquid drops–Part 2. axial symmetry. *J. Fluid Mech.*, 63:487 – 508, 1974.

[12] C. Pozrikidis. *Introduction to Theoritical and Computational Fluid Dynamics.* Oxford University Press, New York, 1997.

Chapter 7

Validation II: Nonlinear Dynamic Problems

In general, the natural and industrial processes involving surface tension phenomena are of dynamic nature. This chapter deals with examples of problems in which dynamic effects are important during the analysis. Two examples are given, the first example is the classical droplet oscillation problem due to surface tension. This particular problem is interesting because the frequency of oscillation can be obtained analytically for small amplitude oscillations of two-dimensional liquid drop [5] and axisymmetric drop [9]. Thus, this problem can provide a means to verify the finite element technique presented in chapters 4 and 5 for dynamic problems. The second example is the stretching of a liquid bridge held between two circular rods. In this problem the liquid experiences complex deformation process involving large deformation and others possible phenomena such as separation of the liquid which causes changes in topology. This problem can be solved using Lagrangian finite element only if an adaptive remeshing procedure is employed to avoid solution degradation due to distorted elements or mesh entanglement.

7.1 Droplet Oscillation

Motivated by space technology applications involving containerless processing, and industrial processes involving spraying and atomization, the last two decades witnessed the increase in the study of drop oscillations in zero-gravity environment or subject to acoustic radiation causing levitation. The nature of the drop oscillation is determined by the initial condition and the amplitude of the motion is governed by the energy imparted in the process of drop formation [15].

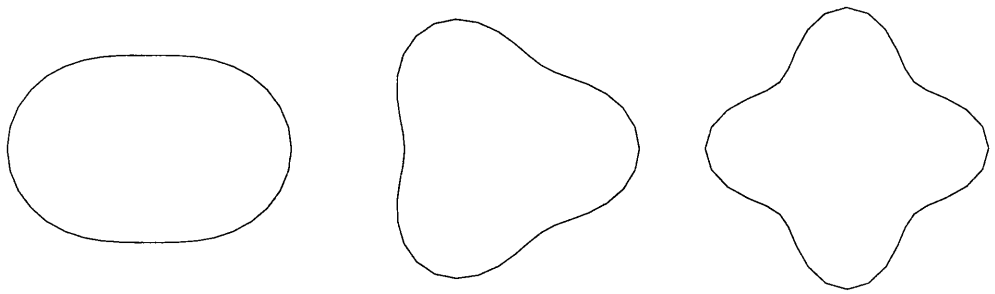

2^{nd} mode 3^{rd} mode 4^{th} mode

Figure 7.1: Eigen mode for 2D liquid drop oscillations

The studies of small amplitude oscillation of inviscid spheroidal liquid drop were initiated by Rayleigh [17] in the context of linear theory. Extension to moderate amplitude was carried out much later by Tsamopoulos and Brown [19]. The authors found that the frequency of oscillation decreases with the square of the amplitude. For oscillations with infinitesimal amplitude the effect of viscosity was for small viscosity first taken into consideration by Lamb [9] and later by Reid [18] for arbitrary viscosity.

The study of large amplitude oscillations is difficult if not impossible without recourse to numerical methods. Different numerical methods have been used in the past; we note among others, finite difference method [4], boundary integral [11, 15], and finite element method [5, 1, 2]. It appears that finite element method has some advantages in comparison to other methodologies. As pointed out by Lungren and Mansour [11], the boundary integral method can not model nonlinear drop oscillation when the viscous effect are large and finite difference method with marker and cell seems to be complicated and computationally inefficient [1].

7.1.1 Two dimensional drop

Before proceed to the finite element analysis of the droplet oscillation problem due to surface tension, the theoretical results pertaining to this problem will be briefly reviewed.

In the context of linear theory, the frequency ω of the small amplitude oscillation of two dimensional inviscid liquid drop suspended in dynamically inactive fluid is given by

$$\omega_n^2 = (n^3 - n)\frac{\gamma}{\rho R^3}, \tag{7.1}$$

where ρ is the density of the liquid drop, R is the unperturbed radius of the drop, and n is the prescribed mode of oscillation in the plane with amplitude A. It is clear that $n = 0$ and $n = 1$ correspond to rigid body motion [5] and the calculations of oscillation start with the lowest oscillating mode $n = 2$. The perturbed surface of the liquid drop is given in polar coordinates (r,θ) by

$$r = R + A\cos(n\theta). \tag{7.2}$$

The liquid used in this example is water. The unperturbed radius of the drop is $R = 0.125 \times 10^{-1}$ cm. Two test cases are presented in this example. The first one is small amplitude case with amplitude of oscillation $A = 0.02\,R$ and the second one is associated with moderate amplitude with $A = 0.2\,R$. For each case, computations are carried out for the lowest three oscillation modes ($n = 2$, $n = 3$, and $n = 4$) (see Figure 7.1). For both cases 300 bilinear quadrilateral F-bar elements are used to discretize the domain of the problem and the problem is integrated implicitly using $\beta = 0.25$ and $\delta = 0.5$ as Newmark integration parameters which correspond to the mid-point rule. Time step size is taken to be $\Delta t = 0.1 \times 10^{-5}$ s and the penalty parameter of $K = 0.1 \times 10^{11}$ has been chosen to enforce incompressibility of the liquid drop. Penalty parameter of this magnitude seems to be too large and there is a danger of causing inaccuracy in the solution. According to Gresho and Sani [7], for 14 digits machine the penalty parameter should be $10^4 \leq K \leq 10^9$. In this work 16 digits machine precision is used. It can be seen from the results that there is no problem with the accuracy. The only consequences are very small time steps that have to be used and the performance of Newton-Rhapson iterative procedure is slightly affected. For this particular example no adaptive remeshing procedure was required during the analysis provided that the size of the liquid drop is kept small to avoid circulation inside the drop.

The period is defined as $\tau = 2\pi/\omega$, so equation (7.1) gives $\tau_2 = 0.41915 \times 10^{-3}$ s, $\tau_3 = 0.20957 \times 10^{-3}$ s, and $\tau_4 = 0.13255 \times 10^{-3}$ s corresponding to $n = 2$, $n = 3$ and $n = 4$, respectively. For small amplitude case in which $A = 0.02\,R$ the finite element analysis gives $\tau_2^{\mathrm{FE}} = 0.420 \times 10^{-3}$ s, $\tau_3^{\mathrm{FE}} = 0.210 \times 10^{-3}$ s, and $\tau_4^{\mathrm{FE}} = 0.135 \times 10^{-3}$ s, while for the large amplitude case with $A = 0.2\,R$ the finite element analysis gives $\tau_2^{\mathrm{FE}} = 0.430 \times 10^{-3}$ s, $\tau_3^{\mathrm{FE}} = 0.224 \times 10^{-3}$ s, and $\tau_4^{\mathrm{FE}} = 0.148 \times 10^{-3}$ s, respectively, for $n = 2$, $n = 3$, and $n = 4$ (see Table 7.1). It is clear that for small amplitude and liquid with low viscosity such as water, the finite element results have a very good agreement with the analytical solutions. For the case with moderate amplitude the period of oscillation is slightly longer as is expected. Figure 7.2 shows the

Table 7.1: Analytical and finite element period for 2D oscillation of liquid drop.

	Analytic (s)	FE, $A = 0.02\,R$ (s)	FE, $A = 0.2\,R$ (s)
$n = 2$	0.41915×10^{-3}	0.420×10^{-3}	0.430×10^{-3}
$n = 3$	0.20957×10^{-3}	0.210×10^{-3}	0.224×10^{-3}
$n = 4$	0.13255×10^{-3}	0.135×10^{-3}	0.148×10^{-3}

comparison of the period of oscillation between analytical and finite element results. The analytical solutions are represented by vertical solid line.

The time history of the amplitude of the point on the surface of the drop that lies on the $r-$ axis and kinetic energy for both $A = 0.02\,R$ and $A = 0.2\,R$ cases are shown in figures 7.3 and 7.4, respectively. Aperiodic damping experienced by the finite element solution confirm the finding by Reid [18] that for a drop of water surrounded by air with radius $R < 0.23 \times 10^{-1}$ cm the drop oscillations will be aperiodically damped. Small amount of volume loss can be observed as a result of using penalty method to enforce incompressibility of the liquid drop.

Figures 7.5, 7.6, and 7.7 depict finite element mesh evolution for $n = 2$, $n = 3$, and $n = 4$, respectively, for drop oscillations with amplitude $A = 0.2\,R$.

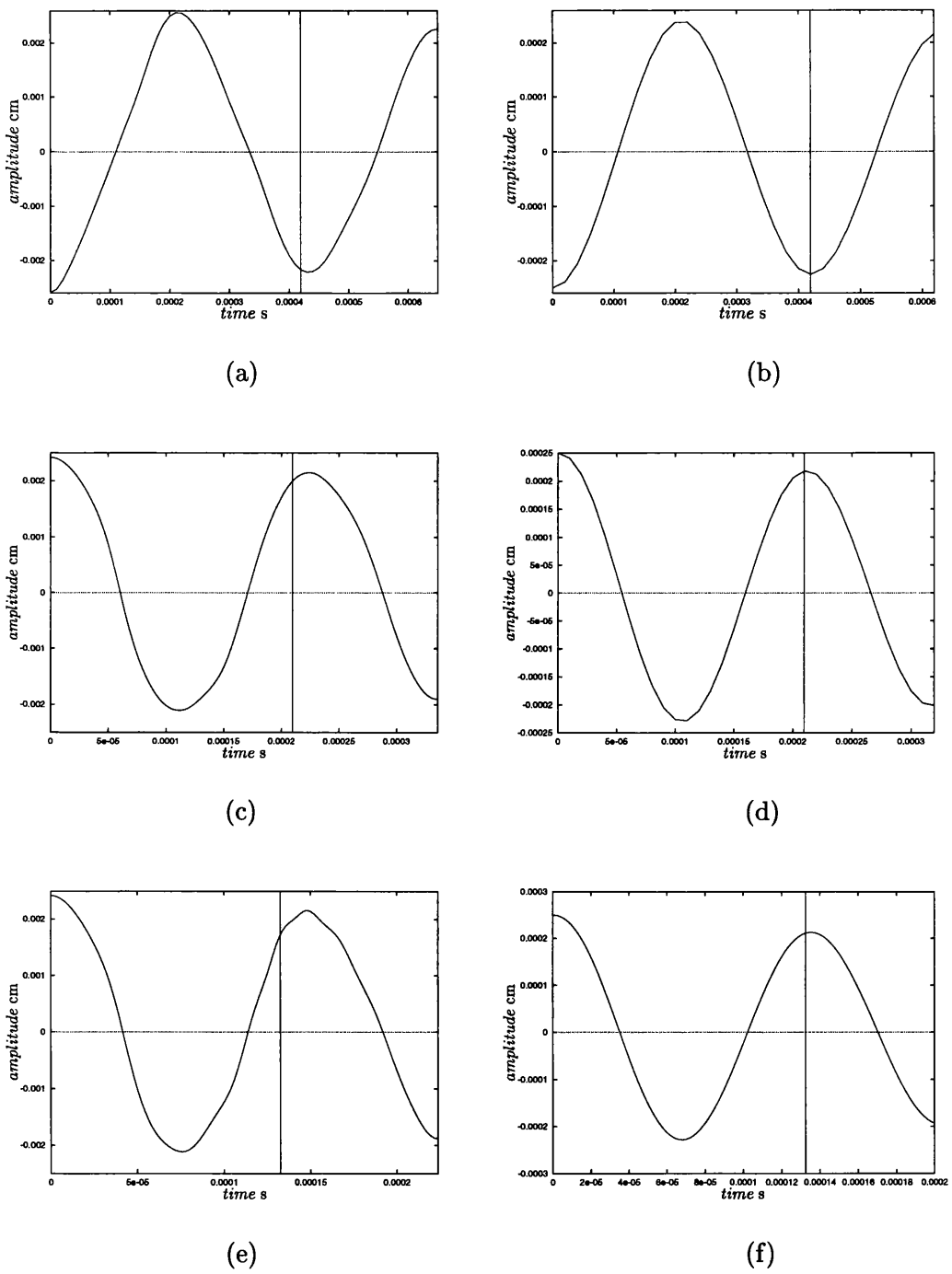

Figure 7.2: Oscillations of a 2D liquid drop: Comparison of the computed period and analytical period. (a) $n = 2$ and $A = 0.2R$, (b) $n = 2$ and $A = 0.02R$, (c) $n = 3$ and $A = 0.2R$, (d) $n = 3$ and $A = 0.02R$, (e) $n = 4$ and $A = 0.2R$, (f) $n = 4$ and $A = 0.02R$, where A is the amplitude of oscillations, n is oscillation mode and R is the unpeturbed radius.

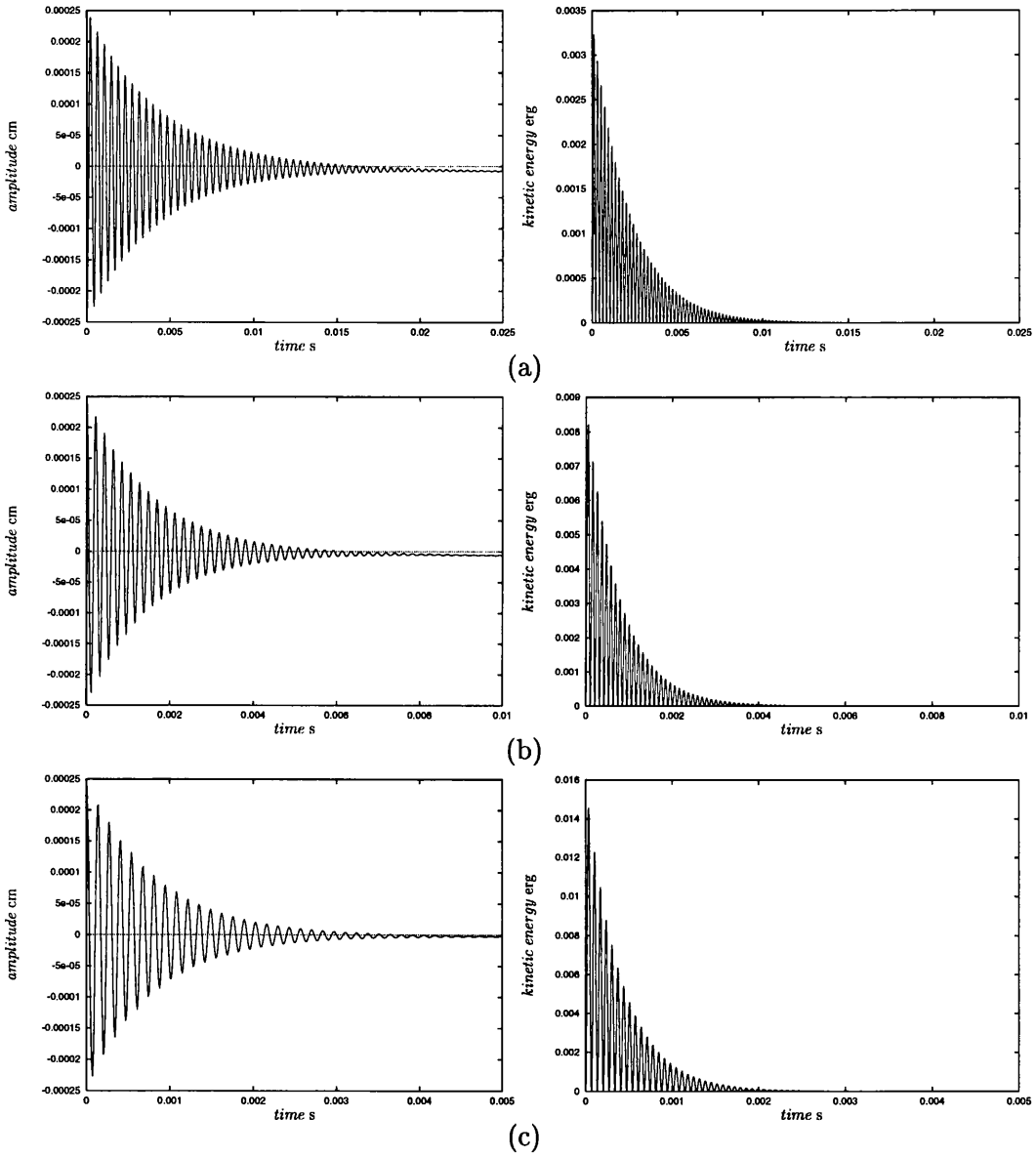

Figure 7.3: Oscillations of a 2D liquid drop. Time history of amplitude and kinetic energy for drop with amplitude $A = 0.02\ R$: (a) Second mode $n = 2$, (b) Third mode $n = 3$, (c) Fourth mode $n = 4$.

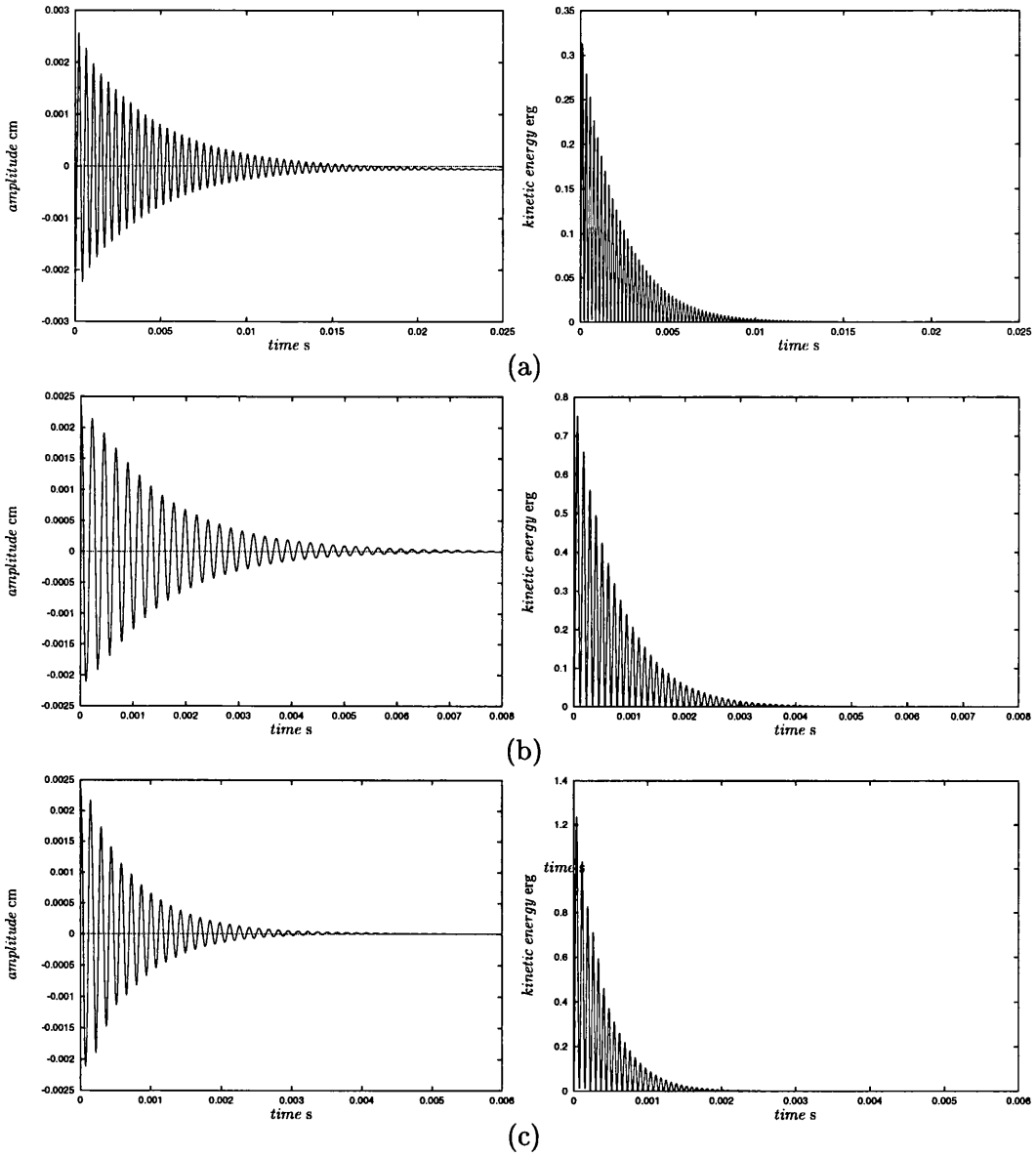

Figure 7.4: Oscillations of a 2D liquid drop. Time history of amplitude and kinetic energy for drop with amplitude $A = 0.2\ R$: (a) Second mode $n = 2$, (b) Third mode $n = 3$, (c) Fourth mode $n = 4$.

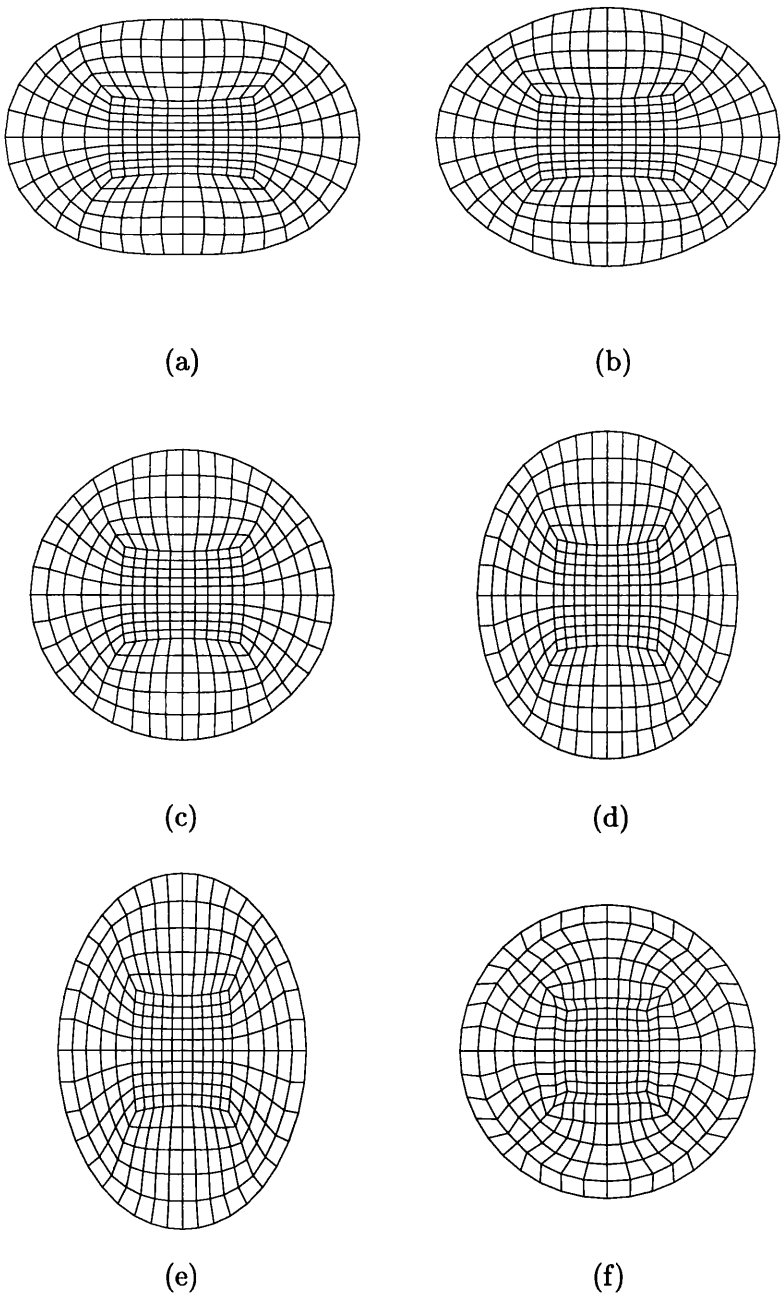

Figure 7.5: Oscillations of a 2D liquid drop. Finite element meshes for second mode ($n = 2$), $R = 0.0125\,\text{cm}$ and $A = 0.2\,R$ at different time instants: (a) $t = 0$, (b) $t = 1/8\,\tau$, (c) $t = 2/8\,\tau$, (d) $t = 3/8\,\tau$, (e) $t = 4/8\,\tau$, (f) $t = \infty$.

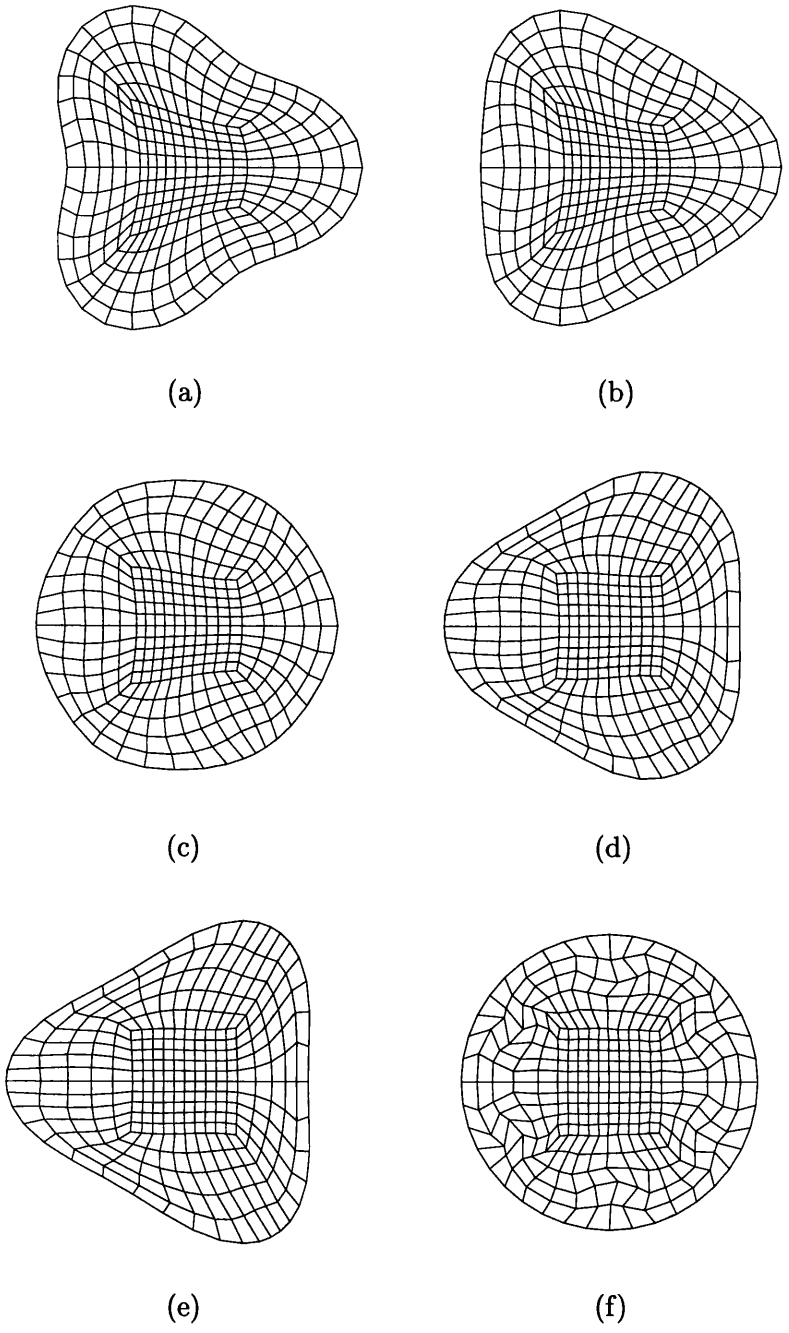

Figure 7.6: Oscillations of a 2D liquid drop. Finite element meshes for third mode ($n = 3$), $R = 0.0125\,\text{cm}$ and $A = 0.2\,R$ at different time instants: (a) $t = 0$, (b) $t = 1/8\,\tau$, (c) $t = 2/8\,\tau$, (d) $t = 3/8\,\tau$, (e) $t = 4/8\,\tau$, (f) $t = \infty$.

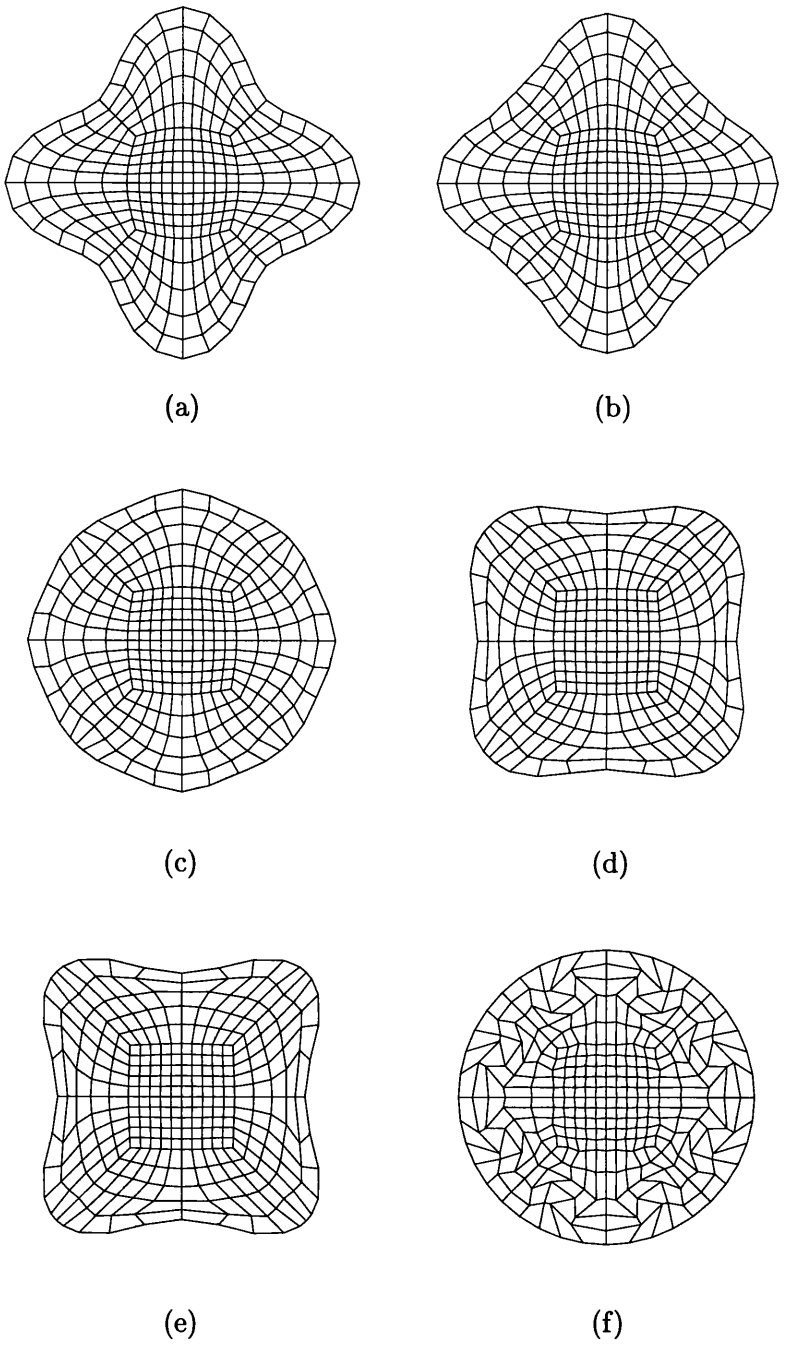

Figure 7.7: Oscillations of a 2D liquid drops. Finite element meshes for fourth mode ($n = 4$), $R = 0.0125\,\text{cm}$ and $A = 0.2\,R$ at different time instants: (a) $t = 0$, (b) $t = 1/8\,\tau$, (c) $t = 2/8\,\tau$, (d) $t = 3/8\,\tau$, (e) $t = 4/8\,\tau$, (f) $t = \infty$.

7.1.2 Axisymmetric drop

The shape of inviscid liquid drop undergoing small oscillations about a spheroidal shape at time t can be represented in spherical coordinates (r, θ, ϕ) as [4]

$$r = R + \sum a_n \, \mathrm{P}_n(\cos\theta), \tag{7.3}$$

where P_n is the n-th order Legendre polynomial, θ is the polar angle, R is the radius of the unperturbed sphere, and a_n are coefficients which are function of time t and given by expression

$$a_n = A_n \cos\omega t, \tag{7.4}$$

where A_n is amplitude associated with mode n and ω is the angular frequency given by

$$\omega^2 = n(n-1)(n+2)\left(\frac{\gamma}{\rho R^3}\right). \tag{7.5}$$

As in two dimensional case, oscillations with $n = 0$ and $n = 1$ correspond to the rigid body motion, and the fundamental mode correspond to $n = 2$.

For the fundamental oscillation the shape of the liquid drop is perturbed using the following expression

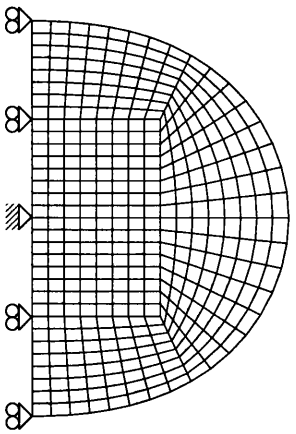

Figure 7.8: Oscillations of axisymmetric liquid drops: Initial mesh and boundary conditions for $n = 2$.

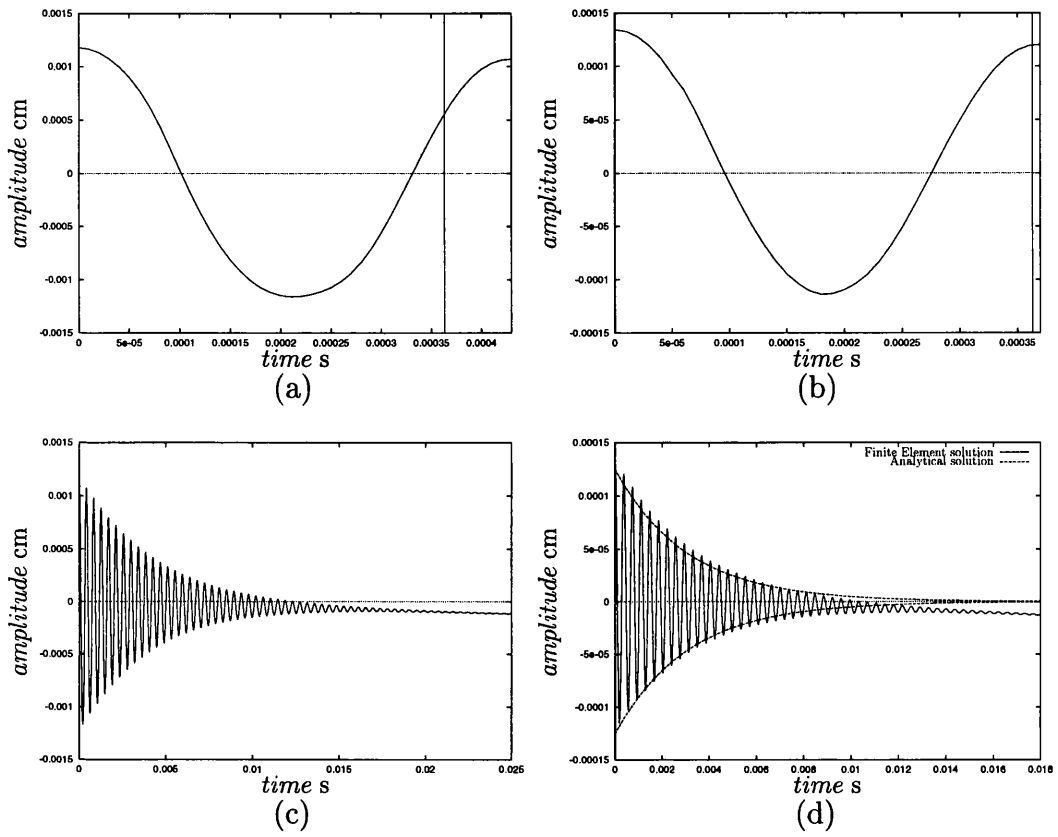

Figure 7.9: Oscillations of axisymmetric liquid drops: (a) and (b) Comparison of analytical and finite element results for $A_2 = 0.1\,R$ and $A_2 = 0.01\,R$, respectively, (c) and (d) time history of amplitude for $A_2 = 0.1\,R$ and $A_2 = 0.01\,R$, respectively.

$$r = R + A_2\,\mathrm{P}_2(\cos\theta). \tag{7.6}$$

Two examples are presented in this subsection. In the first example, the initial amplitude is $A_2 = 0.1R$ and initial amplitude of $A_2 = 0.01R$ is prescribed in the second example. The undisturbed spherical radius is taken to be $R = 0.0125\,\mathrm{cm}$. The type of element used for finite element computation is bilinear quadrilateral F-bar element. The number of elements employed for the computation is 384 and the time step is chosen as $\Delta t = 0.1 \times 10^{-5}\mathrm{s}$. In order to maintain the incompressibility of the fluid, the penalty parameter is taken to be $K = 0.1 \times 10^{11}$.

The analytical period associated with $n = 2$, obtained from equation (7.5), is $\tau = 0.363 \times 10^{-3}\,\mathrm{s}$. The periods of oscillation obtained from finite element analysis are $\tau_2^{\mathrm{FE}} = 0.43 \times 10^{-3}\,\mathrm{s}$ for $A_2 = 0.1\,R$ and $\tau_2^{\mathrm{FE}} = 0.37 \times$

10^{-3} s for $A_2 = 0.01\,R$. As can be seen in figures 7.9(a) and 7.9(b) the linear theory fails to predict the oscillation period for the case of $A_2 = 0.1R$ and there is a slight difference for the case with $A_2 = 0.01R$. Figures 7.9(c) and 7.9(d) show the time history of the amplitude. The viscous effect is clearly visible from the figures. These figures also show that in axisymmetric case the liquid drop experience more volume loss compared to the two dimensional case.

7.2 Stretching Liquid Bridges

A liquid bridge is a column of liquid held captive between two disks, that can be coaxial or non-coaxial. When such a static bridge is stretched uniaxially by moving one or both of the disks apart from each other, the bridge deforms gradually and the middle part of the liquid bridge contracts and eventually breaks into two large volumes of fluid that are pendant from the top disk and sessile on the bottom disk. In the case of fluids with high viscosity and elasticity, at the incipience of breakup a thin liquid thread is formed connecting those two large volumes and when it finally breaks one or more satellite drops may be formed. In addition to stretching the liquid bridge, the breakup process can also be achieved through two other methods. The first one is by extracting liquids from the bridge; in this way the stability limit of the liquid bridge is reduced due to reduction in its volume. The second method is by stabilizing initially unstable liquid bridge and then suddenly switching off the stabilizing effect.

Liquid bridges appear in a large variety of industrial processes such as floating-zone melting technique for crystal growth and purification of high-melting-point materials, spraying and atomization of liquids, fiber spinning process, agglomeration of particles, etc. Particularly for processes involving floating-zone melting technique, the useful idealization provided by statics and dynamics of liquid bridges, has motivated researchers to carry out numerical simulation of such processes. Other examples where liquid bridges have found application include the measurement of various physical properties such as surface tension, shear viscosity and extensional viscosity of molten Newtonian and non-Newtonian liquids.

Since the era of Plateau until about 1980, virtually all experimental and theoretical studies of liquid bridges were focused on the equilibrium shapes and stability of axisymmetric liquid bridge. With the advent of digital computer and development of numerical methods, the study of dynamic of liquid bridges has started to attract the attention of scientific community.

The use of numerical methods in the problems of dynamics of liquid bridges can first be attributed to Meseguer [12] in which finite difference method is used in theoretical study of the breakup of inviscid axisymmetric liquid bridges with initial slenderness ratio (i.e., the ratio of the bridge length to the rod radius) close to those at their limit of static stability. In this study Meseguer employed both the inviscid slice model of Lee [10] and one dimensional Cosserat model of Green [6], initially developed for slender liquid jets. Meseguer and Sanz [13] carried out a theoretical studies using a 1-D inviscid slice model to model the breakup of inviscid slender axisymmetric liquid bridges in microgravity conditions and performed the experiments

in Plateau tank to get neutral buoyancy in order to simulate microgravity condition. In order to relax the assumption that the liquid bridge is inviscid, Zhang and Alexander [22] introduced one dimensional models with viscosity to determine the response of liquid bridges subjected to harmonic disturbances. Later, Perales and Meseguer [14] introduced one dimensional Cosserat equation with viscosity. The most recent work that employed one dimensional model is the work of Ramos *et al.* [16] in which Galerkin finite element method is used to solve the viscous slice model in order to study the breakup of liquid bridge with initial slenderness ratio close to its static stability limits ($2.6 \leq \Lambda \leq 3.5$). The numerical results are validated with results from experiment using alternating current electric field to stabilize initially unstable shape of the liquid bridge under the presence of gravitational field.

Although the use of one dimensional model gives results that are in good agreement with the experimental ones due to the fact that within stretching liquid bridge the flow is predominantly unidirectional, the main drawback of using one dimensional model is that its range of validity is restricted to large values of the slenderness ratio of the liquid bridge being studied.

Two dimensional model is first used by Chen and Tsamopoulos [3] in the study of nonlinear oscillations of liquid bridges to examine the possibility of using it to measure surface tension and viscosity of molten liquids. Recently Yildirim and Basaran [20] compared the one and two dimensional models of stretching bridges of Newtonian and shear-thinning liquids. It is found that the one dimensional model predicts well the liquid bridge response provided that the dimensionless stretching speed $U^* < 1.0$, where $U^* = \sqrt{\rho R U_m^2/\gamma}$. The work of Zhang *et al.* [21] reviews most of the works on dynamics of liquid bridges.

Following the example given by Zhang *et al.*[21], the typical configuration of a liquid bridge with boundary and loading condition is depicted in Fig.7.10. The liquid bridge of fixed volume $V = 0.04\,\mathrm{cm}^3$ is held captive between two coaxial circular rods with radii $R = 0.16\,\mathrm{cm}$. The initial slenderness ratio is $\Lambda \equiv L/R = 2.0$ and the gravitational acceleration $g = 980\ \mathrm{cm/s}^2$ is acting downward along the axis of symmetry. It is assumed that the effects of the surrounding gas are negligible and the liquid is an incompressible Newtonian fluid with constant physical properties. The boundary conditions at the contact between liquid and upper and lower rods are taken as perfect slip conditions. At the three-phase contact lines no movement along the contact interface is allowed throughout the simulation. Surface tension is assumed to be active on the free surface. Stretching process is considered to be isothermal and is carried out by moving the upper rod with a constant velocity U_m while the lower rod is taken as stationary.

As has been pointed out by Kroger *et al.* [8] the effects of inertia can

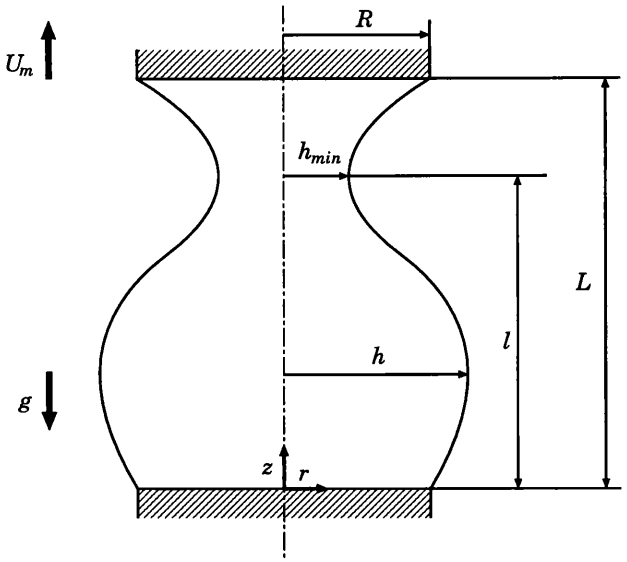

Figure 7.10: Stretching of a liquid bridge: Problem description

not be neglected even for a liquid bridges stretched with velocities as low as 0.1 cm s^{-1}. Therefore, the simulation is carried out dynamically using the equilibrium shape of static liquid bridge as an initial condition. This rises an extra problem due to the fact that the equilibrium shape of a static liquid bridge of particular volume and geometrical constraints is not known *a priori.* Therefore, the computation is carried out in two stages; the first stage is a quasi-static analysis, in which the equilibrium shape of static liquid bridge is obtained starting from a liquid bridge of cylindrical shape. The second stage is a dynamic analysis, in which the liquid bridge is stretched at constant velocity until break-up. The break-up of a liquid bridge is assumed to occur when the ratio of the minimum liquid bridge to the rod radius, h_{min}/R, reaches a prescribed value.

The simulation is performed for stretching velocity of $U_m = 0.60$ cm/s. The adaptive strategy employed in this simulation employs the maximum dissipation error indicator, described in chapter 4, with the value of the maximum error prescribed at 2.0%. The error is evaluated every 500 time steps, and if the error is above the prescribed value new mesh is generated. The initial finite element mesh is shown in figure 7.11(a) while the resulting quasi-static equilibrium shape is depicted in figure 7.11(b). Figure 7.12 presents deformed finite element meshes at different time instants. The time evolution of a liquid bridge profile is shown in figure 7.13 while the time evolution of a dimensionless minimum neck radius, h_{min}/R, is depicted in figure 7.14. The finite element prediction is compared against the exper-

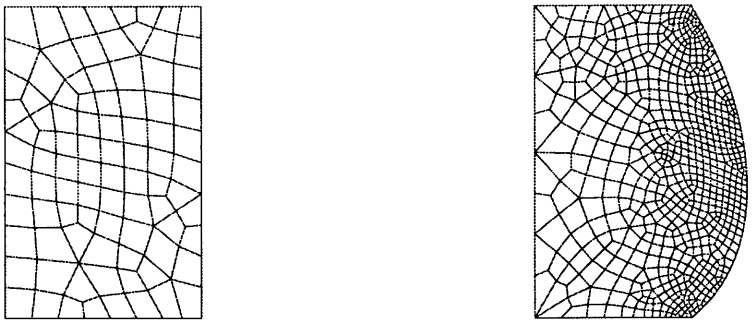

(a) (b)

Figure 7.11: Stretching of a liquid bridge: (a) initial cylindrical FE mesh (b) FE mesh corresponding to static equilibrium.

imental result provided by Zhang *et al.* [21], and good correspondence is obtained, especially considering the difficulties in obtaining a reliable set of experimental results for this type of problems.

In that experiment the liquid bridge is held captive between the parallel surfaces of two stainless steel, cylindrical disks or rods of equal radii that are coaxial with the bridge. The radii of the rods ranged between 0.08 and 0.32 cm. The parallel surfaces of the rods are machined flat and perpendicular to the rod wall so that the liquid wets completely these surfaces and the three-phase contact lines of the bridge remain pinned on the sharp edges of the two surfaces. The upper rod is connected to a translation stage that is reassembled from a Harvard Apparatus syringe pump and allows the top rod to move upward at an adjustable, constant velocity of up to 0.6 cm s^{-1} while providing a sufficiently high ramping acceleration from a state of rest to one of uniform translation.The evolution of the liquid bridge is recorded using a high speed motion analysis/video system. The whole experimental apparatus is placed on a vibration isolation table from Newport. An image digitization system is employed to determined the loci of liquid-gas interface from which the instantaneous shape of the bridge is evaluated.

The stretching velocity is found to influence the breakup mode of the liquid bridge as can be seen from figure 7.15. This confirms what had been found by Zhang *et al.* [21]. As shown in figure 7.15 at stretching velocity $U_m < 23.0\,\mathrm{cm/s}$ the point of inflexion where the breakup takes place is at the lower part of the liquid bridge causing the formation of a sessile drop on the lower plate and a pendent drop hanging from the upper plate after the breakup. There is also possibility of the formation of a satellite drop from the thread after the breakup. At the stretching velocity around $U_m = 23.0\,\mathrm{cm/s}$

two points of inflexion exist. This velocity can be considered as a critical velocity. With the stretching velocity $U_m > 23.0\,\mathrm{cm/s}$ the breakup mode return to a single point inflexion but its position now is in the upper part of the liquid bridge.

It is also evidenced that by increasing the stretching velocity, the maximum height that can be achieved before the liquid bridge starting to break up is increased until it gets to a maximum value and then starts to decrease. This maximum value is obtained when the stretching velocity is around $U_m = 22.0\,\mathrm{cm/s}$.

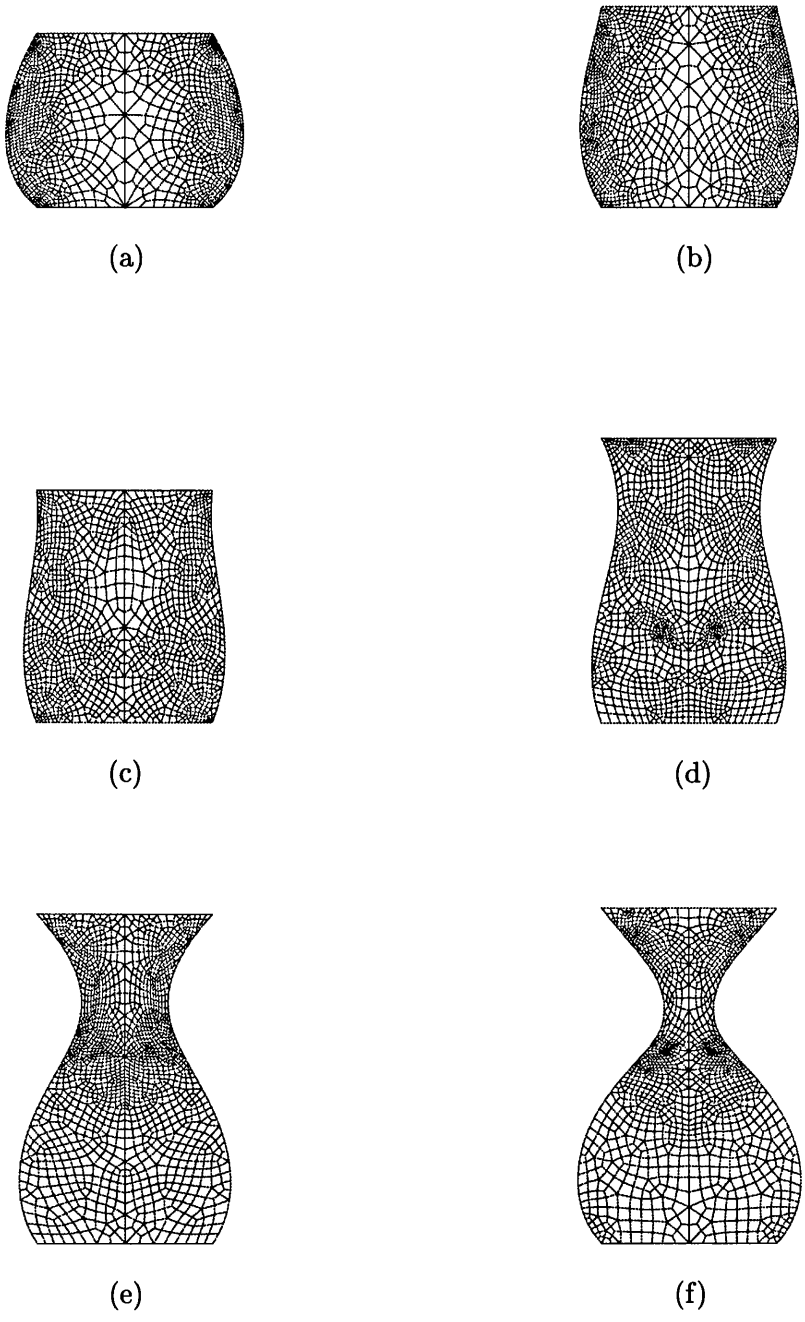

Figure 7.12: Stretching of a liquid bridge: Deformed finite element meshes at different time instants: (a) $t = 0\,\text{ms}$, (b) $t = 80\,\text{ms}$, (c) $t = 188\,\text{ms}$, (d) $t = 350\,\text{ms}$, (e) $t = 472\,\text{ms}$, (f) $t = 487\,\text{ms}$.

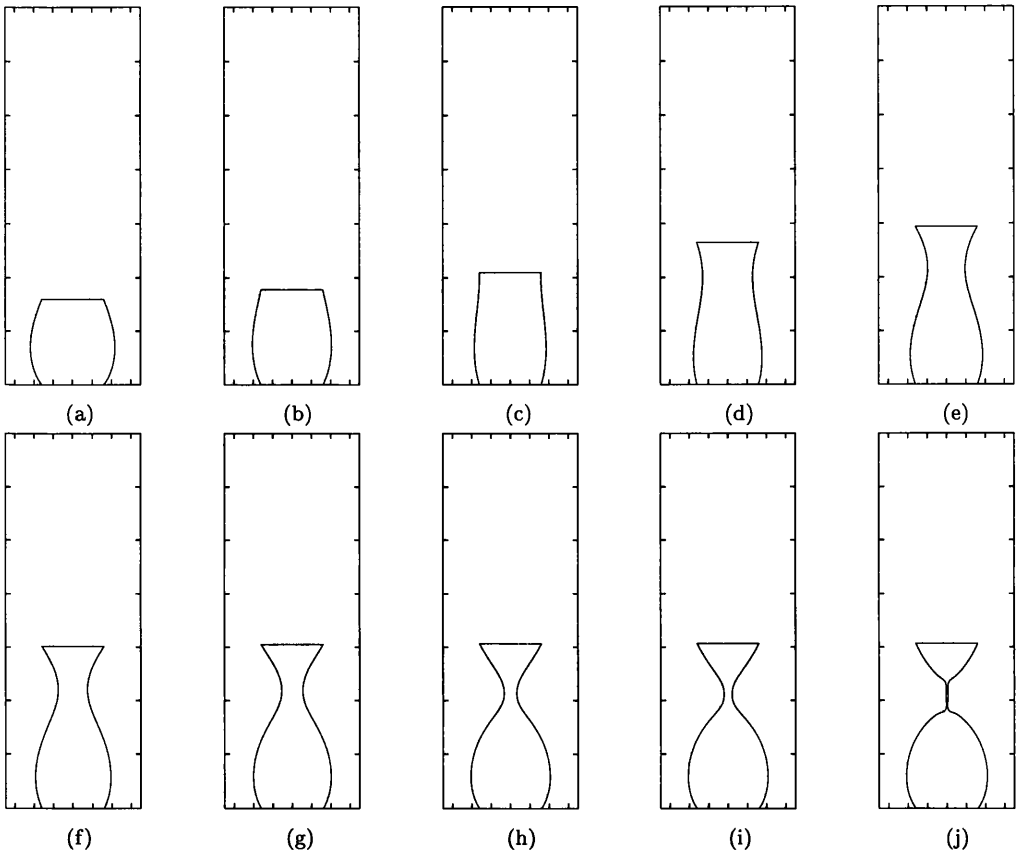

Figure 7.13: Evolution in time of the computed shape of a water bridge of volume of 0.04 cm^3 and slenderness ratio of 2 that is held captive between two circular rod of equal radii of $r = 0.16$ cm and is stretched axially at a constant velocity of 0.6 cm s^{-1}; (a) $t = 0$ ms, (b) $t = 67$ ms, (c) $t = 175$ ms, (d) $t = 350$ ms, (e) $t = 445$ ms, (f) $t = 472$ ms, (g) $t = 482$ ms, (h) $t = 487$ ms, (i) $t = 488$ ms, (j) $t = 492$ ms.

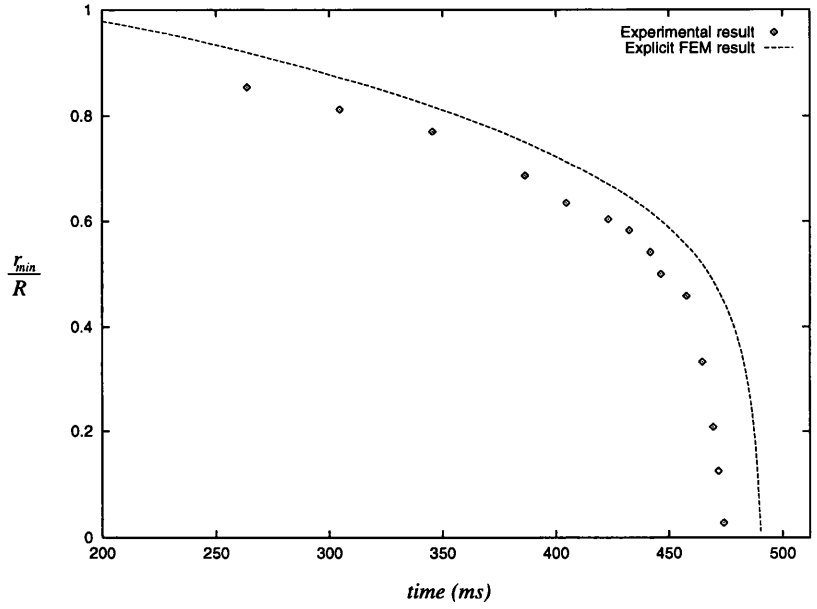

Figure 7.14: Stretching of a liquid bridge: Time evolution of dimensionless minimum radius.

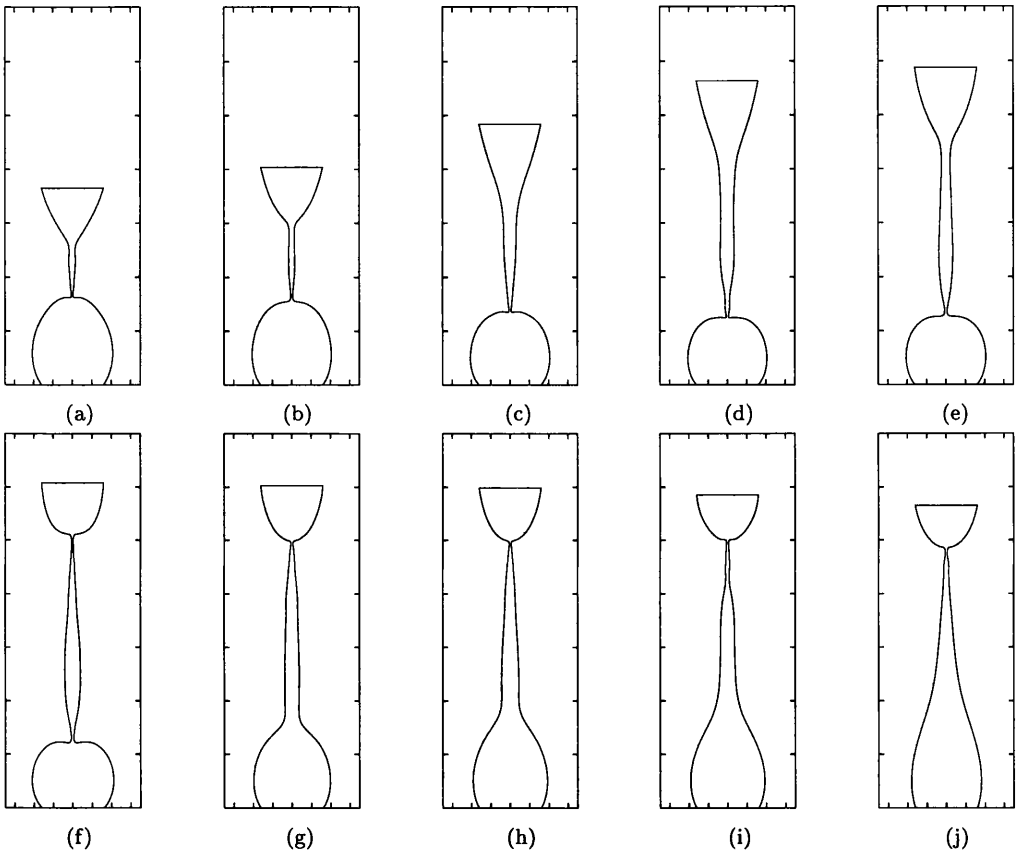

Figure 7.15: Dynamics of a liquid bridge: Computed limiting shapes of water bridges held captive between two circular plates of radius $r = 0.16$ cm as function of plate velocity; (a) $U_m = 5.0$ cm/s, (b) $U_m = 10.0$ cm/s, (c) $U_m = 15.0$ cm/s, (d) $U_m = 20.0$ cm/s, (e) $U_m = 22.0$ cm/s, (f) $U_m = 23.0$ cm/s, (g) $U_m = 25.0$ cm/s, (h) $U_m = 26.5$ cm/s, (i) $U_m = 27.0$ cm/s, (j) $U_m = 30.0$ cm/s.

7.3 Closure

Examples on nonlinear dynamic of liquid drops and liquid bridges have been presented in this chapter. The technique to incorporate surface tension into Lagrangian finite element method for free surface problems presented in Chapter 5 performs satisfactorily for dynamic problems.

The solution for the first example can be obtained without any difficulty as long as the size of the drop is kept relatively small, in order to avoid circulation that can cause mesh entanglement, and the amplitude of oscillation is not too large, to prevent over-distorted elements and possibility of breakup.

Using adaptive remeshing procedure described in Chapter 4 to avoid over-distorted element or mesh entanglement, the experiment on the stretching of a liquid bridge carried out by Zhang *et al.* has been simulated. The results of this numerical simulation prior to breakup are in a good agreement with the experimental one.

Bibliography

[1] O. Basaran. Nonlinear oscillations of viscous liquid drops. *J. Fluid Mech.*, 241:169 – 198, 1992.

[2] E. Becker, W.J. Hiller, and T.A. Kowalewski. Nonlinear dynamics of viscous droplets. *J. Fluid Mech.*, 258:191 – 216, 1994.

[3] T. Chen and J. Tsamopoulos. Nonlinear dynamics of capillary bridges: Theory. *J. Fluid Mech.*, 255:373 – 409, 1993.

[4] G.B. Foote. A numerical method for studying liquid drop behavior: Simple oscillation. *J. Comp. Physics*, 11:507 – 530, 1973.

[5] D.E. Fyfe, E.S. Oran, and M.J. Fritts. Surface tension and viscosity with lagrangian hydrodynamics on triangular mesh. *J. Comp. Physics*, 76:349 – 384, 1988.

[6] A. E. Green. On the nonlinear behaviour of fluid jets. *Int. J. Engng. Sci.*, 14:49 – 63, 1976.

[7] P.M. Gresho and R.L. Sani. *Incompressible Flow and The Finite Element Method: Advection-Diffusion and Isothermal Laminar Flow.* John Wiley & Sons, New York, 1998.

[8] R. Kroger, S. Berg, A. Delgado, and H. J. Rath. Stretching behavior of large polymeric and newtonian liquid bridges in plateau simulation. *J. Non-Newtonian Fluid Mech.*, 45:385 – 400, 1992.

[9] H. Lamb. *Hydrodynamics.* Cambridge University Press, Cambridge, 6^{th} edition, 1932.

[10] H. C. Lee. Drop formation in a liquid jet. *IBM J. Res. Dev.*, 18:364 – 369, 1974.

[11] T.S. Lundgren and N.N. Mansour. Oscillations of drops in zero gravity with weak viscous effects. *J. Fluid Mech.*, 194:479 – 510, 1988.

[12] J. Meseguer. The breaking of axisymmetric slender liquid bridges. *J. Fluid Mech.*, 130:123 – 151, 1983.

[13] J. Meseguer and A. Sanz. Numerical and experimental study of the dynamics of axisymmetric slender liquid bridges. *J. Fluid Mech.*, 153:83 – 101, 1985.

[14] J. M. Perales and J. Meseguer. Theoritical and experimental study of the vibration of axisymmetric viscous liquid bridges. *Phys. Fluids A*, 4:1110 – 1130, 1992.

[15] C. Pozrikidis. Three-dimensional oscillations of inviscid drops induced by surface tension. *Comp. Fluids*, 30:417 – 444, 2001.

[16] A. Ramos, F. J. Garcia, and J. M. Valverde. On the breakup of slender liquid bridges: Experiments and a 1-d numerical analysis. *Eur. J. Mech. B/Fluids*, 18:649 – 658, 1999.

[17] Lord Rayleigh. On the capillary phenomena of jets. *Proc. R. Soc. Lond.*, 29:71 – 97, 1879.

[18] W.H. Reid. The oscillation of a viscous liquid drop. *Q. Appl. Math.*, 18:86 –89, 1960.

[19] J.A. Tsamopoulos and R.A. Brown. Nonlinear oscillations of inviscid drops and bubles. *J. Fluid Mech.*, 127:519 – 537, 1983.

[20] O. E. Yildirim and O. A. Basaran. Deformation and breakup of stretching bridges of newtonian and shear-thinning liquids: Comparison of one and two-dimensional models. *Chem. Engng. Scie.*, 56:211 – 233, 2001.

[21] X. Zhang, R. S. Padgett, and O. A. Basaran. Nonlinear deformation and breakup of stretching liquid bridges. *J. Fluid Mech.*, 329:207 – 245, 1996.

[22] Y. Zhang and J. I. D. Alexander. Sensitivity of liquid bridges subject to axial residual acceleration. *Phys. Fluid A*, 2:1966 – 1974, 1990.

Chapter 8

Conclusions

Topics related to finite element modelling of surface tension phenomena for fluid flows with free surfaces and interfaces have been discussed in this thesis. The approach adopted in this work was based on a Lagrangian framework and moving meshes which describe explicitly the interface evolution. The Lagrangian formulation allows accurate tracking of the free surface and provides a simple and natural framework for computational modelling of surface tension. Attention is focused on the development of finite element procedure for solving Lagrangian free surface flow based on incremental flow formulation and a technique to incorporate the surface tension effects into this finite element procedure. The procedure was validated using some classical problems for which the analytical solutions exist and available experimental results.

8.1 Summary and Conclusions

8.1.1 Free surface flows

To provide the basis for the finite element modelling of surface tension phenomena, a finite element procedure for solving free surface flow problems was developed and discussed in detail in Chapter 4. The Lagrangian formulation was adopted. The use of the so-called incremental flow formulation gave rise to the constitutive equations being approximated by time integration. Upon the spatial discretization using finite elements the weak form of the governing equations yielded a set of ordinary differential equations. The Newmark method was used for time integration of this set of ordinary differential equation. For implicit case the resulting nonlinear algebraic equation was solved using Newton-Raphson iterative procedure. Emphasis was placed on

the consistent linearization of residuals associated with the Newton-Raphson procedure.

The resulting finite element procedure was tested using three different problems commonly used as benchmarks for a free surface flow solver, namely the breaking dam, the large amplitude oscillations and the free oscillation problems. In general, the procedure performed very well for all problems considered. The only problem experienced relates to the apparent volume loss was in the free oscillation problem and a long time interval of interest, as a consequence of employing penalty method to impose incompressibility constraint.

8.1.2 Surface tension

A technique to incorporate surface tension into Lagrangian finite element free surface flow problems was presented in Chapter 5 for both two dimensional and axisymmetric cases. The surface tension model employed in this work is the inviscid fluid surface model which is known traditionally as the Laplace-Young equation. By using the surface divergence theorem the weak form of the Laplace-Young equation has been transformed into the term associated with the condition at the contact line and a term associated with the surface tension. In this way the required C^1 continuity across element boundary has been circumvented. Emphasis was put on the derivation of the element surface tension force vector and its consistent linearization associated with the Newton-Rhapson iterative solution procedure.

The performance of the adopted technique was tested for both quasi-static and dynamic simulations. The generalized Plateau problem was employed as a benchmark for quasi-static case. In all three examples the finite element results are in a very good agreement with the analytical solutions obtained by numerical integration of the set of ordinary differential equations resulting from a parameterization of the Laplace-Young equation. For dynamic case two problems were employed to test the adopted technique. The first one was a droplet oscillations and the second one was the stretching of a liquid bridge. In the first problem the finite element solutions were compared against the analytical solutions and in the second problem the finite element solutions were compared against the experimental results. For both problems the finite element solutions show a very good agreement with both analytical solutions and experimental results.

8.2 Suggestions for Future Research

Issues related to the finite element modelling of surface tension phenomena addressed in this thesis can be considered as a preliminary in nature. Therefore, research on this particular subject is far from complete and a great deal of issues are still widely open for research.

The following subsections bring up some issues for the further research of the finite element modelling of surface tension phenomena.

8.2.1 Finite element method for free-surface flow

Obtaining a robust finite element method for solving free-surface flow is considered as a primary concern of further research. The use of multi-field variational principle in imposing incompressibility constraint seems inevitable due to the fact that penalty method experiences problems in modelling incompressible fluid flows though it works quite well for incompressible solids.

Another aspect of finite element method that needs to be considered is the use of Arbitrary Lagrangian-Eulerian framework to reduce the required expensive adaptive remeshing process to the minimum. Moreover by reducing the number of adaptive remeshing required the numerical diffusion due to this process can also be reduced.

8.2.2 Surface tension model

Although the surface tension model employed in this work is valid for most of liquid-liquid and liquid-vapor interfaces there are cases where this model is not applicable. Grossly contaminated interfaces, polymerized interfaces, and biological interfaces consisting of lipids and protein are examples where the inviscid fluid surface model cannot model the complex physical behavior of these types of interfaces. Including these models into the present finite element code will widen the range of the problems that can be solved.

Another consideration related to the surface tension model is to extend the two dimensional and axisymmetric model currently available into a three dimensional one. The three dimensional model could, for instance, be used in simulation of more realistic granulation processes.

8.2.3 Contact angle

Regarding contact angle, the present assumption in which constant contact angle is prescribed, is not realistic enough to simulate problems with dynamic contact line such as, for instance, liquid drop impacting upon a surface. The

extension of the present treatment of contact angle to take into account the difference between advancing and receding contact angles can follow the one proposed by Fukai *et. al.* [2].

8.2.4 Merging and separation

One of the features in modelling agglomeration processes that has not been addressed in this thesis is the topological changes that are associated with merging and separation of the liquid phase. Some studies of these processes have been published, both theoretical and experimental, by several authors. The published works are mainly related to droplet formation either from liquid jet break-up or pendent drop. Only a limited number are devoted to numerical simulations. Most of them are based on the finite difference or finite element solutions of one-dimensional approximation of the Navier-Stokes equations [4, 5, 1, 6, 9], or finite difference solutions or finite element modelling of free surface flows using VOF/CSF method in the Eulerian framework [3, 7, 8]. To the best of our knowledge there is no published work on merging and separations simulation performed by using finite element solutions in the Lagrangian framework.

Bibliography

[1] J. Eggers and T.F. Dupont. Drop formation in a one-dimensional approximation of the Navier-Stokes equation. *J. Fluid Mech.*, 262:205 – 221, 1994.

[2] J. Fukai, Y. Shiiba, T. Yamamoto, O. Miyatake, D. Poulikakos, C. M. Megaridis, and Z. Zhao. Wetting effects on the spreading of a liquid droplet colliding with a flat surface: Experiment and modeling. *Phys. Fluids*, 7:236 – 247, 1995.

[3] B. Lafaurie, C. Nardone, R. Scardovelli, S. Zaleski, and G. Zanetti. Modelling merging and fragmentation in multiphase flows with SURFER. *J. Comp. Physics.*, 113:134 – 147, 1994.

[4] H. C. Lee. Drop formation in a liquid jet. *IBM J. Res. Dev.*, 18:364 – 369, 1974.

[5] J. Meseguer. The breaking of axisymmetric slender liquid bridges. *J. Fluid Mech.*, 130:123 – 151, 1983.

[6] X.D. Shi, M.P. Brenner, and S.R. Nagel. A cascade of structure in a drop falling from a faucet. *Science*, 265:219 – 222, 1994.

[7] J. Wu, S.T. Yu, and B.N. Jiang. Simulation of two-fluid flows by the least-squares finite element method using a continuum surface tension model. *Int. J. Num. Meth. Engng*, 42:583 – 600, 1998.

[8] X. Zhang. Dynamics of drop formation in viscous flows. *Chem. Engng. Sci.*, 54:1759 – 1774, 1998.

[9] X. Zhang, R. S. Padgett, and O. A. Basaran. Nonlinear deformation and breakup of stretching liquid bridges. *J. Fluid Mech.*, 329:207 – 245, 1996.

Appendix A

Some Results from Differential Geometry

A surface $\mathcal{S}$ in $\mathcal{E}$ is a subset of $\mathcal{E}$ endowed with a structure defined at each $\boldsymbol{x} \in \mathcal{S}$ by two dimensional subspace $\mathcal{T}_{\boldsymbol{x}}$ of $\mathcal{V}$ and a mapping $\pi_{\boldsymbol{x}}$ such that

i.) $\pi_{\boldsymbol{x}} : \mathcal{N}_{\boldsymbol{x}} \to \mathcal{S}$ is a class C^2 mapping with domain $\mathcal{N}_{\boldsymbol{x}}$ an open neighborhood of zero in $\mathcal{T}_{\boldsymbol{x}}$.

ii.) For some neighborhood $\mathcal{M}$ of $\boldsymbol{x}$ in $\mathcal{E}$, $\pi_{\boldsymbol{x}}(\mathcal{N}_{\boldsymbol{x}}) \cap \mathcal{M} = \mathcal{S} \cap \mathcal{M}$.

iii.) $\pi_{\boldsymbol{x}}(\boldsymbol{y}) - (\boldsymbol{x} + \boldsymbol{y})$ belongs to $\mathcal{T}_{\boldsymbol{x}}^{\perp}$ for every $\boldsymbol{y} \in \mathcal{N}_{\boldsymbol{x}}$ and is of order $O(|\boldsymbol{y}|)$ as $\boldsymbol{y} \to \boldsymbol{0}$.

iv.) There exists a continuous field $\boldsymbol{n} : \mathcal{S} \to \mathcal{V}$ that never vanishes and has $\boldsymbol{n}(\boldsymbol{x}) \in \mathcal{T}_{\boldsymbol{x}}^{\perp}$ at each $\boldsymbol{x} \in \mathcal{S}$

$\mathcal{T}_{\boldsymbol{x}}$ is called the *tangent space* at $\boldsymbol{x}$ and $\pi_{\boldsymbol{x}}(\boldsymbol{y})$ is the projection, perpendicular to $\mathcal{T}_{\boldsymbol{x}}$, of $\boldsymbol{x} + \boldsymbol{y}$ onto $\mathcal{S}$. It follows from (iii) that $\pi_{\boldsymbol{x}}$ is injective, $\pi_{\boldsymbol{x}}(\boldsymbol{0}) = \boldsymbol{x}$, and

$$\nabla \pi_{\boldsymbol{x}}(\boldsymbol{0}) = \mathsf{I}(\boldsymbol{x}),$$

where $\mathsf{I}(\boldsymbol{x}) \in \mathrm{Lin}(\mathcal{T}_{\boldsymbol{x}}, \mathcal{V})$ is the *inclusion* map

$$\mathsf{I}(\boldsymbol{x})\boldsymbol{y} = \boldsymbol{y} \qquad \forall \boldsymbol{x} \in \mathcal{T}_{\boldsymbol{x}}$$

Let $\mathsf{1}(\boldsymbol{x}) \in \mathrm{Lin}(\mathcal{T}_{\boldsymbol{x}}, \mathcal{T}_{\boldsymbol{x}})$ be the *identity* map on $\mathcal{T}_{\boldsymbol{x}}$ and $\boldsymbol{P}(\boldsymbol{x}) \in \mathrm{Lin}(\mathcal{V}, \mathcal{T}_{\boldsymbol{x}})$ be a *perpendicular projection* from $\mathcal{V}$ onto $\mathcal{T}_{\boldsymbol{x}}$, then for every $\boldsymbol{y} \in \mathcal{T}_{\boldsymbol{x}}$, $\boldsymbol{v} \in \mathcal{V}$

$$\boldsymbol{y} \cdot \boldsymbol{P}(\boldsymbol{x})\boldsymbol{v} = \mathsf{I}(\boldsymbol{x})\boldsymbol{y} \cdot \boldsymbol{v},$$

so that

$$\mathsf{I}(\boldsymbol{x})^T = \boldsymbol{P}(\boldsymbol{x}), \tag{A.1}$$

and

$$\boldsymbol{P}(\boldsymbol{x})\boldsymbol{P}(\boldsymbol{x})^T = \mathsf{1}(\boldsymbol{x}) = \mathsf{I}(\boldsymbol{x})^T\mathsf{I}(\boldsymbol{x}). \tag{A.2}$$

In addition

$$\mathsf{I}(\boldsymbol{x})\boldsymbol{P}(\boldsymbol{x}) = \boldsymbol{I} - \boldsymbol{n}(\boldsymbol{x}) \otimes \boldsymbol{n}(\boldsymbol{x}) \tag{A.3}$$

The *gradient* of a smooth function f on $\mathcal{S}$ also known as the *surface gradient* is defined by

$$\nabla_s f(\boldsymbol{x}) = \nabla(f \circ \pi_{\boldsymbol{x}})(\boldsymbol{0}),$$

so that $\nabla_s f(\boldsymbol{x}) \in \mathscr{T}_{\boldsymbol{x}}$. A similar definition applies to a vector or point field $\boldsymbol{u}$ on $\mathcal{S}$, thus $\nabla_s \boldsymbol{u}(\boldsymbol{x}) \in \mathrm{Lin}(\mathscr{T}_{\boldsymbol{x}}, \mathscr{V})$.

A *tangential vector field* is a map $\boldsymbol{t} : \mathcal{S} \to \mathscr{V}$ such that $\boldsymbol{t}(\boldsymbol{x}) \in \mathscr{T}_{\boldsymbol{x}}$ at each $\boldsymbol{x} \in \mathcal{S}$. The *tangential derivative* of a smooth vector field $\boldsymbol{u} : \mathcal{S} \to \mathscr{V}$ is defined by

$$D\boldsymbol{u}(\boldsymbol{x}) = \boldsymbol{P}(\boldsymbol{x})\nabla\boldsymbol{u}(\boldsymbol{x}), \tag{A.4}$$

so that $D\boldsymbol{u}(\boldsymbol{x}) \in \mathrm{Lin}(\mathscr{T}_{\boldsymbol{x}}, \mathscr{T}_{\boldsymbol{x}})$ maps each tangent vector $\boldsymbol{y} \in \mathscr{T}_{\boldsymbol{x}}$ into that portion of $\nabla\boldsymbol{u}(\boldsymbol{x})\boldsymbol{y}$ which lies in $\mathscr{T}_{\boldsymbol{x}}$.

Let $\boldsymbol{n}$ be an orientation of $\mathcal{S}$, the field

$$\mathsf{L} = -D\boldsymbol{n}, \tag{A.5}$$

is called the *Weingarten map* and

$$H = \frac{1}{2}\mathrm{tr}[\mathsf{L}], \tag{A.6}$$

is the *mean curvature.*

The *surface divergence* div_s of a smooth vector field $\boldsymbol{u} : \mathcal{S} \to \mathscr{V}$ is defined by

$$\mathrm{div}_s[\boldsymbol{u}] = \mathrm{tr}[D\boldsymbol{u}]. \tag{A.7}$$

A *tangential tensor field* is a field T on $\mathcal{S}$ that assigns to each $\boldsymbol{x} \in \mathcal{S}$ a linear transformation $\mathsf{T}(\boldsymbol{x}) : \mathscr{T}_{\boldsymbol{x}} \to \mathscr{T}_{\boldsymbol{x}}$.

Bibliography

[1] M.E. Gurtin and A.I. Murdoch. A continuum theory of elastic material surfaces. *Arch. Rat. Mech. Anal.*, 57:291 – 323, 1975.

[2] A.I. Murdoch. A thermodynamical theory of elastic material interfaces. *J. Mech. Appl. Math.*, 29:245 – 275, 1976.

Appendix B

Computation of general isotropic tensor functions of one tensor and their derivatives

B.1 General isotropic tensor valued functions of one tensor

In 2-D, the general isotropic tensor valued functions of one tensor is constructed as follows. Given a scalar function $y : \mathbb{R}^n \to \mathbb{R}$, the tensor function $\boldsymbol{Y}$: $\text{sym}(V_n) \to \text{sym}(V_n)$ is defined by:

$$\boldsymbol{Y}(\boldsymbol{X}) := \sum_{i=1}^{p} y_i \boldsymbol{E}_i \tag{B.1}$$

where, the eigenvalues y_i of $\boldsymbol{Y}$ are obtained from the eigenvalues x_i of $\boldsymbol{X}$ as

$$\begin{aligned} y_1 &:= y(x_1, x_2) \\ y_2 &:= y(x_2, x_1) \end{aligned} \tag{B.2}$$

B.2 Function computation

Practical computation of isotropic tensor functions is carried out as follows:

i.) Given $\boldsymbol{X}$, compute its eigenvalues x_i by

$$\begin{aligned} x_1 &= \frac{I_{\boldsymbol{X}}+\sqrt{I_{\boldsymbol{X}}^2-4II_{\boldsymbol{X}}}}{2} \\ x_2 &= \frac{I_{\boldsymbol{X}}-\sqrt{I_{\boldsymbol{X}}^2-4II_{\boldsymbol{X}}}}{2} \\ \boldsymbol{E}_\alpha &= \frac{1}{2x_\alpha - I_{\boldsymbol{X}}}\left[\boldsymbol{X} + (x_\alpha - I_{\boldsymbol{X}})\,\mathbf{1}\right] \end{aligned} \tag{B.3}$$

where $I_{\boldsymbol{X}} = \mathrm{tr}[\boldsymbol{X}]$ and $II_{\boldsymbol{X}} = \det[\boldsymbol{X}]$

ii.) With x_i, evaluate eigenvalues y_i of $\boldsymbol{Y}$ using (B.2)

iii.) Compute $\boldsymbol{Y}$ as:

$$\boldsymbol{Y} = \begin{cases} \sum_{i=1}^{2} y_i \boldsymbol{E}_i & if \quad x_1 \neq x_2 \\ y_1 \mathbf{1} & if \quad x_1 = x_2 \end{cases} \tag{B.4}$$

with $\boldsymbol{E}_\alpha$ is given by expression (B.3).

B.3 Computation of the derivative

Computation of the derivative of isotropic tensor functions is carried out as follows:

i.) Given $\boldsymbol{X}$, compute its eigenvalues x_α ($\alpha = 1, 2$) by means expression (B.3).

ii.) With x_α, evaluate eigenvalues y_α of $\boldsymbol{Y}$ using (B.2).

iii.) Compute $d\boldsymbol{Y}/d\boldsymbol{X}$ as

$$\frac{d\boldsymbol{Y}}{d\boldsymbol{X}} = \begin{bmatrix} A & if \quad x_1 \neq x_2 \\ B & if \quad x_1 = x_2 \end{bmatrix} \tag{B.5}$$

where

$$\begin{aligned} A &= \frac{y_1 - y_2}{x_1 - x_2}[\boldsymbol{I} - \boldsymbol{E}_1 \otimes \boldsymbol{E}_1 - \boldsymbol{E}_2 \otimes \boldsymbol{E}_2] + \sum_{\alpha=1}^{2}\sum_{\beta=1}^{2} \frac{\partial y_\alpha}{\partial x_\beta} \boldsymbol{E}_\alpha \otimes \boldsymbol{E}_\beta \\ B &= \left(\frac{\partial y_1}{\partial x_1} - \frac{\partial y_1}{\partial x_2}\right)\boldsymbol{I} + \frac{\partial y_1}{\partial x_2}\mathbf{1} \otimes \mathbf{1} \end{aligned}$$

Bibliography

[1] D.E. Carlson and A. Hoger. The derivative of a tensor-valued function of a tensor. *Quart. Appl. Math.*, 44(3):409–423, 1986.

[2] E.A. de Souza Neto, D. Perić, and D.R.J. Owen. Continuum modelling and numerical simulation of material damage at finite strains. *Arch. Comp. Meth. Engng.*, 5:311–384, 1998.